Center for Seismic Studies
Semiannual Technical Report
March - October 1992

Jerry Carter
John Coyne
Lori Grant
Anne Henson
Hans Israelsson
Florence Riviere
Vlad Ryaboy

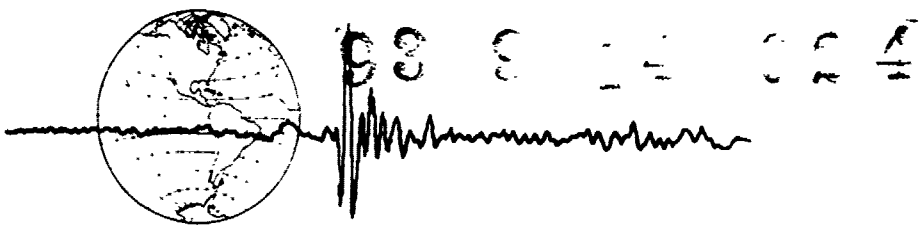

Center for Seismic Studies
1300 N. 17th Street, Suite 1450
Arlington, Virginia 22209-3871
Telephone: (703) 276-7900

Semiannual Technical Report C92-04

November 30, 1992

Center for Seismic Studies
Semiannual Technical Report
March - October 1992

Jerry Carter
John Coyne
Lori Grant
Anne Henson
Hans Israelsson
Florence Riviere
Vlad Ryaboy

APPROVED FOR PUBLIC RELEASE - DISTRIBUTION UNLIMITED

Science Applications International Corporation
Center for Seismic Studies
1300 N. 17th Street, Suite 1450
Arlington, VA 22209

ADVANCED RESEARCH PROJECTS AGENCY
3701 NORTH FAIRFAX DRIVE
ARLINGTON, VA 22203-1714

August 17, 1993

MEMORANDUM FOR PHILLIPS LABORATORY/PKVA
ATTN: Ms Lynne Adams

SUBJECT: Approval for Unlimited Distribution CSS Semiannual Technical Report, March - October 1992
Report C92-04, Contract No. F29601-92-C-0005

ARPA/NMRO has carefully reviewed the subject scientific report submitted by Science Applications International Corporation under the subject contract, and certifies that this report contains no critical or sensitive data, information, or technology. As a result of this investigation, the report is approved for public release, distribution unlimited.

The contractor shall include a copy of this letter with each copy of the subject report released to individuals or organizations outside of the US Government or their contractors, as documentation that the contents have been reviewed and that unlimited distribution of the report has been approved.

The procedure described above is consistent with the distribution procedures specified in the subject contract, and with procedures agreed upon in our phone conversation of 8 July 1993. Please let me know if you have any questions.

Steven R. Bratt
Program Manager
Nuclear Monitoring Research Office

REPORT DOCUMENTATION PAGE

Form Approved
OMB No. 0704-0188

1. AGENCY USE ONLY (Leave blank)	2. REPORT DATE	3. REPORT TYPE AND DATES COVERED
	November 30, 1992	Semiannual Technical Report

4. TITLE AND SUBTITLE
Center for Seismic Studies Semiannual Technical Report March - October 1992

5. FUNDING NUMBERS
F29601-92-C-0005

6. AUTHOR(S)
J. Carter, J. Coyne, L. Grant, A. Henson, H. Israelsson, F. Riviere, V. Ryaboy

7. PERFORMING ORGANIZATION NAME(S) AND ADDRESS(ES)
Science Applications International Corporation
Center for Seismic Studies
1300 N. 17th Street, Suite 1450
Arlington, VA 22209

8. PERFORMING ORGANIZATION REPORT NUMBER
CSS 92-04

9. SPONSORING/MONITORING AGENCY NAME(S) AND ADDRESS(ES)
Advanced Research Projects Agency
3701 N.Fairfax Drive
Arlington, VA 22203

10. SPONSORING/MONITORING AGENCY REPORT NUMBER

11. SUPPLEMENTARY NOTES

12a. DISTRIBUTION/AVAILABILITY STATEMENT
Approved for Public Release
Distribution Unlimited

12b. DISTRIBUTION CODE

13. ABSTRACT *(Maximum 200 words)*

The first chapter of this report describes a ground-truth database that is being constructed for discrimination research. It includes waveforms, source parameters, and arrival information for earthquakes, mine blasts, and mine tremors at regional distances with magnitudes between 2 and 4. The next four chapters are devoted to improving the performance of the IMS. A new method of azimuth estimation using regional knowledge of azimuth bias is proposed that also decreases the scatter in azimuth estimates. An examination of S-phases at near-regional distances in refraction profiles shows complexity that is not accounted for in the IMS that leads to large event mis-locations (20 km in one case). It is also demonstrated that RMS Lg magnitudes are more stable magnitude estimators than the current IMS magnitude estimators. The next chapter describes the results of event identification research for Kola Peninsula events using cluster analysis. Evidence of the method's ability to group events from the same source region (mine) comes from the time distribution of events that comprise a cluster. The final chapter examines the use of polarization filtering to enhance depth phases. Improvement is shown in some cases, but further research is warranted.

14. SUBJECT TERMS	15. NUMBER OF PAGES
Ground Truth Database, Azimuth Estimation, Phase Identification, RMS Lg Magnitudes, Event Identification, Depth Phases	158
	16. PRICE CODE

17. SECURITY CLASSIFICATION OF REPORT	18. SECURITY CLASSIFICATION OF THIS PAGE	19. SECURITY CLASSIFICATION OF ABSTRACT	20. LIMITATION OF ABSTRACT
UNCLASSIFIED	UNCLASSIFIED	UNCLASSIFIED	NONE

Table of Contents

Azimuth Variations at NORESS and ARCESS

Identification of Kola Peninsula Events

Polarization Filtering of Depth Phases

List of Figures

List of Tables

A Ground-Truth Database for Seismic Discrimination Research

Lori Grant, John Coyne

Introduction

To facilitate research on the seismic discrimination problem, there is a need for a standardized database of events of known type. This select suite of events could be used to develop, test and compare various algorithms and systems that identify the source type of seismic events. The objective of this project is to develop such a standard set of events. Of primary concern is that the resulting database will contain parameter and waveform data linked to "ground-truth" about the event. By this we mean that non-seismic information that identifies source type and location is available for each event. This paper describes the database under development and shows three sample datasets.

Target Attributes of Database

The first step in this project has been to define goals for the content of the database. The target attributes of the database are as follows:

- Events that are well-documented with supporting evidence for identification of source type. For example, felt earthquake reports have been used to identify earthquakes, while blaster's logs from mine operators have been used in the case of industrial explosions. The intention is to exclude events identified by seismic analysis alone.
- A variety of source types including: industrial shots (quarry and mine blasts, ripple-fired and single shots), earthquakes, exploration activity, nuclear explosions, collapse from nuclear explosions, mine collapse, rockbursts and other unusual sources.
- A variety of geographic regions, preferably where earthquakes and explosions are co-located.
- Waveforms in the distance range between 2 and 15 degrees. Waveforms from any distance will be included, but the emphasis is on events with regional data.
- Events with magnitude between 2 and 4.

The approach taken in this project has been to identify interesting events for which ground-truth is available and then collect the waveform data necessary to make the event useful in a seismic discrimination project. Once the database is populated with a diverse set of events meeting the target attributes, the entire dataset will be carefully analyzed in a

consistent manner. Eventually, all data in this database will be stored on-line at the Center for Seismic Studies (CSS).

New Relations

While developing the discrimination database, extensions have been added to the CSS Version 3.0 Database Schema (Anderson *et al.*, 1990) for handling more detailed shot information and for storing and quickly retrieving technical references, general comments, and ground-truth information. An attempt has been made to draw from the experience of others in designing new schema, relying on standard CSS Version 3.0 schema where possible.

In addition to database extensions, the scope of the *etype* (event type) attribute in the CSS ORIGIN Table has been expanded as shown in Table 1. A distinction is made between

Table 1: Range of ETYPE Attributes in Origin Relation

ETYPE	DESCRIPTION
qb	Quarry or mine blast confirmed by quarry
qb+	Quarry or mine blast with designed shot information- ripple fired
qb++	Quarry or mine blast with observed shot information- ripple fired
qbx	Quarry or mine blast - single shot
qmt	Quarry or mining-induced events: tremors and rockbursts
ex	Explosion of known origin; i.e. exploration, construction, calibration
nu	Nuclear explosion
nc	Nuclear cavity collapse
eq	Earthquake
eq+	Earthquakes in a swarm or aftershock sequence
eq++	Felt earthquake
o	Other source of known origin
u	Undetermined or conflicting information

quarry blasts with different levels of information. The designation **qb** indicates that the mine or quarry has confirmed the shot and there is no other "ground-truth" information

available (e.g., Wüster, 1992). The **qb+** designation means the quarry has confirmed the shot and has given at least some specifics of the blast design, usually from the blaster's logs (e.g., Chapman *et al.* 1991). The **qb++** designation is reserved for the few experimental quarry or mine shots that have been observed and fully documented by seismologists or mining engineers for research purposes (e.g., Reamer *et al* , 1992).

Similarly for earthquakes, there are different designations for different levels of ground-truth. Examples of the lowest level of confidence for earthquakes, **eq**, are the events denoted "probable earthquake" in regional seismic bulletins. Earthquake identifications based on their temporal and spatial relationships to a known earthquake, such as swarms and aftershock series are denoted **eq+**. The highest level of confidence, **eq++**, refers earthquakes that are very well documented and/or felt, such as those events denoted "Earthquake, Felt" in regional seismic bulletins.

Mining induced seismic events are denoted by the *etype* **qmt** (quarry or mine tremor). This classification includes both rockbursts and mining tremors and excludes the registration of the mine or quarry blast itself. The occurance of two types of mining-induced seismicity is well documented by several authors. S. J. Gibowicz (1984) attributes the distinction to work by Hurtig *et al.* (1979): "mining-induced shocks caused directly by sudden failure of brittle rocks in a stope area, resulting from stress concentration around the excavations, and seismic events in mining disctricts where a tectonic stess field and additional mining-induced stresses are the main factors generating mining tremors." Events of the first type are rockbursts, i.e. they actually have some effect on the mine such as the collapse of a cavity or thrusting of coal seams into a tunnel. Because these events are the source of much of the danger and destruction in underground mining operations, they are very closely monitored by the mine operators, often by seismic instrumentation at depth in the mines. Because of liability issues, information about these events is often difficult to obtain from mining authorities. Events in the second group involve tectonic stress release, are generally larger, and may occur some distance from the active area in the mine. As a result, these mine tremors may be more difficult to associate with a specific mine. Several examples of large mining tremors are documented by Gibowicz (1984). At this point, our aim is to distinguish between blasts (**qb**) and any other type of mining induced seismicity (**qmt**), where the latter is defined broadly as an event which would not have occured without the presence of mining in the area.

Six of the primary ground-truth database tables are shown in Figure 1. The ORIGIN and EVENT Tables are in the CSS Version 3.0 Database Schema (Anderson et al., 1990). The NOTEBOOK, NOTELINK, REFERENCE and XTAG Tables are new. The NOTEBOOK Table is a "menu" of standard statements, or *notes*. Using a set "menu" statements about events will aid in data retrieval. Each *note* has a integer identifier, *noteid*, and is linked to

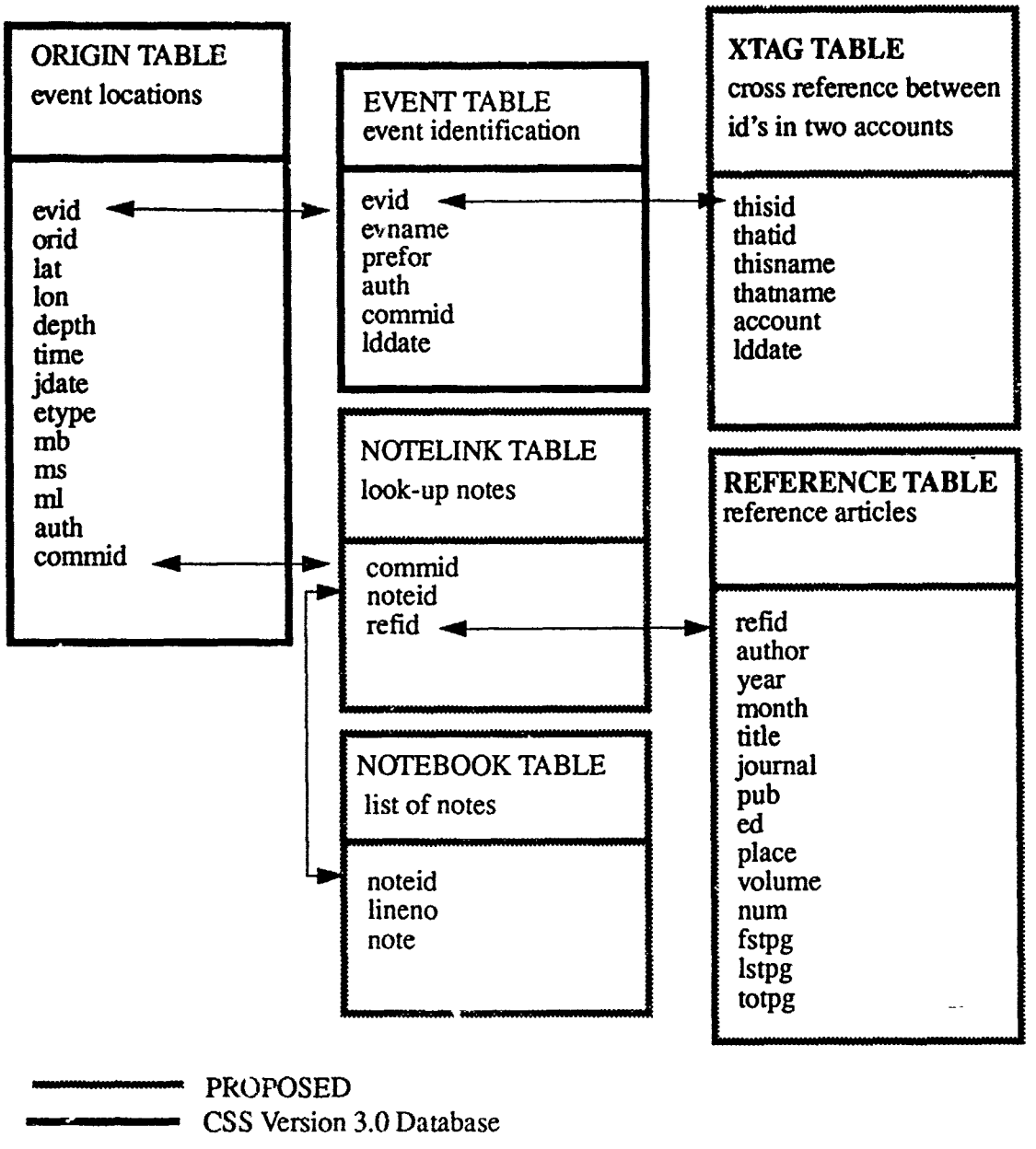

Figure 1: *Relations for storing and tracking ground-truth information. The ORIGIN and EVENT Tables are standard CSS 3.0 Schema (Anderson et al., 1990) . New tables, NOTEBOOK, NOTELINK and REFERENCE store notes and references and are keyed on the commid attribute in the standard CSS 3.0 ORIGIN Relation. The new XTAG Relation is a cross-reference to other CSS database accounts.*

the ORIGIN through the *commid* attribute through the NOTELINK Table. Any number of different notes can be combined and linked to one *commid* in the ORIGIN Table to tell a unique story about each event. The REFERENCE relation houses references to journal articles and reports about the events in the database. Each article is assigned a unique identifier, *refid*, which is linked to the ORIGIN Table through the NOTELINK Table This NOTELINK Table provides a reference for each statement that is made about an event.

The XTAG Table is a cross-reference between identifiers in two different CSS Database accounts. For example, *orid* 25 in this database could be linked to *orid* 56784 in the IMS-2 account so that the user who wishes to refer to additional tables existing in the IMS-2 account will have the IMS-2 *orid* for that event. This concept is essential for tracking data between database accounts.

PHASE 1 DATASETS

The database currently contains three distinct datasets named for their geographic locations: #1: Vogtland, #2: Steigen, and #3: Lubin. Locations of the three datasets are shown in Figure 2. There are a total of 95 distinct events in the database: 49 earthquakes, 15 quarry blasts and 31 rockbursts. Most of the events were recorded by one or all of the arrays in the IMS-2 network and 16 of the events occurred within the GSETT-2 time period, so reported GSETT-2 data is available for these events. Thus, all the waveform data currently in the database comes from either the IMS-2 network or the GSETT-2 network. The earliest event is March 11, 1991 and the most recent event is February 12, 1992. Local magnitudes (ml) range from 1.0 to 4.0 with 73 of the 95 events having a local magnitude estimate (ml) greater than 2.0.

In accordance with the CSS 3.0 format, each event can have multiple tuples (rows) in the ORIGIN Table with the preferred ORIGIN indicated in the EVENT Table as *prefor*. There are 225 origins for the 91 events distributed as follows: 13 events with 1 origin; 29 events with 2 origins; 42 events with 3 origins; 7 events with 4 origins. All 225 origins are listed in "Appendix A: ORGIN TABLE" on page 16. The Vogtland dataset includes *evids* 1-27; *evids* 28-64 are the Steigen dataset; *evids* 65-95 are the Lubin dataset. Each dataset is described below.

The origin information in Appendix A comes from 7 different authors as referenced in the *auth* attribute. The seven different sources, or authors, are described below:

"IMS2" - from the analyst-reviewed IMS-2 account;

"WASCEL" - from the final Current Event List from the GSETT-2 Washington EIDC (Experimental International Data Center);

"HELSINKI" - Seismological Bulletin published by the University of Helsinki;

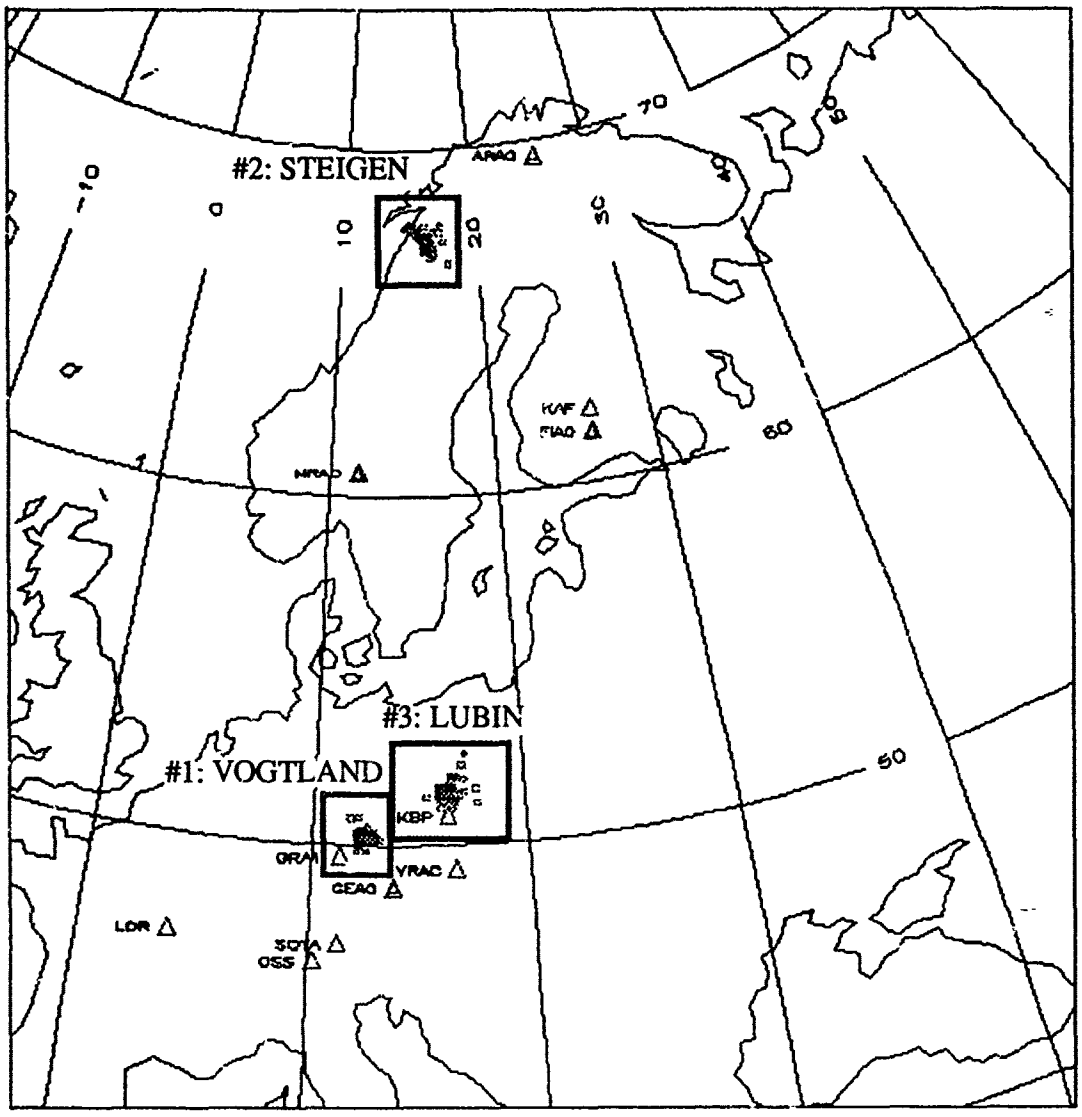

Figure 2: *Three datasets that comprise the Phase 1 release of the database. Vogtland is 11 earthquakes and 16 quarry blasts. Steigen is 31 earthquakes and Lubin is 31 rockbursts.*

"BERGEN" - Seismological Bulletin published in Bergen, Norway;
"WUSTER" - origin times and locations published by Jan Wüster (1992);
"HARJES" - sent by H.-P. Harjes, obtained from Weijacz at the Polish Academy of Sciences;
"GERESS-EPX" - automatic processing system solutions, sent by Harjes.

The origin table listed in Appendix A will eventually be updated and renumbered (1 through 225) so that each *orid* is unique. Original *orids* referring to other accounts will be tracked through the XTAG table.

The *etype* attribute in the origin table is left blank ("-") unless the source identification was specifically associated with the origin information. For example, in the Vogtland dataset, the IMS-2 origins are not labeled as **qb** or **eq** because there are no source types associated with these origins. However, for the Steigen events, the IMS-2 origin tuples have **eq+** as *etype* because these *orids* were specifically associated with the earthquake swarm as reported by Tormod Kværna (pers. comm.).

Table 2: Summary of Three datasets in Phase 1 Database

dataset	auth	number of events	qb	qmt	eq	ml>=2.0
#1: Vogtland	IMS2	27	-	-	-	20
#1: Vogtland	WASCEL	6	-	-	-	(6 mb > 2.0)
#1: Vogtland	WUSTER	27	16	-	11	14
#2: Steigen	IMS2	31	-	-	31	6
#2: Steigen	BERGEN	22	-	-	1	22
#2: Steigen	HELSINKI	14	-	-	14	14
#3: Lubin	IMS2	31	-	-	-	30
#3: Lubin	HARJES	31	-	31	-	a
#3: Lubin	GERESS-EPX	29	-	-	-	a
#3:Lubin	WASCEL	7	-	-	-	(7 mb > 2.0)

a. ml not given

Dataset #1: Vogtland

The events in the first dataset are located in Germany and Czechoslovakia in a region of Western Bohemia known as Vogtland, about 180 km northwest of the GERESS array. Figure 3 shows the locations of the Vogtland events. Ground-truth information for these events is based on work by Jan Wüster at Ruhr University Bochum, Germany (Wüster, 1992). The dataset includes 11 natural earthquakes in a swarm (*etype* = **eq+**) and 16 confirmed quarry blasts (*etype* = **qb**). The WFDISC Table contains 1818 entries with waveforms mostly from the IMS-2 arrays and a few GSETT-2 stations. This includes all raw data channels of each array as well as the beams retained as a result of IMS-2 processing.

Wüster obtained the earthquake locations from Dr. Schmedes (pers. comm.). These earthquakes occurred within a 13-station network and the locations are thus very accurate. However, we do not currently have the depth information for all of these events. Mr. Wüster provided us with the Bulletin of Microearthquakes from the Vogtland Region by Nuenhöfer *et al.* (1992) which covers 1987 through 1990. But these events, having occurred in 1991, are in the Preliminary Bulletin in which only the origin times of the arrivals at each station are given for most of the earthquakes. Very accurate depth information should be available in the near future. Another significant swarm occurred in the area in 1985 and 1986 and is well documented by German and Czech seismologists (Bormann, 1989).

Wüster obtained the locations of the quarry blasts from Dr. Klinge at MOXA Seismological Observatory who regularly notes the occurrence of quarry blasts. The blasts are from the strip coal mines near the town of Karlovy Vary, Czechoslovakia.There are at least four distinct mines near this town but the locations provided by Dr. Klinge are not accurate enough to distinguish between individual mines. Further requests about these particular mines have been sent to Dr. Petr Firbas in Czechoslovakia.

Wüster's events were compared with the IMS-2 Bulletin and the WASCEL Bulletin (GSETT-2) to find matching events. This search resulted in 16 quarry blasts and 11 earthquakes with corresponding IMS2 locations, and 5 quarry blasts and 1 earthquake with corresponding WASCEL locations.

Dataset #2: Steigen

This dataset consists of 33 earthquakes related to a swarm near Steigen, Norway which began in January of 1992. The events are shown in Figure 4 . The first, and largest of these events was felt by residents of the town of Steigen, 21 km south of the epicenters, as reported in both the Bergen and Helsinki Bulletins. Subsequent events were identified as earthquakes on the basis of location and temporal distribution and because there was no

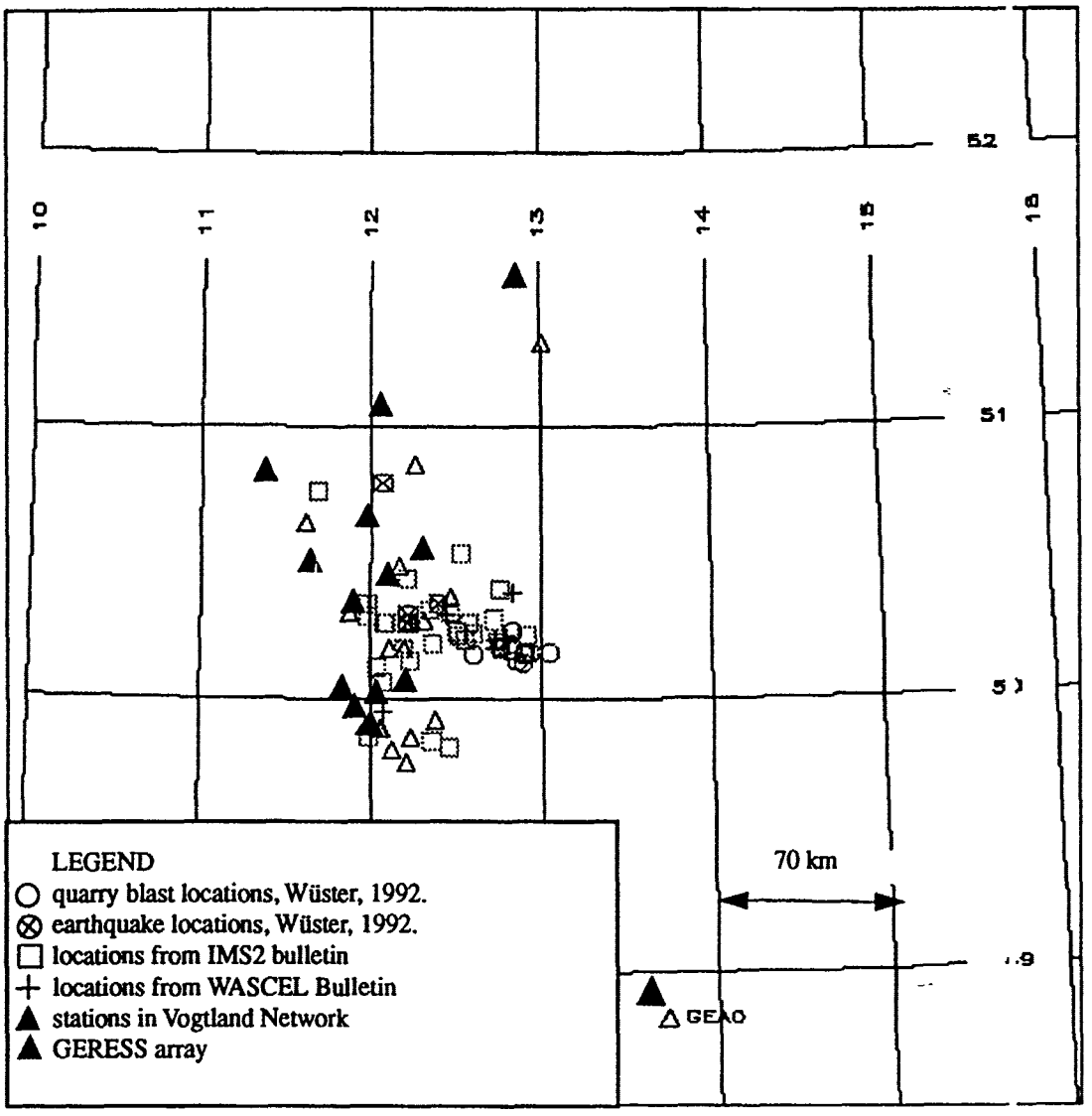

Figure 3: *Locations of events in the Vogtland dataset. Circles indicate locations from Wüster, 1992. Squares indicated locations from the IMS-2 Bulletin and pluses indicate locations from the WASCEL Bulletin. Stations in the Vogtland Region which contribute to the locations published in the Vogtland Region Bulletin (Neunhöfer et al., 1992) are shown by solid triangles.*

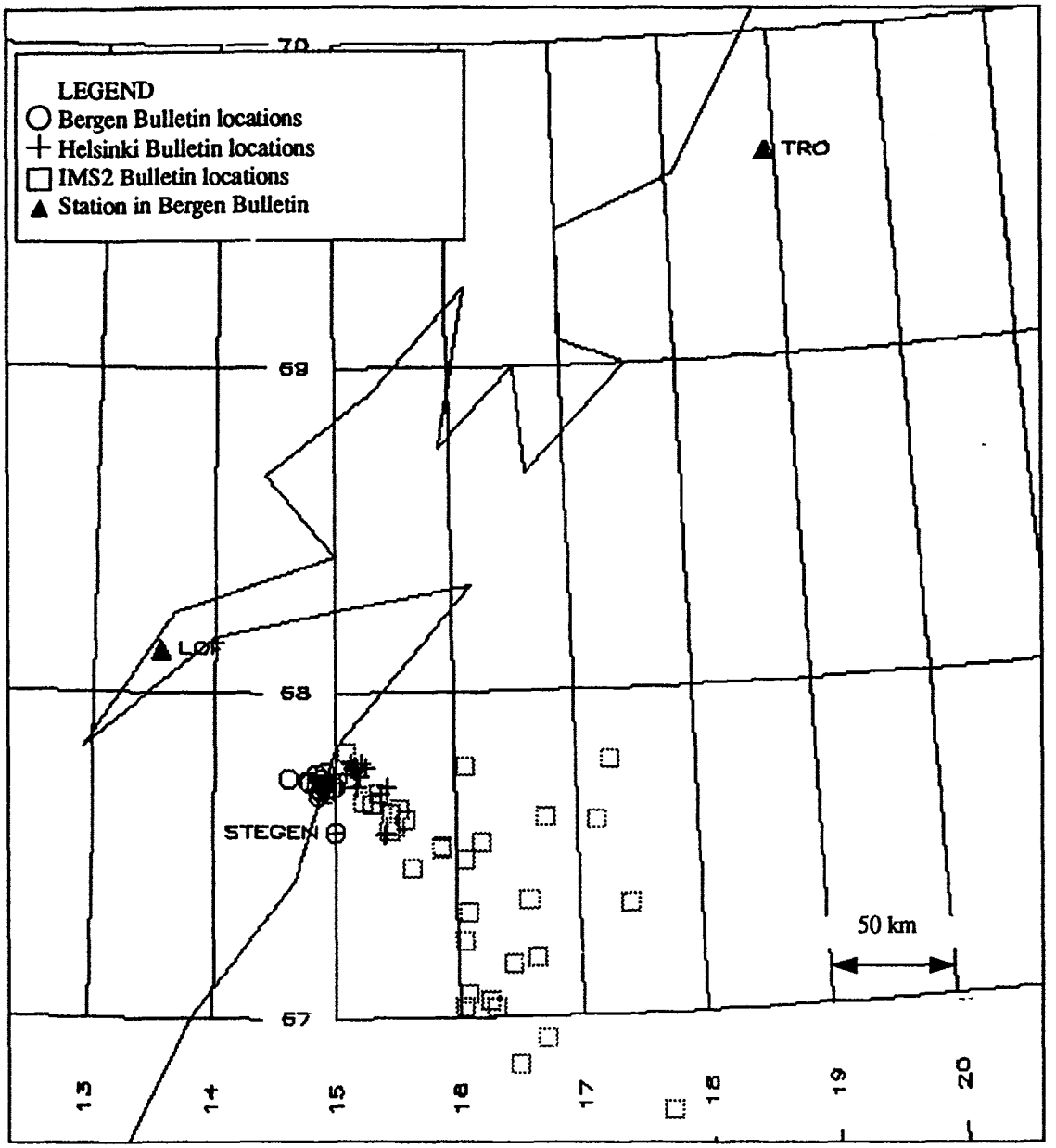

Figure 4: *Locations of the events in the 1992 Steigen Earthquake swarm. Some of the smaller magnitude events were recorded only at ARCESS and the large scatter in the IMS-2 locations is due to poor azimuth estimates. The locations in the Bergen Bulletin are well-contrained by stations LOF and TRO. The town of Steigen, where the larger earthquakes were felt, is 21 km south of the epicenters.*

significant industrial (explosion) activity in the area (Tormod Kværna, pers. comm.).

As these are earthquakes related to a swarm, the *etype* designation for the IMS-2 origins was updated to **eq+** after copying the origin tuples from the IMS-2 account. The WFDISC Table contains waveforms recorded by the IMS-2 arrays in Scandinavia: ARCESS at 4.3°, NORESS at 7.2°, and FINESSA at 7.9°.

All of these events were reported in the IMS2 Bulletin. Although 29 of the 33 events were listed in the Bergen Bulletin, only the first event had an earthquake source type designated in the bulletin. In addition, 6 of the 33 events where listed as "Felt Earthquake" and another 8 events where reported as "Probable Earthquake" in the Helsinki Bulletin.

The Bergen Bulletin locations are the preferred locations because stations TRO (Tromsø, Norway), approximately 270 km northeast of the epicenters, and LOF, approximately 69 km northwest of the epicenters, were used in the location of these earthquakes.

Eleven of the smaller magnitude events in the Steigen dataset are reported in the IMS-2 Bulletin but not reported in either the Bergen or Helsinki Bulletins and thus have only one ORIGIN tuple for each *evid*. These include eight IMS-2 events with local magnitude (ml) below 1.5 and three events with no IMS-2 magnitude (ml) given. The smaller-magnitude events were poorly located by IMS-2 because they were recorded only by the ARCESS array. Another two events were included in the Steigen dataset which were listed in the Bergen Bulletin but not in the IMS-2 or in the Helsinki Bulletin.

Dataset #3: Lubin

This dataset illustrates the importance and usefulness of the ground-truth database, for there is no assurance that an event with a seismic location on top of a mine is the result of a blast. All of the 31 events in this dataset were originally thought to be blasts and are now known to be artifically induced seismic events resulting from mining activity in the Lubin Copper Basin in Poland, where 4 distinct underground copper mines are located about 280 km northeast of the GERESS array.

The "ground-truth" information on these events, sent to us by H.-P. Harjes, consists of (seismic) locations reported by Mr. Wiejacz who works at the Polish Academy of Sciences. The seismic locations are determined by analysis of records from seismic instruments in the mining area. The mining companies closely monitor this induced seismicity with attention to location but the origin times are of less importance and thus the times can be off by several seconds. Depth estimates are not included in the information from Weicjac. *Etype* designations are **qmt**. For each event a specific mine and field within the mine is reported.

Locations are shown in Figure 5 . There are 3 different locations for 29 of the 31 events: an IMS-2 location (after analyst review); the GERESS automatic system location (before analyst review), and the location provided by Harjes from Weijacz. Additionaly, seven of the events are listed in the WASCEL Bulletin (GSETT-2).

Future Work

Although the first three datasets will be available soon, more events are obviously needed to make the database more useful. Some of the pending datasets are described below:

- Blasts and earthquakes recorded by the Canadian Seismic Telemetry Network.
- LLNL recordings of small NTS explosions.
- Quarry blasts in West Virginia and Russia: data recorded by station BLA and other regional stations operated by Virginia Polytechnical Institute with blasting logs; and data recorded at KIV and other regional stations operated by EME with blasting logs.
- A subset of CSS's Nuclear Explosion Database. (an estimated 60 events fit the target attributes of this database and will be included).
- Waveforms for events in the MINEX table compiled at NORSAR (Dahle, *et al.*, 1989). The MINEX Table currently has over 400 individual explosions starting in 1985. For the years in which data are stored at CSS, we will retrieve data from tape and in incorporate them into the database.
- All "FELT" earthquakes in the Bergen and Helsinki Bulletins. Recent events in the Bergen and Helsinki Bulletins will be matched with IMS and IMS-2 events.

Other necessary steps include: (1) QC entire dataset for problems that the user should be aware of: glitches, drop-outs, conflicting information, missing data. (2) Add instrument responses for all instruments included in the data set. (3) Analyze the entire data set to verify all the picks, locations, data integrity. (4) Document each event with maps, plots, descriptions, references and addresses of the source of the ground-truth information.

Summary

A plan for identifying and collecting a standardized set of events for discrimination research has been presented. New schema that are both easy to use and general enough to house a large variety of information have been presented. Events in the three datasets comprising Phase 1 are those for which waveform data were easy to obtain because the data were already on-line at CSS. Now that the tables are in place, we anticipate that the process of adding new datasets will be straight-forward. Of course, any new datasets recorded at stations that we do not have experience with will involve additional work to document the stations.

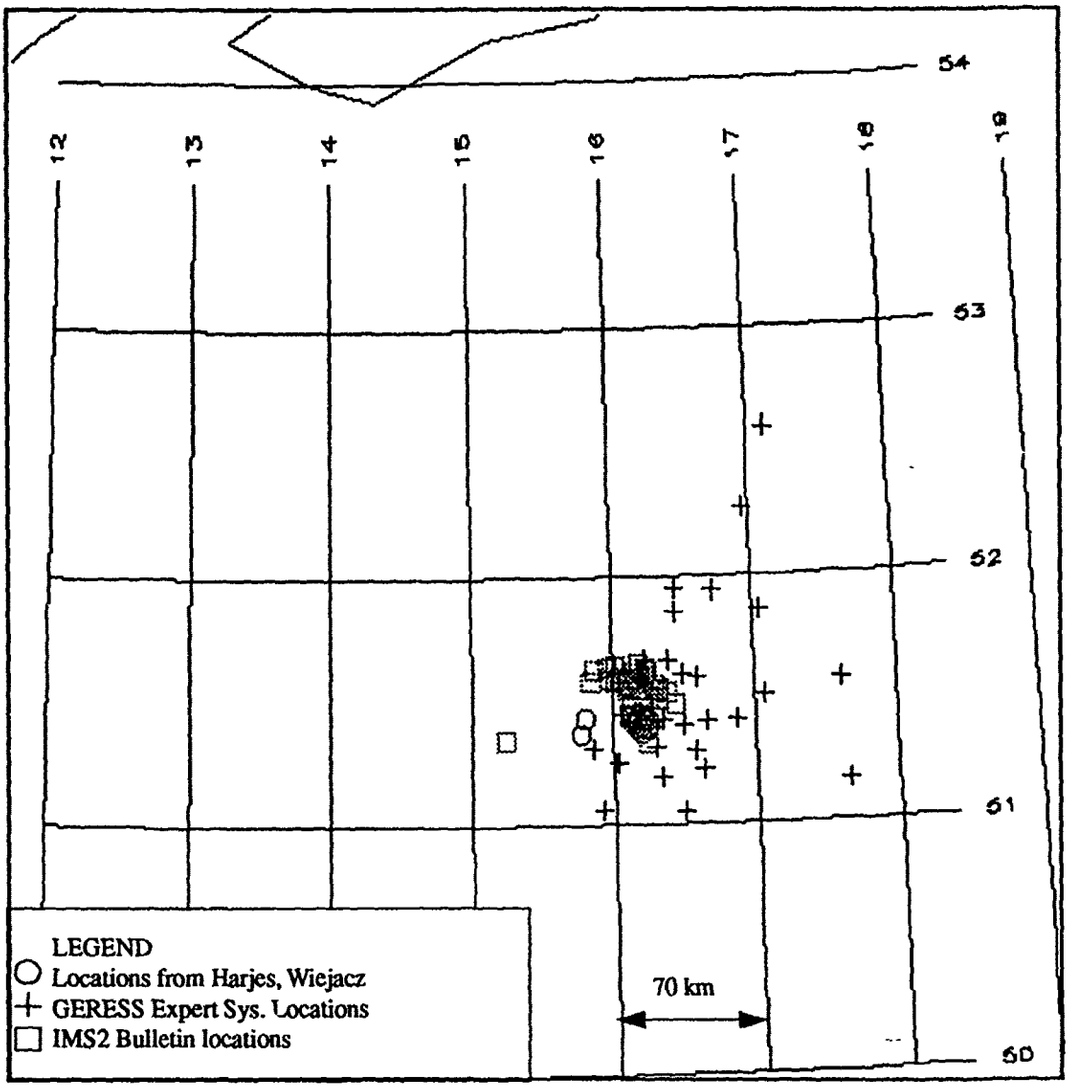

Figure 5: *Locations of the events in the Lubin dataset. Circles denote locations sent to us by H.-P. Harjes from Weicjac. There is a possible error in the two western-most locations. Pluses indicate locations from the GERESS Expert system. The sqaures denote origin information copied from the IMS-2 account.*

One weakness in the data sets described in this report is the poor constraint on the depths of the events. Continued effort to contact those who operate seismic stations nearest the events will most likely lead to better depth estimates for at least some of the events.

For more information on this database or if you wish to make suggestions or contributions, please contact the authors at grant@seismo.CSS.GOV or coyne@seismo.CSS.GOV.

Acknowledgments

The planning of this dataset benefited from discussions with many researchers including all of the Center Research Staff. In addition, we are especially grateful to Jan Wüster, Tormod Kværna and H.-P. Harjes for information on the three datasets in this report.

References

Anderson, J., W. E. Farrell, K. Garcia, J. Given, and H. Swanger (1990). Center for Seismic Studies Version 3.0 Database: Schema Reference Manual, *SAIC Tech. Rep.* C90-01, Arlington, VA., 61 pp.

Bormann, Peter, Ed., (1989). Monitoring and analysis of the earthquake swarm 1985/86 in the region Vogtland/Western Bohemia. Zentralinstitut für Physik der Erde. Veröffentlichung Nr. 110, ISSN 0514-8790. Potsdam.

Champan, M. C., G. A. Bollinger, and M. S. Sibol (1991). Spectral studies of the elastic wave radiation from Appalachian earthquakes and explosions - explosion source spectra modeling using blaster's logs, *Proceedings of the 13th Annual PL/DARPA Seismic Research Symposium*, Keystone, Colorado, 138-144.

Dahle, A., A. Alsker, S. Mykkeltveit (1989). Establishment of a mining explosion database, *NORSAR Sci. Rep. 1-89/90*, NORSAR, Kjeller, Norway, 83-102.

Gibowicz, S. J. (1984). The mechanism of large mining tremors in Poland. *Proceedings of the 1st International Congress on Rockbursts and Seismicity in Mines*, Johannesburg, 1982. SAIMM. Johannesburg.

Gibowicz, S. J., H.-P. Harjes, and M. Schäfer (1990). Source parameters of seismic events at Heinrich Robert Mine, Ruhr Basin, Federal Republic of Germany: evidence for non-double-couple events.Bull. Seism. Soc. Am., **80**, 88-109.

Hurtig, E., P. Bormann, P. Knoll, and F. Tauber (1979). Seismological and geomechanical studies of a strong seismic event in the potash mines of the GDR: implications for predicting mining tremors, *Proc. Int. Symposium on Earthquake Prediction*, UNESCO, Paris, 2-6 April, 1979.

Neunhöfer, H. E. Schmedes, B. Tittel, H.-A. Dahlheim, and D. Guth (1992). Bulletin of Microearthquakes from the Vogtland Region; Period 1987-1990.

Reamer, S. K., K.-G. Hinzen, and B. W. Stump (1992). Analysis of spatial and temporal finiteness observed in the seismic wavefield radiated from quarry blasts, *Bull. Seism. Soc. Am.*, submitted for publication.

Wüster, J. (1992). Discrimination of chemical explosions and earthquakes in Central Europe - a case study, *Bull. Seism. Soc. Am.*, submitted for publication.

Table 3: Appendix A: ORGIN TABLE

evid	etype	date	time	lat	lon	depth	ml	orid	auth
1	-	03/11/91	12:03:24	50.06	12.07	.0	2.5	13746	IMS2
1	qb	03/11/91	12:03:26	50.17	13.05	-999.0	2.0	1	WUSTER
2	-	03/21/91	12:04:13	50.32	12.46	.0	2.5	15242	IMS2
2	qb	03/21/91	12:04:16	50.17	12.92	-999.0	2.1	7	WUSTER
3	-	03/22/91	12:33:19	50.54	12.53	.0	2.6	15551	IMS2
3	qb	03/22/91	12:33:27	50.16	12.89	-999.0	2.0	9	WUSTER
4	-	03/23/91	12:00:55	50.24	12.50	.0	2.5	16310	IMS2
4	qb	03/23/91	12:00:56	50.20	12.82	-999.0	2.0	10	WUSTER
5	-	03/24/91	05:05:02	50.35	11.98	.0	2.7	16607	IMS2
5	eq	03/24/91	05:05:04	50.28	12.21	-999.0	2.6	516	WUSTER
6	-	03/24/91	05:35:25	50.14	12.23	.0	1.7	16609	IMS2
6	eq	03/24/91	05:35:19	50.28	12.22	-999.0	1.6	517	WUSTER
7	-	03/24/91	06:58:10	49.85	12.35	.0	1.4	14875	IMS2
7	eq	03/24/91	06:58:00	50.31	12.22	-999.0	1.5	518	WUSTER
8	-	03/24/91	09:38:36	50.19	12.19	.0	1.9	16612	IMS2
8	eq	03/24/91	09:38:33	50.31	12.22	-999.0	1.8	520	WUSTER
9	-	03/24/91	14:33:27	50.28	12.08	.0	3.0	14892	IMS2
9	eq	03/24/91	14:33:28	50.28	12.21	-999.0	3.0	521	WUSTER
10	-	03/24/91	15:00:42	50.35	11.94	.0	2.4	16618	IMS2
10	eq	03/24/91	15:00:44	50.28	12.22	-999.0	2.1	523	WUSTER
11	-	03/24/91	15:41:07	50.12	12.04	.0	2.0	16619	IMS2
11	eq	03/24/91	15:41:04	50.28	12.22	-999.0	1.9	524	WUSTER
12	-	03/25/91	14:54:13	50.30	11.99	.0	3.2	15951	IMS2
12	eq	03/25/91	14:54:14	50.28	12.21	-999.0	2.6	526	WUSTER
13	-	03/25/91	22:32:02	49.82	12.46	.0	1.5	16080	IMS2
13	eq	03/25/91	22:31:47	50.31	12.22	-999.0	1.7	532	WUSTER
14	-	04/03/91	09:57:13	50.28	12.58	.0	2.2	16056	IMS2
14	qb	04/03/91	09:57:14	50.16	12.60	-999.0	1.8	11	WUSTER

Table 3: Appendix A: ORGIN TABLE

evid	etype	date	time	lat	lon	depth	ml	orid	auth
15	-	05/02/91	11:06:10	50.20	12.36	.0	2.2	21324	IMS2
15	qb	05/02/91	11:06:11	50.19	12.76	-999.0	1.9	12	WUSTER
16	-	05/02/91	12:47:39	49.86	11.98	.0	1.4	21335	IMS2
16	-	05/02/91	12:47:40	49.95	12.07	.0	-999.0	44744	WASCEL
16	qb	05/02/91	12:47:58	50.18	12.19	-999.0	2.0	13	WUSTER
17	-	05/08/91	11:14:38	50.24	12.60	.0	2.3	22298	IMS2
17	-	05/08/91	11:14:37	50.38	12.83	.0	-999.0	55254	WASCEL
17	qb	05/08/91	11:14:39	50.18	12.82	-999.0	2.0	14	WUSTER
18	-	05/10/91	20:02:50	50.76	11.69	.0	1.6	21578	IMS2
18	eq	05/10/91	20:03:19	50.79	12.07	-999.0	1.4	537	WUSTER
19	-	05/19/91	03:22:11	50.28	12.09	.0	2.4	23275	IMS2
19	-	05/19/91	03:22:13	50.31	12.44	21.6	-999.0	73395	WASCEL
19	eq	05/19/91	03:22:10	50.35	12.40	-999.0	2.9	538	WUSTER
20	-	05/23/91	11:01:07	50.21	12.75	.0	2.4	23615	IMS2
20	qb	05/23/91	11:01:07	50.13	12.89	-999.0	2.1	15	WUSTER
21	-	05/25/91	11:01:29	50.22	12.55	.0	2.3	24308	IMS2
21	-	05/25/91	11:01:32	50.21	12.73	.0	-999.0	86747	WASCEL
21	qb	05/25/91	11:01:30	50.17	12.90	-999.0	2.1	16	WUSTER
22	-	05/26/91	11:00:28	50.44	12.21	.0	2.0	24346	IMS2
22	-	05/26/91	11:00:34	50.18	12.72	650.0	-999.0	88482	WASCEL
22	qb	05/26/91	11:00:34	50.14	12.85	-999.0	2.1	17	WUSTER
23	-	05/28/91	11:03:48	50.32	12.35	.0	2.4	24156	IMS2
23	-	05/28/91	11:03:53	50.22	12.79	.0	-999.0	92547	WASCEL
23	qb	05/28/91	11:03:52	50.20	12.74	-999.0	2.0	18	WUSTER
24	-	06/20/91	11:01:16	50.29	12.72	.0	2.2	27165	IMS2
24	qb	06/20/91	11:01:18	50.16	12.90	-999.0	2.0	20	WUSTER
25	-	06/20/91	11:45:35	50.40	12.76	.0	2.4	26825	IMS2
25	qb	06/20/91	11:45:36	50.25	12.83	-999.0	1.8	21	WUSTER

Table 3: Appendix A: ORGIN TABLE

evid	etype	date	time	lat	lon	depth	ml	orid	auth
26	-	06/22/91	10:58:37	50.23	12.92	.0	2.4	26911	IMS2
26	qb	06/22/91	10:58:35	50.18	12.80	-999.0	2.2	22	WUSTER
27	-	06/27/91	11:04:40	50.23	12.51	.0	2.1	27850	IMS2
27	qb	06/27/91	11:04:41	50.17	12.93	-999.0	1.9	23	WUSTER
28	eq++	01/01/92	08:03:58	67.75	14.84	12.1	3.6	1	BERGEN
28	eq++	01/01/92	08:03:58	67.71	15.43	15.0	3.9	69	HELSINKI
28	eq+	01/01/92	08:03:57	67.66	15.30	.2	3.2	303265	IMS2
29	eq+	01/01/92	08:18:08	67.36	16.59	7.3	-999.0	312921	IMS2
31	-	01/01/92	08:39:02	67.72	14.85	12.1	2.6	3	BERGEN
31	eq++	01/01/92	08:39:00	67.77	15.17	15.0	2.6	71	HELSINKI
31	eq+	01/01/92	08:39:04	67.52	15.87	9.3	2.0	303251	IMS2
32	eq+	01/01/92	08:57:09	67.48	16.06	1.8	-999.0	312922	IMS2
33	-	01/01/92	10:15:12	67.72	14.88	12.3	2.5	4	BERGEN
33	eq	01/01/92	10:15:09	67.74	15.19	15.0	2.5	72	HELSINKI
33	eq+	01/01/92	10:15:08	67.03	16.04	8.1	1.8	312925	IMS2
34	eq+	01/01/92	14:46:11	66.94	16.70	7.5	1.4	312926	IMS2
35	-	01/04/92	03:43:43	67.71	14.93	.0	3.0	9	BERGEN
35	eq+	01/04/92	03:43:44	67.46	15.63	.0	1.9	303471	IMS2
36	-	01/04/92	04:15:04	67.71	14.90	12.1	3.2	10	BERGEN
36	eq++	01/04/92	04:15:03	67.78	15.13	15.0	3.4	74	HELSINKI
36	eq+	01/04/92	04:15:05	67.58	15.49	8.2	-999.0	312934	IMS2
37	-	01/04/92	05:33:27	67.68	14.87	12.1	2.5	11	BERGEN
37	eq+	01/04/92	05:33:24	66.86	16.47	.0	1.1	303473	IMS2
38	-	01/04/92	06:00:53	67.70	14.87	12.1	3.5	12	BERGEN
38	eq++	01/04/92	06:00:52	67.77	15.24	15.0	4.0	75	HELSINKI
38	eq+	01/04/92	06:00:52	67.82	15.09	10.0	-999.0	312938	IMS2
39	-	01/04/92	09:06:31	67.76	14.92	12.1	3.3	13	BERGEN

Table 3: Appendix A: ORGIN TABLE

evid	etype	date	time	lat	lon	depth	ml	orid	auth
39	eq++	01/04/92	09:06:29	67.78	15.22	15.0	3.3	76	HELSINKI
39	eq+	01/04/92	09:06:29	67.66	15.22	2.3	2.2	303256	IMS2
40	-	01/05/92	01:20:50	67.73	14.78	15.5	2.9	16	BERGEN
40	eq	01/05/92	01:20:47	67.71	15.17	15.0	2.9	77	HELSINKI
40	eq+	01/05/92	01:20:50	67.32	16.10	.0	1.7	303395	IMS2
41	-	01/05/92	02:31:04	67.72	14.79	12.1	2.3	17	BERGEN
41	eq+	01/05/92	02:31:20	67.60	17.16	.0	1.2	303428	IMS2
42	-	01/05/92	05:11:56	67.71	14.99	.0	3.0	18	BERGEN
42	eq	01/05/92	05:11:56	67.76	15.16	15.0	3.0	78	HELSINKI
42	eq+	01/05/92	05:11:56	67.57	15.45	.0	1.6	303433	IMS2
43	-	01/05/92	07:53:38	67.70	14.87	2.0	2.7	20	BERGEN
44	eq+	01/05/92	07:57:10	67.34	17.42	.0	1.0	303125	IMS2
45	-	01/05/92	20:00:07	67.70	14.95	.4	2.0	21	BERGEN
46	-	01/06/92	08:26:22	67.70	14.97	.0	2.3	22	BERGEN
46	eq+	01/06/92	08:26:23	67.16	16.44	.0	1.6	303493	IMS2
48	eq+	01/10/92	22:07:15	67.78	17.29	.0	1.1	313180	IMS2
49	-	01/10/92	22:25:42	67.71	14.98	2.2	3.2	32	BERGEN
49	eq++	01/10/92	22:25:42	67.72	14.97	15.0	3.0	81	HELSINKI
49	eq+	01/10/92	22:25:42	67.63	15.46	.0	2.1	313181	IMS2
50	-	01/11/92	01:17:29	67.70	14.91	.0	2.8	33	BERGEN
50	eq+	01/11/92	01:17:30	67.03	16.29	11.7	1.5	313018	IMS2
51	-	01/11/92	01:45:37	67.74	14.88	12.1	2.7	34	BERGEN
51	eq+	01/11/92	01:45:35	67.07	16.09	9.9	1.5	313020	IMS2
52	eq+	01/13/92	12:51:43	67.53	16.21	4.0	-999.0	313147	IMS2
55	-	01/22/92	18:58:25	67.72	14.89	12.1	3.3	52	BERGEN
55	eq++	01/22/92	18:58:23	67.77	15.15	15.0	3.5	83	HELSINKI
55	eq+	01/22/92	18:58:30	67.61	16.74	.0	2.9	312622	IMS2
56	eq+	01/22/92	19:26:54	66.69	17.69	.0	1.3	312625	IMS2

Table 3: Appendix A: ORGIN TABLE

evid	etype	date	time	lat	lon	depth	ml	orid	auth
57	eq+	01/22/92	21:38:00	67.77	16.08	.0	1.1	312628	IMS2
58	-	01/25/92	11:57:34	67.69	14.93	.0	2.9	56	BERGEN
58	eq	01/25/92	11:57:35	67.56	15.40	15.0	2.9	85	HELSINKI
58	eq+	01/25/92	11:57:35	67.64	15.53	7.8	1.9	313091	IMS2
59	-	01/25/92	12:16:48	67.71	14.88	12.1	3.3	57	BERGEN
59	eq++	01/25/92	12:16:47	67.75	15.09	15.0	3.0	86	HELSINKI
59	eq+	01/25/92	12:16:46	67.69	15.35	.0	2.7	313094	IMS2
60	-	01/25/92	12:26:29	67.73	15.11	.0	3.0	58	BERGEN
60	eq	01/25/92	12:26:30	67.69	15.37	15.0	2.9	87	HELSINKI
60	eq+	01/25/92	12:26:30	67.61	15.59	2.2	1.8	313099	IMS2
61	-	01/25/92	19:12:52	67.74	14.61	12.1	2.9	59	BERGEN
61	eq	01/25/92	19:12:53	67.57	15.42	15.0	2.9	88	HELSINKI
61	eq+	01/25/92	19:12:54	67.52	15.88	.0	1.8	313112	IMS2
62	eq+	02/03/92	04:15:43	67.23	16.04	14.5	1.1	315636	IMS2
63	eq+	02/03/92	23:39:09	67.18	16.63	10.0	1.5	315678	IMS2
64	eq+	02/12/92	14:37:27	67.05	16.25	5.6	1.5	317841	IMS2
65	-	03/12/91	00:00:11	51.42	16.67	-999.0	-999.0	5490	GERESS-EPX
65	qmt	03/12/91	00:00:13	51.43	16.17	-999.0	-999.0	66	HARJES
65	-	03/12/91	00:00:12	51.57	16.01	.0	2.9	13784	IMS2
66	-	03/29/91	03:40:11	52.27	16.95	-999.0	-999.0	980	GERESS-EPX
66	qmt	03/29/91	03:40:19	51.39	16.24	-999.0	-999.0	86	HARJES
66	-	03/29/91	03:40:25	51.59	15.97	.0	2.3	16066	IMS2
67	-	03/29/91	13:04:52	51.60	16.19	-999.0	-999.0	1150	GERESS-EPX
67	qmt	03/29/91	13:04:46	51.42	16.12	-999.0	-999.0	87	HARJES
67	-	03/29/91	13:04:56	51.55	16.30	.0	2.5	16654	IMS2

Table 3: Appendix A: ORGIN TABLE

evid	etype	date	time	lat	lon	depth	ml	orid	auth
68	-	04/07/91	08:35:07	51.95	16.45	-999.0	-999.0	2120	GERESS-EPX
68	qmt	04/07/91	08:35:08	51.39	16.24	-999.0	-999.0	94	HARJES
68	-	04/07/91	08:35:13	51.64	15.96	.0	2.3	17185	IMS2
69	-	04/18/91	04:37:50	51.19	16.34	-999.0	-999.0	1400	GERESS-EPX
69	qmt	04/18/91	04:37:37	51.43	16.17	-999.0	-999.0	108	HARJES
69	-	04/18/91	04:37:39	51.63	15.87	.0	2.8	18742	IMS2
70	-	04/30/91	03:40:21	51.17	17.66	-999.0	-999.0	3230	GERESS-EPX
70	qmt	04/30/91	03:40:36	51.41	16.26	-999.0	-999.0	123	HARJES
70	-	04/30/91	03:40:36	51.55	16.33	.0	3.0	20297	IMS2
70	-	04/30/91	03:40:39	51.54	16.23	8.7	-999.0	40508	WASCEL
71	-	05/07/91	03:02:42	51.60	16.60	-999.0	-999.0	4230	GERESS-EPX
71	qmt	05/07/91	03:02:39	51.41	16.14	-999.0	-999.0	129	HARJES
71	-	05/07/91	03:02:44	51.48	16.44	.0	2.7	20935	IMS2
71	-	05/07/91	03:02:47	51.47	16.28	2.8	-999.0	54787	WASCEL
72	-	05/18/91	11:15:39	51.66	16.24	-999.0	-999.0	5950	GERESS-EPX
72	qmt	05/18/91	11:15:39	51.43	15.81	-999.0	-999.0	137	HARJES
72	-	05/18/91	11:15:40	51.52	16.23	.0	2.5	23217	IMS2
72	-	05/18/91	11:15:42	51.51	16.24	4.0	-999.0	71776	WASCEL
73	-	05/21/91	23:15:36	52.59	17.14	-999.0	-999.0	6410	GERESS-EPX
73	qmt	05/21/91	23:15:56	51.39	16.24	-999.0	-999.0	138	HARJES
73	-	05/21/91	23:15:59	51.35	15.24	.0	3.0	23247	IMS2
73	-	05/21/91	23:15:55	51.52	15.85	.0	-999.0	77772	WASCEL
74	-	05/23/91	19:42:45	51.87	17.04	-999.0	-999.0	6910	GERESS-EPX

Table 3: Appendix A: ORGIN TABLE

evid	etype	date	time	lat	lon	depth	ml	orid	auth
74	qmt	05/23/91	19:42:54	51.43	16.24	-999.0	-999.0	139	HARJES
74	-	05/23/91	19:42:54	51.59	16.07	.0	2.8	23958	IMS2
74	-	05/23/91	19:42:55	51.58	16.08	5.4	-999.0	82707	WASCEL
75	-	05/28/91	03:52:46	51.66	16.39	-999.0	-999.0	7410	GERESS-EPX
75	qmt	05/28/91	03:52:50	51.42	16.18	-999.0	-999.0	143	HARJES
75	-	05/28/91	03:52:48	51.50	16.33	.0	2.7	24129	IMS2
75	-	05/28/91	03:52:50	51.53	16.39	.0	-999.0	92523	WASCEL
76	-	05/30/91	21:18:15	51.94	16.72	-999.0	-999.0	8050	GERESS-EPX
76	qmt	05/30/91	21:18:22	51.39	16.18	-999.0	-999.0	147	HARJES
76	-	05/30/91	21:18:23	51.62	16.24	.0	2.4	24593	IMS2
76	-	05/30/91	21:18:27	51.26	16.44	32.9	-999.0	97483	WASCEL
77	-	06/15/91	12:51:32	51.45	16.06	-999.0	-999.0	10430	GERESS-EPX
77	qmt	06/15/91	12:51:13	51.40	16.20	-999.0	-999.0	159	HARJES
77	-	06/15/91	12:51:28	51.54	16.39	.0	2.6	27379	IMS2
78	-	06/28/91	02:32:44	51.52	17.07	-999.0	-999.0	12430	GERESS-EPX
78	qmt	06/28/91	02:32:55	51.44	16.12	-999.0	-999.0	171	HARJES
78	-	06/28/91	02:32:56	51.56	16.13	.0	2.3	28063	IMS2
79	qmt	07/10/91	11:33:13	51.44	16.13	-999.0	-999.0	185	HARJES
79	-	07/10/91	11:33:22	51.54	16.11	.0	3.0	29367	IMS2
80	-	07/10/91	23:57:20	51.42	16.35	-999.0	-999.0	15070	GERESS-EPX
80	qmt	07/10/91	23:57:16	51.42	16.22	-999.0	-999.0	189	HARJES
80	-	07/10/91	23:57:20	51.55	16.20	.0	2.2	29396	IMS2
81	-	07/21/91	22:50:53	51.06	15.91	-999.0	-999.0	17420	GERESS-EPX
81	qmt	07/21/91	22:50:40	51.37	15.77	-999.0	-999.0	206	HARJES

Table 3: Appendix A: ORGIN TABLE

evid	etype	date	time	lat	lon	depth	ml	orid	auth
81	-	07/21/91	22:50:41	51.60	16.22	.0	1.8	31416	IMS2
82	-	07/24/91	03:17:36	51.57	17.62	-999.0	-999.0	17950	GERESS-EPX
82	qmt	07/24/91	03:17:44	51.39	16.24	-999.0	-999.0	211	HARJES
82	-	07/24/91	03:17:45	51.64	16.02	.0	2.7	31610	IMS2
83	-	07/28/91	23:32:34	51.58	16.22	-999.0	-999.0	18750	GERESS-EPX
83	qmt	07/28/91	23:32:40	51.39	16.18	-999.0	-999.0	216	HARJES
83	-	07/28/91	23:32:43	51.52	16.13	.0	2.3	32441	IMS2
84	qmt	08/23/91	12:11:19	51.37	16.20	-999.0	-999.0	234	HARJES
84	-	08/23/91	12:11:23	51.60	16.04	.0	2.7	36122	IMS2
85	-	09/28/91	00:37:53	51.42	16.87	-999.0	-999.0	26710	GERESS-EPX
85	qmt	09/28/91	00:37:52	51.41	16.15	-999.0	-999.0	268	HARJES
85	-	09/28/91	00:37:52	51.51	16.25	.0	2.5	41792	IMS2
86	-	10/22/91	19:19:26	51.32	16.31	-999.0	-999.0	31000	GERESS-EPX
86	qmt	10/22/91	19:19:26	51.43	16.24	-999.0	-999.0	295	HARJES
86	-	10/22/91	19:19:?6	51.59	16.20	.0	3.3	300639	IMS2
87	-	11/01/91	05:49:05	51.31	15.86	-999.0	-999.0	32750	GERESS-EPX
87	qmt	11/01/91	05:48:00	51.41	16.15	-999.0	-999.0	302	HARJES
87	-	11/01/91	05:49:02	51.58	16.11	.0	2.5	300993	IMS2
88	-	11/12/91	20:57:10	51.25	16.03	-999.0	-999.0	34790	GERESS-EPX
88	qmt	11/12/91	20:57:09	51.42	16.22	-999.0	-999.0	307	HARJES
88	-	11/12/91	20:57:08	51.65	16.18	.0	2.6	301256	IMS2
89	-	11/16/91	22:22:35	51.58	16.05	-999.0	-999.0	35510	GERESS-EPX
89	qmt	11/16/91	22:22:37	51.40	16.20	-999.0	-999.0	312	HARJES

Table 3: Appendix A: ORGIN TABLE

evid	etype	date	time	lat	lon	depth	ml	orid	auth
89	-	11/16/91	22:22:37	51.61	16.15	.0	2.5	301726	IMS2
90	-	11/20/91	15:40:57	51.60	16.50	-999.0	-999.0	36020	GERESS-EPX
90	qmt	11/20/91	15:41:03	51.39	16.24	-999.0	-999.0	319	HARJES
90	-	11/20/91	15:41:04	51.57	16.18	.0	2.5	301885	IMS2
91	-	11/29/91	17:47:00	51.30	16.59	-999.0	-999.0	37910	GERESS-EPX
91	qmt	11/29/91	17:47:00	51.39	16.24	-999.0	-999.0	334	HARJES
91	-	11/29/91	17:47:02	51.58	15.85	.0	2.5	302453	IMS2
92	-	12/01/91	03:32:22	51.86	16.45	-999.0	-999.0	38020	GERESS-EPX
92	qmt	12/01/91	03:32:34	51.39	16.18	-999.0	-999.0	335	HARJES
92	-	12/01/91	03:32:36	51.58	16.14	.0	2.4	302663	IMS2
93	-	12/16/91	18:06:45	51.05	16.50	-999.0	-999.0	40090	GERESS-EPX
93	qmt	12/16/91	18:07:51	51.37	16.20	-999.0	-999.0	350	HARJES
93	-	12/16/91	18:08:01	51.33	16.24	.0	3.1	302914	IMS2
94	-	12/17/91	23:24:49	51.23	16.64	-999.0	-999.0	40310	GERESS-EPX
94	qmt	12/17/91	23:24:45	51.43	16.24	-999.0	-999.0	351	HARJES
94	-	12/17/91	23:24:50	51.56	16.30	.0	3.0	302961	IMS2
95	-	12/20/91	06:32:51	51.40	16.49	-999.0	-999.0	40630	GERESS-EPX
95	qmt	12/20/91	06:32:52	51.39	16.18	-999.0	-999.0	355	HARJES
95	-	12/20/91	06:32:57	51.56	16.10	.0	2.8	303184	IMS2

Improvement of Azimuth Estimation in the IMS

Anne Suteau-Henson

Summary

In many regional monitoring situations, most of the detected events are chemical explosions. The exact location of such events can potentially be known using information from mines and quarries as "ground truth". Therefore, comparing actual locations with those estimated by the Intelligent Monitoring System (IMS, Bache *et al.*, 1990) can point out location errors. For example, the near-regional seismicity at ARCESS shows clusters of events scattered about points that are not known mine locations. This indicates a need to improve azimuth and distance estimation in the IMS by reducing both scatter and systematic bias. In the current implementation of the IMS location algorithm, azimuth measurements (from *f-k* analysis for "defining" phases) are not corrected for any bias, and are weighted using a method developed for data recorded at the NORESS array (Bratt and Bache, 1988). In this study we show how azimuth estimation can be improved using near-regional data at ARCESS as examples. Region-specific corrections and weights are applied to the *f-k* azimuth estimates for each phase type before they are used to locate events. The weights are based on observed rather than "a priori" variance of the estimates. This technique takes into account the fact that in some regions, some phases are more consistently picked than others, and therefore, should be given a larger weight. At ARCESS, for example, *Pn* is often much more consistently picked than *Lg*, resulting in smaller azimuth variance, although *Pn* and *Lg* azimuths are currently assigned similar weights in the IMS. Other ongoing studies at the Center focus on improving identification and picks for *S*-type phases, and therefore, the reliability of their azimuth and arrival time measurements (Suteau-Henson *et al.*, 1992).

Introduction

In a previous study (Suteau-Henson, 1992) we began to evaluate azimuth estimation at the NORESS and ARCESS arrays using estimates from both *f k* analysis and polarization that are automatically calculated and stored by the Intelligent Monitoring System. The results indicated some variation of both systematic bias and scatter with azimuth and distance, as well as the expected decrease in scatter with increasing SNR. A phase dependence of the scatter of azimuth estimates from *f-k* analysis was also found at ARCESS for events from the Apatity mining area in the Kola Peninsula.

The previous study has been extended here in several ways. Based on the Apatity data, a new method has been devised for correcting and weighting *f-k* azimuth estimates from dif-

ferent phases before input to the location algorithm. This method has been applied to other event clusters within about 500 km of ARCESS, thus emphasizing improvement of single-array locations for which azimuth estimation is crucial. The resulting scatter is compared to that for the azimuth estimates corresponding to the IMS locations. Known mine locations are used to correct azimuth estimates for systematic bias.

Analysis Technique

A new technique of azimuth estimation has been developed using events from the Apatity mining area in the Kola Peninsula. This area has a very high level of activity, and the locations of the mines are approximately known (Mykkeltveit *et al.*, 1991; Figure 6). The IMS locations show a significant scatter, as seen in Figure 6, where they are plotted for the time periods November 4, 1990 - September 30, 1991 and October 15, 1991 - March 7, 1992. Most of these events have single-array locations, and therefore, their azimuth from ARCESS is constrained by the azimuths from *f-k* analysis for all phases selected as defining by the IMS analyst (Bratt and Bache, 1988). Defining phases can be any of the following: *Pn*, *Pg*, *Sn*, *Lg*, *Px*, *Sx*, *Rg*, where *Px* and *Sx* refer to unidentified *P*- or *S*-type arrivals, respectively. In the IMS location algorithm, the standard deviation (s.d.) for the azimuth of each defining phase is estimated based on the product of a geometric term, an estimate of the quality of the *f-k* measurement, and an empirical scaling factor determined for NORESS observations. For single-array locations the resulting azimuth is a weighted average of the azimuth observations for individual phases with the inverse of the s.d. estimates used as weights (Bratt and Bache, 1988).

Figure 7 compares the *f-k* azimuth as a function of signal-to-noise ratio (SNR) for the *Pn* and *Lg* phases of events located by the IMS within the geographical limits 67.0 - 67.9° latitude N and 32.9 - 34.7° longitude E, and presumed to originate from the Apatity mining area. The following observations can be made:

- The scatter is much less for *Pn* than for *Lg*;
- The scatter decreases with increasing SNR, and this effect is particularly strong for *Pn* because of the much larger SNR range;
- There is a systematic difference between the azimuth mean for *Pn* and that for *Lg*.

The small scatter in the *Pn* azimuth for large SNR is consistent with the observation that the mines in this area tend to align along the same azimuth from ARCESS. Using these observations we have devised a method to improve azimuth estimates using a new weighting scheme combined with relative azimuthal corrections for each phase:

- For each cluster of events and each phase type the mean and SNR-dependent s.d. of the *f-k* azimuths are derived from observations. The SNR dependence is

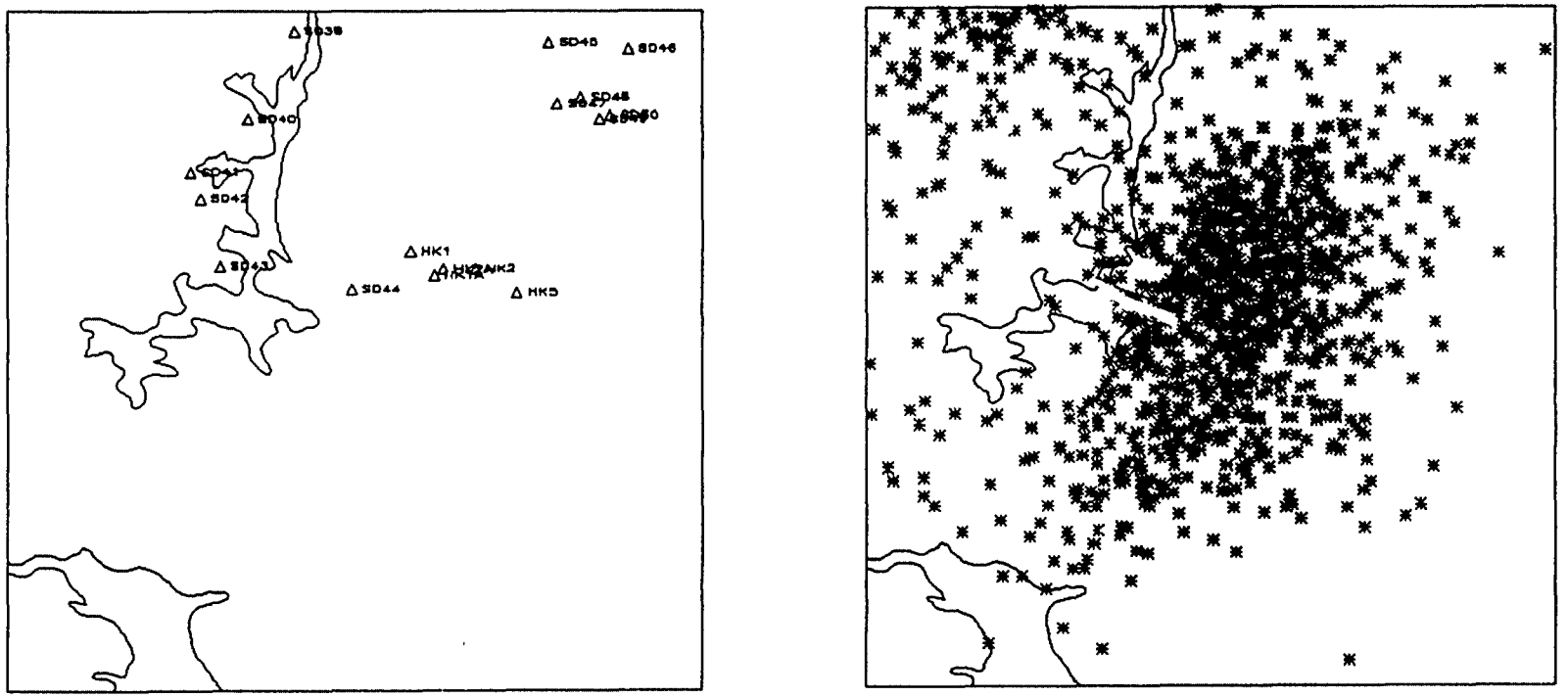

Figure 6: *Map of the Apatity mining area in the Kola Peninsula. The left shows known mine locations, provided by SPOT satellite images ("SD") or the University of Helsinki ("HK"). The right shows corresponding IMS event locations for the time period studied.*

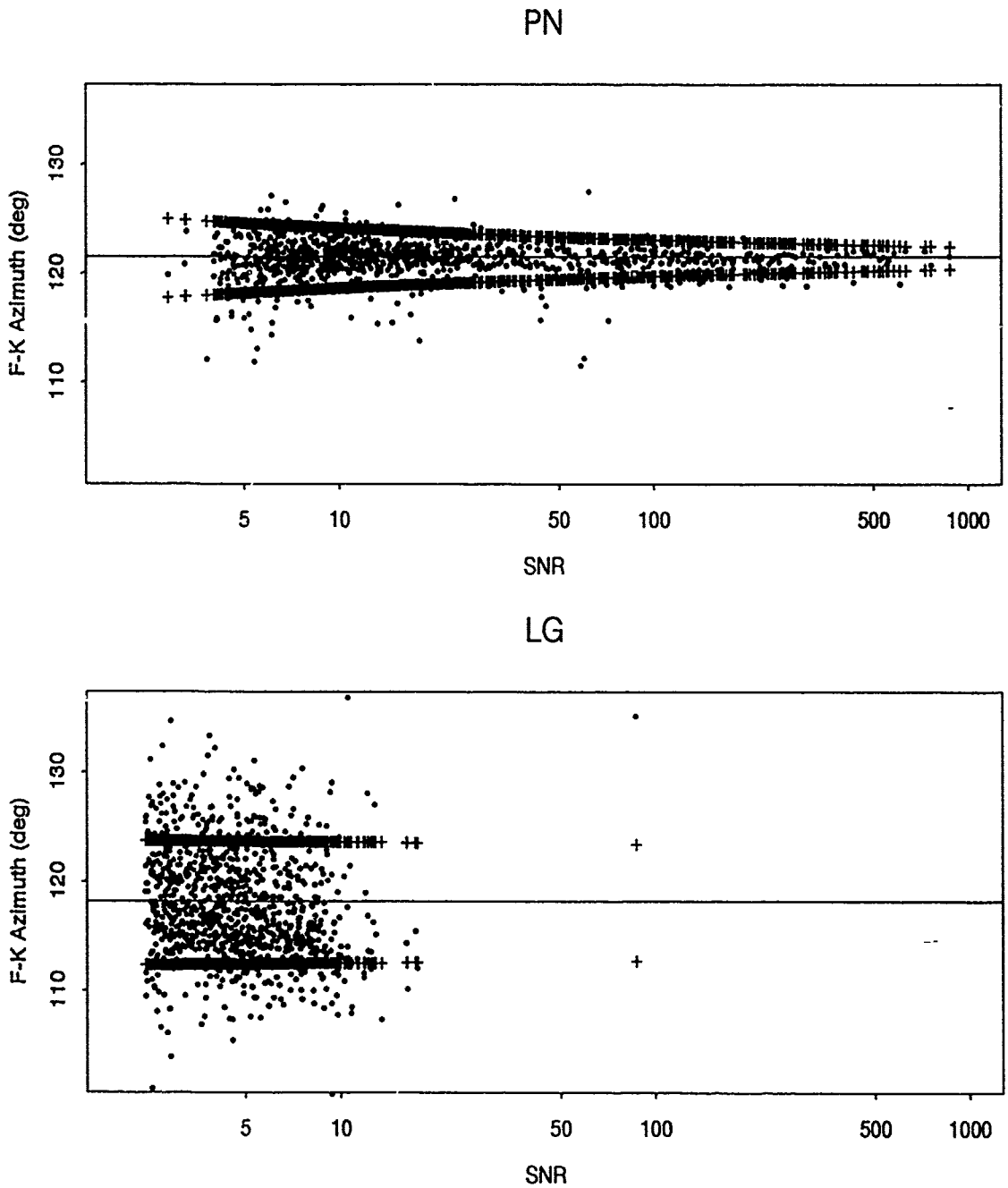

Figure 7: *The f-k azimuth is plotted as a function of SNR for Pn (top) and Lg (bottom) arrivals of events from the Apatity mining area. The scale is the same for easier comparison. The lines marked with plus signs represent two standard deviations (see text for details). The solid line indicates the mean of the observations, which is significantly different for Pn and Lg.*

assumed to be linear on a log-log scale. This is consistent with theoretical predictions (Harris, 1991), and reasonably fits our observations, especially for *Pn*.

- A trial location is obtained for each new event using the current IMS procedure.
- For each new event located within one of the clusters a new average azimuth is estimated using the corrections and weights previously determined for each contributing phase for this cluster.

Application to Apatity Events

This method of azimuth estimation was applied to the Apatity cluster (see Figure 6). The statistics (means and SNR-dependent standard deviations) were determined using all phases (defining and non-defining, from events with single- and multiple-array locations), and are shown in Figure 7 for *Pn* and *Lg*. The resulting azimuth, however, was calculated for single-array events only, using defining arrivals for averaging. With the new method the s.d. decreases from 2.89° to 1.95° after removing some outliers. Figure 8 shows histograms of the *Pn* and *Lg f-k* azimuths, azimuths from the IMS location, and the new azimuth estimates. The s.d. of the new estimates is still somewhat larger than that of the *Pn f-k* azimuth (1.95° compared to 1.70°) reflecting limitations in our modelling of the *f-k* azimuth data. There are two apparent reasons for the improvement obtained over the IMS with the new azimuth estimation method:

- The IMS location procedure does not currently allow for a different azimuth bias for each phase type. This effect, however, can be important, as demonstrated for the Apatity area where there is an average difference of 3.3° between the means of *Pn* and *Lg f-k* azimuths (see Figure 7).
- The weights used in the IMS do not reflect the actual s.d. variation as a function of SNR (see Figure 7), and are underestimated for *Pn*. Figure 9 compares the IMS weights with those from this study for *Pn* and *Lg* at Apatity. The distributions of the IMS weights are affected by the fact that the quantity used to measure the "*f-k* quality" is an integer. A more serious problem is the overall underestimation of the IMS weights for *Pn*. In this case, similar weights are used in the IMS for *Pn* and *Lg*, which does not account for the larger scatter in the azimuth estimates for *Lg* or the bias. A more realistic distribution of weights is obtained using the method of this study.

One factor not taken into account in the IMS error estimation is the consistency of measurements for different phases. Figure 10 shows that for Apatity events, measurements of the slowness vector are very consistent for *Pn*, while a large scatter is observed for the *Lg* population. In particular, at frequencies above 4 Hz, *Lg* has anomalously high phase

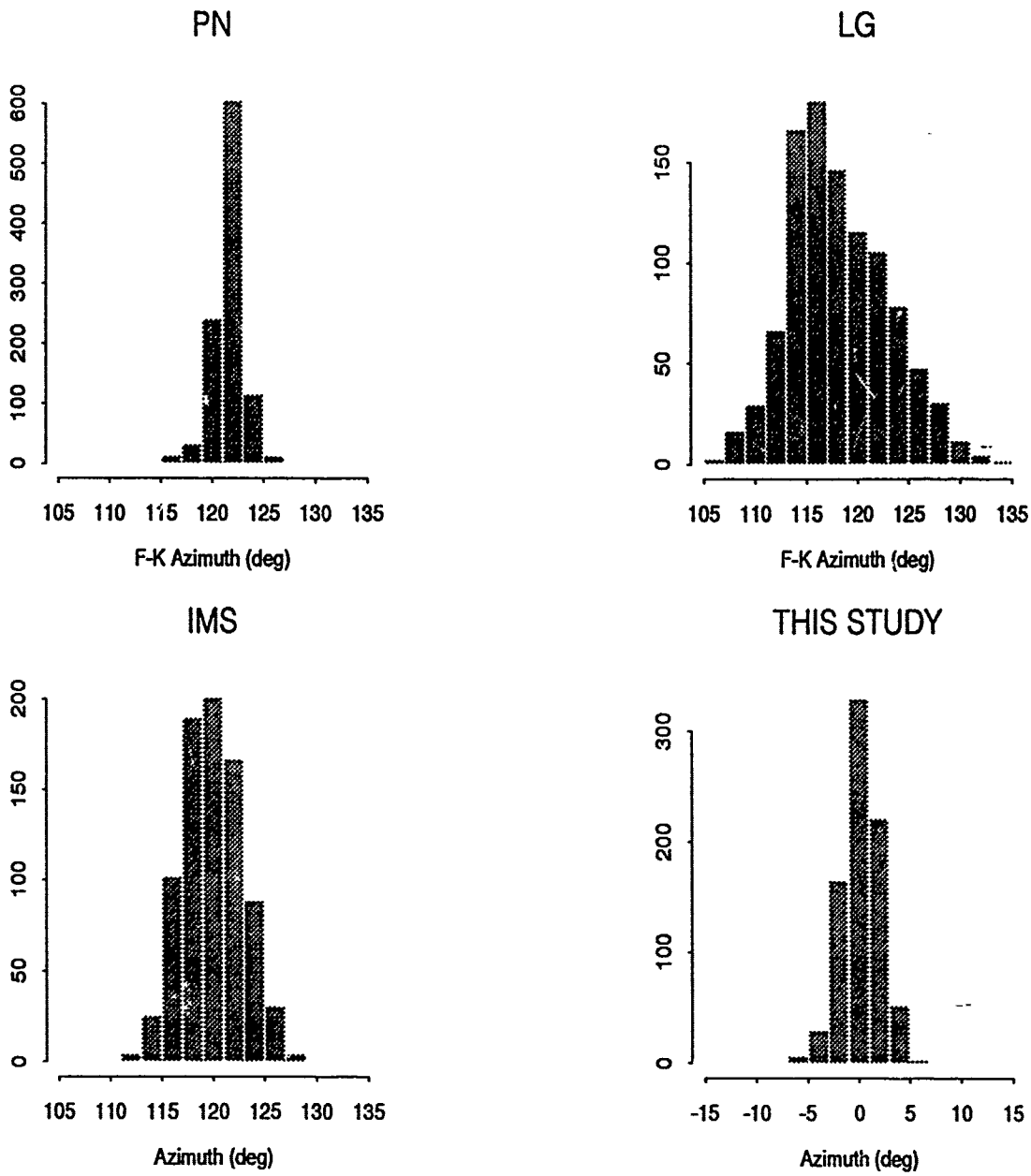

Figure 8: *Histograms of azimuth estimates for events in the Apatity mining area, using four different methods of estimation: top left: Pn f-k azimuth, top right: Lg f-k azimuth, bottom left: azimuth from the IMS location, bottom right: weighted average from this study (relative to the mean of the population).*

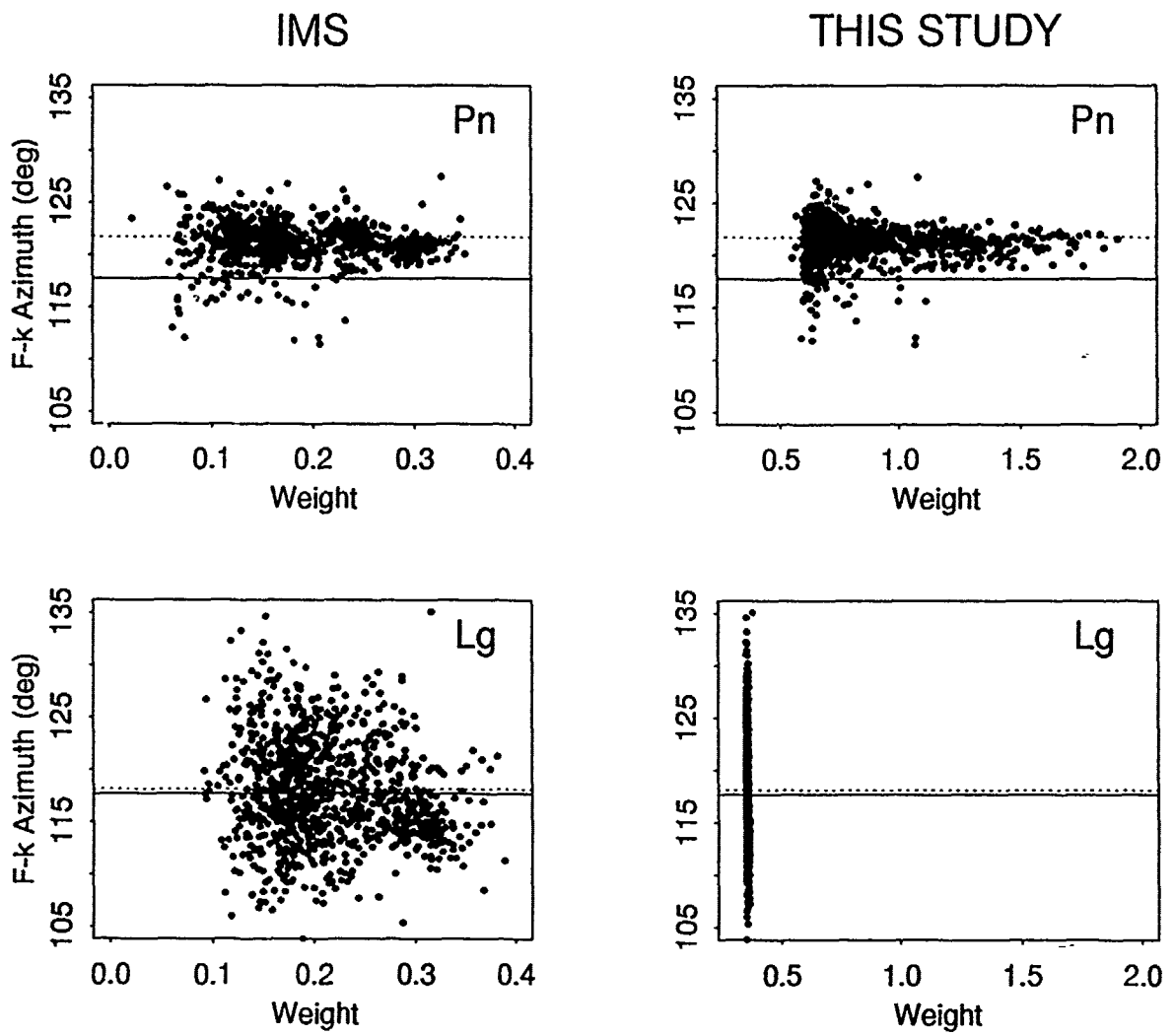

Figure 9: *The weights assigned to the f-k azimuths before input to location are compared for Pn and Lg from events in the Apatity mining area. To the left are shown the weigths used in the IMS. To the right are displayed the weights used in this study, that are based on the inverse of the s.d. of mining event distributions as a function of SNR for each phase (see Figure 7).*

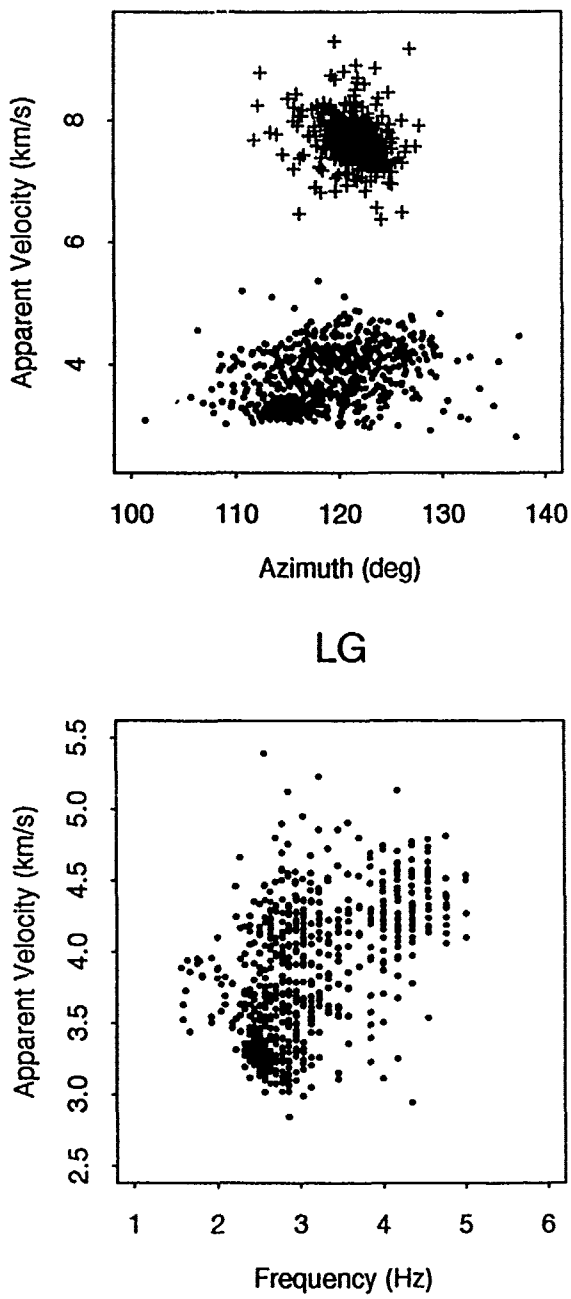

Figure 10: *Azimuth and apparent velocity from f-k analysis are plotted for Pn (crosses) and Lg (dots) phases from Apatity events (top). The dispersion is much larger for Lg than for Pn. Apparent velocity is plotted against frequency for Lg (bottom). Higher frequencies (> 4 Hz) correspond to higher velocities (> 4 km/s).*

velocities (> 4 km/s), presumably due to contamination by *Sn*-coda. Systematic bias and large scatter in time picks for the phase identified in the IMS as "*Lg*" contribute to azimuth as well as distance errors and are studied in detail elsewhere (Suteau-Henson *et al.*, 1992).

Application to Kiruna Events

As a second illustration of this technique, events from a large cluster near the town of Kiruna (Northern Sweden) were analyzed. The geographical boundaries of the cluster are 67.5 - 68.2° latitude N and 20 - 22° longitude E. The location and extent of the mine are known, as well as its shooting practices. It is 4 km by 200 m large, and ripple-fired blasts are shot every night around 00:35 local time (Israelsson, personal communication, 1992). Examination of the origin times for events within that area confirmed that about half of them occurred very close to the expected time. The data set was accordingly divided into two subsets: 3a for events occurring around the expected time, 3b for other events.

Figure 11 compares the distributions of *Pn* and *Lg f-k* azimuths as a function of SNR for Kiruna (cluster 3a) and Apatity. Azimuth estimation for Kiruna using the method developed above for Apatity results in a slightly smaller s.d. (1.67°) than that of the azimuths from the IMS locations (1.90°). Contrary to our observation for Apatity, there is no difference between the mean of the *f-k* azimuths for *Pn* and *Lg* (225.9°), but it differs by 5° from the true azimuth of the Kiruna mine (231.1°).

Application to Other Event Clusters

In view of the success of this method for the Apatity and Kiruna mining areas, it was applied to the entire region around ARCESS. The study was restricted to a radius of 500 km from ARCESS, as most events beyond this distance have multiple-array locations. Also, tight clustering of events, presumably explosions from specific mines or quarries, was only observed on land, so offshore events were not included. Figure 12 is a map of the near-regional seismicity around ARCESS for the time period studied. A total of eigtheen clusters were identified on this map, and their geographical limits are given in Table 4. Note that cluster 15 corresponds to the Apatity area, and cluster 3 to the Kiruna area (all events included, regardless of origin time), that were studied above. Clearly, the limits given in Table 4 are somewhat arbitrary and are likely to include some mislocated events, as well as miss events that should have been included. However, this does not significantly affect the results of this study which are based on statistics over large numbers of events. This was tested by modifying the boundaries for some clusters, and comparing the results. In a few cases (clusters 6, 13, and 16), the boundaries had to be corrected after the statistical analysis indicated a non-uniform event distribution.

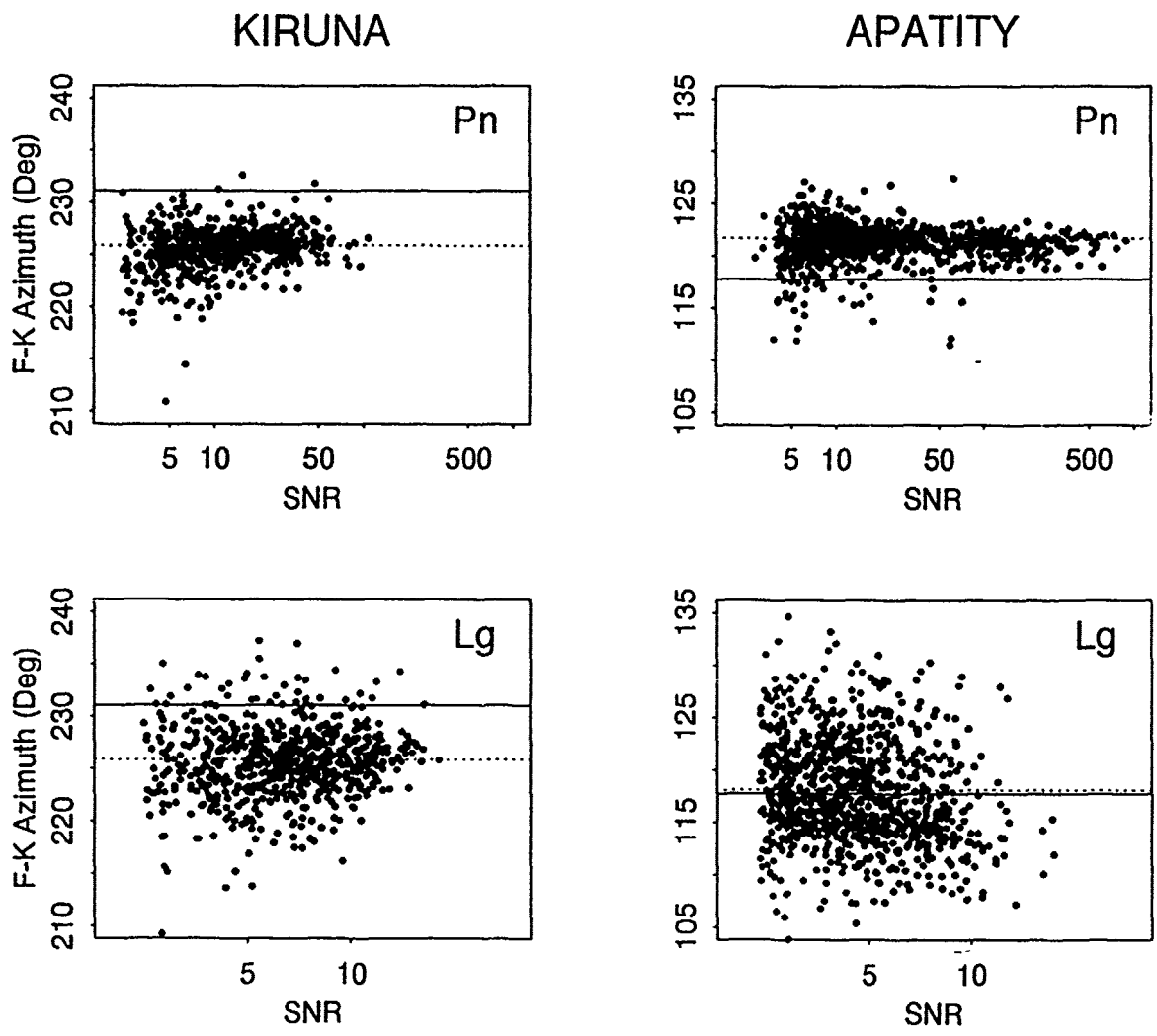

Figure 11: *The distributions of f-k azimuth as a function of SNR are compared fcr Pn (top) and Lg (bottom) arrivals of events from the Kiruna (left) and Apatity (right) mining areas. Note the region- and phase-dependence of the difference between the actual mine azimuth (solid line) and the mean of the f-k azimuth (dotted line).*

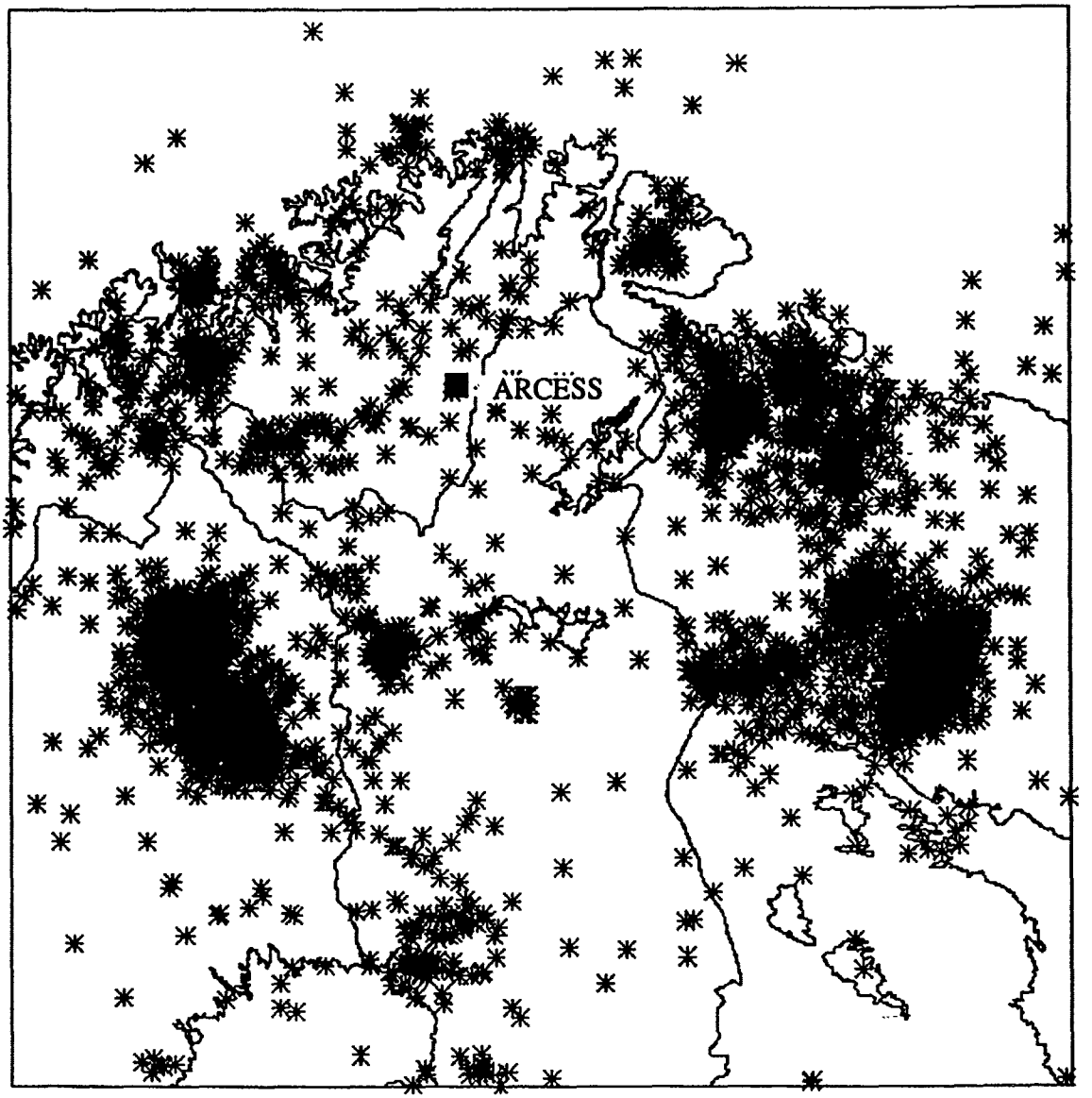

Figure 12: *Map of the seismicity recorded at ARCESS (filled square) during the period studied. Note that many events form clusters. The geographical limits of the event clusters identified and analyzed in this study are given in Table 4.*

Table 4: Geographical Limits of Clusters

Cluster #	Latitude Limits (°N)		Longitude Limits (°E)	
1	69.8	70.3	20.0	20.8
2	69.3	69.8	20.2	20.9
3	67.5	68.2	20.0	21.7
4	66.8	67.5	20.8	22.6
5	67.5	68.1	24.0	25.0
6a	69.0	69.3	21.5	23.2
7	69.9	70.4	21.0	22.5
8	70.8	71.4	23.8	24.8
9	70.8	71.3	25.7	27.0
10	70.2	70.54	28.5	29.7
11	69.1	69.5	29.9	31.1
12	69.3	69.8	31.3	31.7
13a	69.25	69.8	31.7	32.3
13b	68.5	69.2	32.1	33.2
14	67.9	68.4	32.0	33.1
15	67.0	67.9	32.9	34.7
16a	67.5	67.8	29.5	31.0
17	65.5	66.3	24.5	26.5

For each cluster Table 4 gives the number of detections in each phase type. As expected, the most numerous detections were either "*Pn*" or "*Pg*", and "*Lg*", as identified in the IMS. Figure 13 shows the locations of the known mines at the time of this study, for comparison.

For events with single-array locations in each cluster, a new azimuth estimate was obtained using the method described above. Some modifications, however, had to be made to account for smaller data sets:

- For a given cluster, statistics were only obtained for phase types with enough

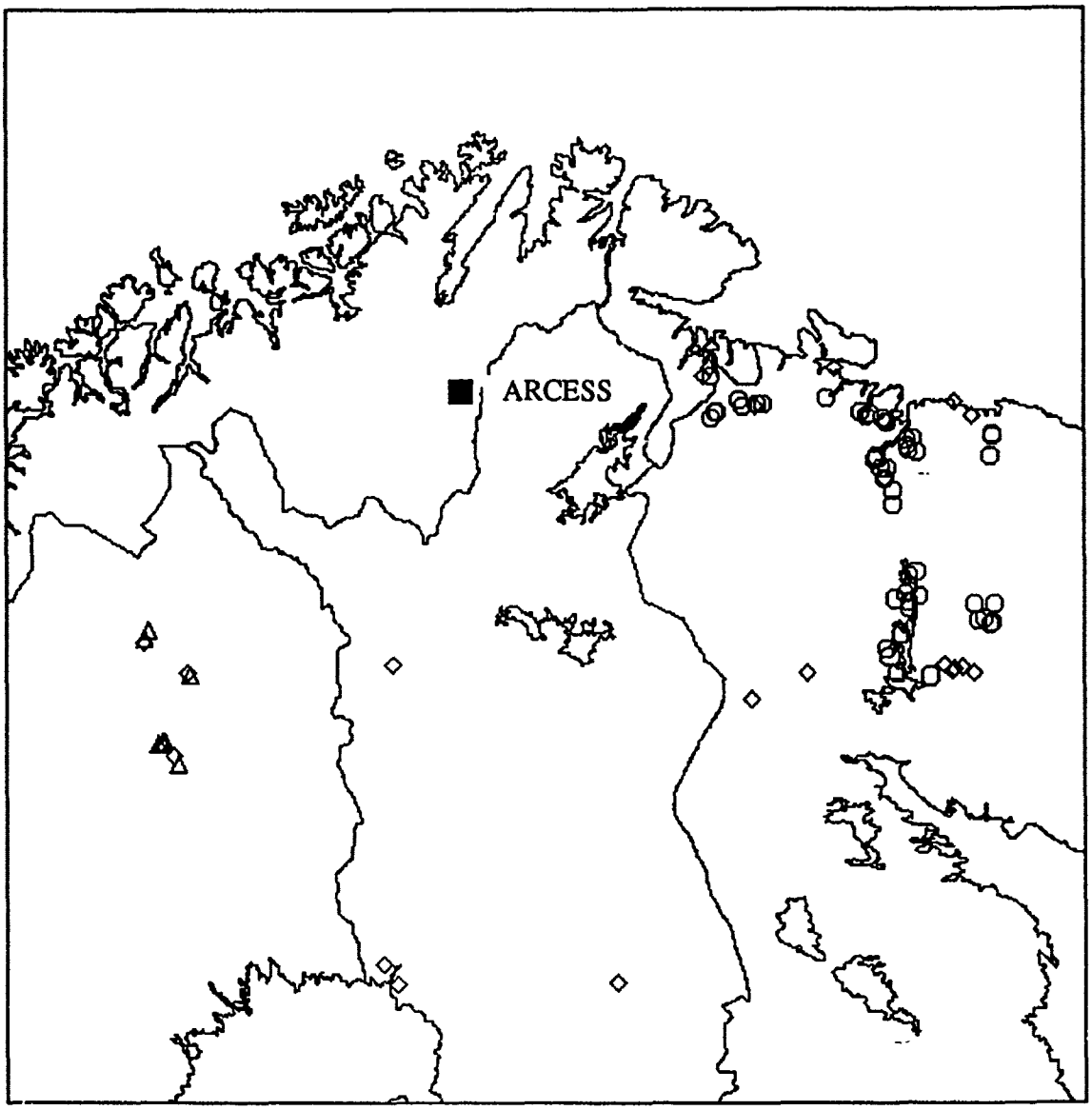

Figure 13: *Map showing the locations of known mines at the time of this study for the area displayed on the map of Figure 12. Mine locations indicated with diamonds, circles, and triangles, originate from NORSAR or the University of Helsinki, SPOT satellite images, and DMA maps, respectively.*

Table 5: Number of Detections per Phase Type for Each Cluster

Cluster #	Pn	Pg	Sn	Lg	Px	Sx	Rg
1	7	58	2	64	19	4	1
2	6	73	1	79	18	16	0
3	1489	42	35	1528	425	668	1
4	695	92	35	698	258	390	2
5	33	145	1	178	21	18	0
6a	1	42	1	42	15	22	1
7	3	33	1	34	23	21	1
8	0	27	0	27	3	1	1
9	0	29	0	29	0	3	0
10	3	56	0	58	30	20	0
11	96	387	8	478	87	107	82
12	85	3	1	94	33	69	0
13a	70	6	3	81	37	61	0
13b	126	17	11	124	72	96	1
14	151	28	38	148	114	162	51
15	1042	387	575	1022	273	552	12
16a	118	12	26	121	95	132	4
17	74	35	53	68	27	55	0

detections.

- When no proper fit could be obtained for the SNR dependence of the s.d. (due to a small data set or limited SNR range), a constant s.d. was used instead.

For each cluster, Table 6 and Figure 14 compare the s.d. of the azimuths from the IMS locations to that for the azimuths estimated with the new method. Note that the s.d. was measured after removal of outliers that tend to be more numerous with the new method. This may reflect the effect of factors not taken into account in this analysis. However, these outliers may also correspond to events that were significantly mislocated by the

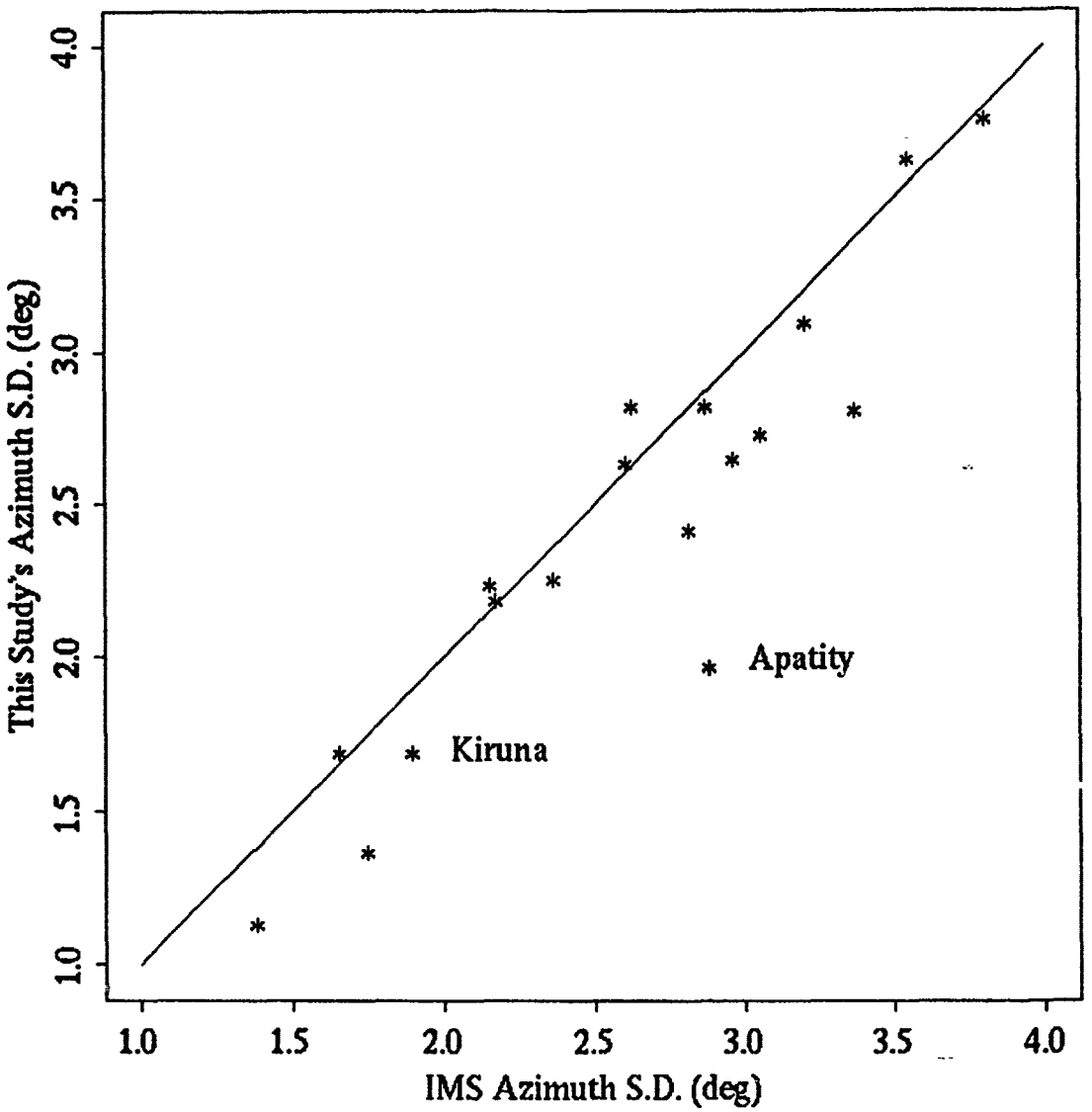

Figure 14: *For the 18 clusters defined in Table 4, the standard deviation of the azimuth estimates derived in this study is plotted against the standard deviation of the azimuths from the IMS locations. The line indicates equal s.d. for the two methods. A significant reduction in scatter is obtained for half of the clusters when using the new weights.*

Table 6: Comparison of Standard Deviation of Azimuth Estimates

Cluster #	IMS	This Study
1	1.75	1.35
2	2.82	2.40
3	2.42	2.33
4	3.38	2.79
5	1.39	1.11
6a	2.37	2.24
7	3.81	3.75
8	2.61	2.62
9	2.88	2.80
10	2.16	2.22
11	2.63	2.80
12	1.66	1.67
13a	3.21	3.08
13b	3.56	3.61
14	2.18	2.17
15	2.89	1.95
16a	3.06	2.71
17	2.97	2.63

IMS. The results show the following:

- There is no significant increase in scatter for any of the clusters studied, when using the new method of azimuth estimation.
- A significant improvement (i.e., reduction in scatter) is obtained for half of the clusters.

Determination of Azimuth Bias

We have shown that the method proposed here for azimuth estimation can reduce the azimuth scatter for specific event clusters. Next, we attempt to determine any systematic bias between the average azimuth of a given population and the "true" azimuth for those events. Table 7 compares the average azimuth (for both single-array and multiple-array

Table 7: Comparison of Mean of Azimuth Estimates With Mine Azimuths

Cluster #	Single-Array Azimuth (°)	Multiple-Array Azimuth (°)	Mine Azimuth (°)
1	289.1	NA	NA
2	273.5	NA	NA
3	225.6	226.7	Kiruna (231.1)
4	212.6	213.3	Malmberget (219.4)
5	193.5	NA	Saattopora (193.2)
6a	252.0	NA	NA
7	297.4	NA	NA
8	346.7	NA	NA
9	10.7	NA	NA
10	54.2	NA	NA
11	95.7	94.2	Nikel (91.1)
12	87.4	NA	SD10 (90.0)
13a	87.8	NA	NA
13b	99.2	NA	SD24-SD32 (97.7-103.5)
14	116.5	116.0	SD33-SD39 (110.3-114.5)
15	119.9	119.0	Apatity (117.2-118.1)
16a	135.3	135.3	Kodvor (135.2)
17	180.9	181.4	Elijaervi (185.0), Kalkkimaa (186.7)

locations) to the corresponding mine azimuths, when available, for each cluster. Note that for some clusters, several mines spanning an azimuth range, were included. Only seven of the clusters had enough multiple-array locations to derive an average azimuth.

The average multiple-array azimuth usually differs from the "mine azimuth" by up to ±6°. It is smaller south (cluster 17) and southwest (clusters 3 and 4), and larger east (clusters 11, 14, 15) of ARCESS. For the six clusters at which both are available (excluding 16a for which all estimates are similar), the single- and multiple-array azimuths differ slightly (by up to 1.5°). Interestingly, the multiple-array estimate is consistently closer to the average mine azimuth. This indicates that the multiple-array locations tend to be closer to "ground truth". However, the ARCESS observations have the largest weights in the location estimation, because of the proximity of the events to ARCESS. Therefore, in general, multiple-array locations also significantly differ from "ground truth".

In summary, a systematic bias of several degrees generally exists between the average multiple-array azimuth for each cluster, and the average azimuth of the corresponding mine (or mines). The bias is even greater for single-array locations. Therefore, it is necessary to apply a correction to the observed azimuths. Clearly, more information is needed to establish "ground truth" for each area with mining activity.

Conclusions and Discussion

This study has shown that *a priori* estimates for the variance of *f-k* azimuths which are used to weight individual observations before input to location need to be revised as more knowledge is acquired. Such knowledge consists of the observed mean and s.d. of *f-k* azimuths for specific phases from events located at known mines or quarries along with the actual mine azimuth. For near-regional events recorded at ARCESS, we have demonstrated that the use of phase-dependent weights and azimuth corrections based on such knowledge can significantly reduce the resulting azimuth scatter in a given mining area.

Methods are currently being developed to accurately locate events from known mines (Rivière-Barbier and Grant, 1992). This will make it possible to "eliminate" the large number of events from such sources and to focus on "unknown" events. More accurate and precise locations for the latter will be obtained as full use is made of the knowledge acquired from all other events. Clearly, events from known mines do not uniformly cover the area around a given station (see Figure 12). Therefore, it is necessary to interpolate the observed azimuth bias and s.d. between mining areas in order to derive estimates for areas where such knowledge is not available. In future work, we will perform such an interpolation and thereby obtain a map of azimuth bias and s.d. for the main regional phases around ARCESS.

This work is dependent on the availability of "ground truth". A "Ground Truth Database" is currently being assembled at the Center (Grant and Coyne, 1992), that will comprise a large number of reference events of various types (mine blasts, earthquakes, etc.) for which the exact location is known. This database will be invaluable for determining appropriate azimuth corrections and weights to improve automatic location in the IMS.

References

Bache, T. C., S. R. Bratt, J. Wang, R. M. Fung, C. Kobryn, and J. W. Given (1990). "The Intelligent Monitoring System", *Bull. Seism. Soc. Am.* **80**, 1833-1851.

Bratt, S. R. and T. C. Bache (1988). "Locating events with a sparse network of regional arrays", *Bull. Seism. Soc. Am.* **78**, 780-798.

Grant, L. and J. Coyne (1992). "A Ground-Truth Database for Seismic Discrimination Research", this report.

Harris, D. B. (1990). "Comparison of the direction estimation performance of high-frequency seismic arrays and three-component stations", *Bull. Seism. Soc. Am.* **80**, 1951-1968.

Mykkeltveit, S., A. Dahle, J. Fyen, T. Kvaerna, P. W. Larsen, R. Paulsen, F. Ringdal, and E. O. Kremenetskaya (1991). "Extensions of the Northern Europe Regional Array Network -- a new three-component station at Apatity, USSR, and a planned array at Spitsbergen", in *NORSAR Sci. Rep. 1-91/92*, p. 100-111.

Rivière-Barbier, F. and L.T. Grant (1992). "Cluster Analysis of Closely Spaced Mining Blasts as a Method of Event Location", submitted to *Bull. Seism. Soc. Am.*

Suteau-Henson, A. (1992). "Azimuth Variations at NORESS and ARCESS", this report.

Suteau-Henson, A., V. Z. Ryaboy, F. Rivière-Barbier, H. Israelsson, and J. A. Carter (1992). "Analysis of IMS Locations of Mine Blasts and RMS *Lg* Magnitudes in Scandinavia", in *Proceedings of the 14th Annual PL/DARPA Seismic Research Symposium*, 16-18 September 1992, Tucson, AZ, p. 401-407.

Regional Phase Identification in the IMS

Vlad Ryaboy

Introduction

A prototype regional seismic monitoring system, the IMS (Bache *et al.*, 1990), uses data from short-period regional seismic arrays in Scandinavia and Central Europe (NORESS, ARCESS, FINESA, and GERESS) to detect, locate, and identify low-magnitude local, regional, and far-regional events for use in verification monitoring. The effectiveness of the IMS is critically dependent on the accuracy of its event locations, many of which are determined using a single array.

For single station locations, mistiming a regional phase arrival can significantly change the location of an event; mis-identifying the phase has an even larger effect. Variations of regional phase travel-times make phase identification a difficult task where the moveout information is generally limited, as in the case of arrays, or not available at all. DSS profile data serves as an aid in both identifying and timing regional phases. Because DSS data is sampled at fairly regular distance intervals on reversed and overlapping profiles, regional phases can be identified more reliably by their moveout and their association with neighboring traces.

A detailed study of the locations of mine blasts from the Kiruna mine in northern Sweden (290 km southwest of the ARCESS array) was performed. In the study we compared the location of the Kiruna mine to mine blast locations from the ARCESS array. An average 20 km bias in distance toward ARCESS and 5° in azimuth was observed for these events (Suteau-Henson, 1991; Suteau-Henson *et al.*, 1992). The distance bias is much greater than would be expected from the variations caused by regional perturbations in the travel-time curves (Ryaboy, 1992). In addition, examination of DSS data in the northern Baltic shield shows that pronounced *Pn*-wave travel-time anomalies are not observed in this area. Thus, the bias is likely the result of mistiming or mis-identification of phases. Our study explores this issue using deep seismic sounding (DSS) data as ground truth. Specifically, we show that phases labeled as *Lg* by the IMS at distances between approximately 100 and 400 km do not have typical *Lg* travel-times, velocities, or frequencies. The characteristics of this phase match well the characteristics of the *SmS* phase, a shear-wave Moho reflection identified on long-range seismic profiles.

Data

Figure 15 shows ARCESS recordings from the central vertical short-period channel of

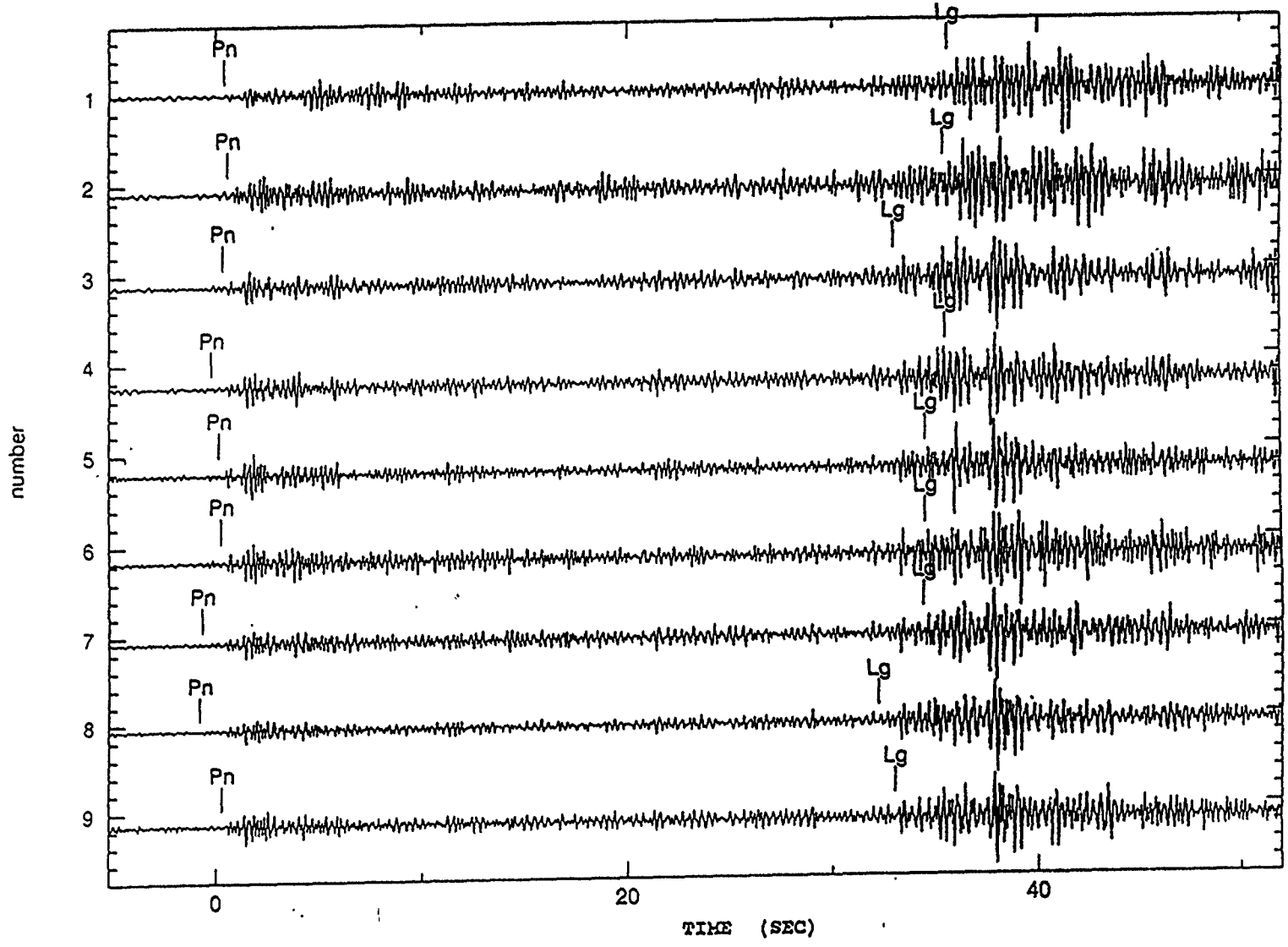

Figure 15: *ARCESS recordings (a bandpass filter of 2 to 8 Hz) of nine selected Kiruna mine blasts (central vertical short-period channels). Pn and Lg phase identifications based on the IMS bulletin.*

nine Kiruna mine blasts and the phase identifications assigned by the IMS. Phase identifications in the IMS are determined using an automated procedure which are reviewed by an analyst (Bache *et al.*, 1990). For these events, the *P*-wave first arrivals are identified as *Pn* and the phases in the *S*-wave group are identified as *Lg*. Despite the similarity in the waveforms, there is a considerable amount of scatter in the *Lg* picks which is the cause of the distance scatter in the event locations.

Detailed observations based on recordings of *P*- and *S*-waves were carried out in this area along the FENNOLORA (Guggisberg, 1986; Hauser and Stangl, 1990; Stangl, 1990) and POLAR (Luosto *et al.*, 1989) DSS profiles. Figure 16 shows the record sections of *P*- and *S*-waves constructed for the POLAR DSS profile. *Pn* emerges as a first arrival at distances greater than 200 km. High amplitude reflected *P*-waves from the Moho (*PmP*) are observed in the later arrivals. *SmS* (reflected shear wave from the Moho) is the highest amplitude *S*-wave at distances from at least 100 to 350 km. At greater distances, *PmP* and *SmS* waves were not reliably recorded because of attenuation and poor SNR. At distances less than 100-120 km, the dominant phases in the later arrivals of *P*- and *S*-waves are reflected waves from intermediate crustal boundaries (Figure 16).

Comparison of IMS and DSS Phase Identifications

Figure 17 shows a comparison of the IMS phase identifications and arrival times from DSS observations on a coherent beam formed for one of the Kiruna blasts. The arrival times of the phases identified along the POLAR DSS profile were measured at a distance of 290 km, the true distance between the ARCESS array and the Kiruna mine. The wave labeled as *Lg* by the IMS, corresponds to *SmS* identified from the DSS data. The *SmS* interpretation is consistent with studies of major regional phases recorded by the NORESS, ARCESS, and FINESA arrays within the Baltic shield (Vogfjord *et al.*, 1991; Vogfjord and Langston, 1992) and results of modelling *Lg*-wave propagation (Kennett, 1992a, 1992b).

SmS consists of pre-critical, critical, and post critical reflected shear waves from the Moho. Analysis of DSS data suggests that *SmS* has a phase velocity larger than that reported for *Lg* at greater distances (for a review of Lg group and phase velocity measurements see Blandford, 1982). Figure 18 shows the apparent velocity for the phase identified as *Lg* by the IMS vs. distance from the ARCESS array. Also shown in Figure 18 is the *SmS* apparent velocity curve inferred from the POLAR DSS profile. The *SmS* curve is a good fit to the IMS data within the distance range from 100 to 400 km. At distances between 400 and 1,000 km, typical *Lg* apparent velocities (slightly above 3.5 km/sec) are observed. At distances less than 100 km, however, the apparent velocity inferred from the IMS observations is between 4.0-5.0 km/sec. These values are too large for *Lg* and too small for

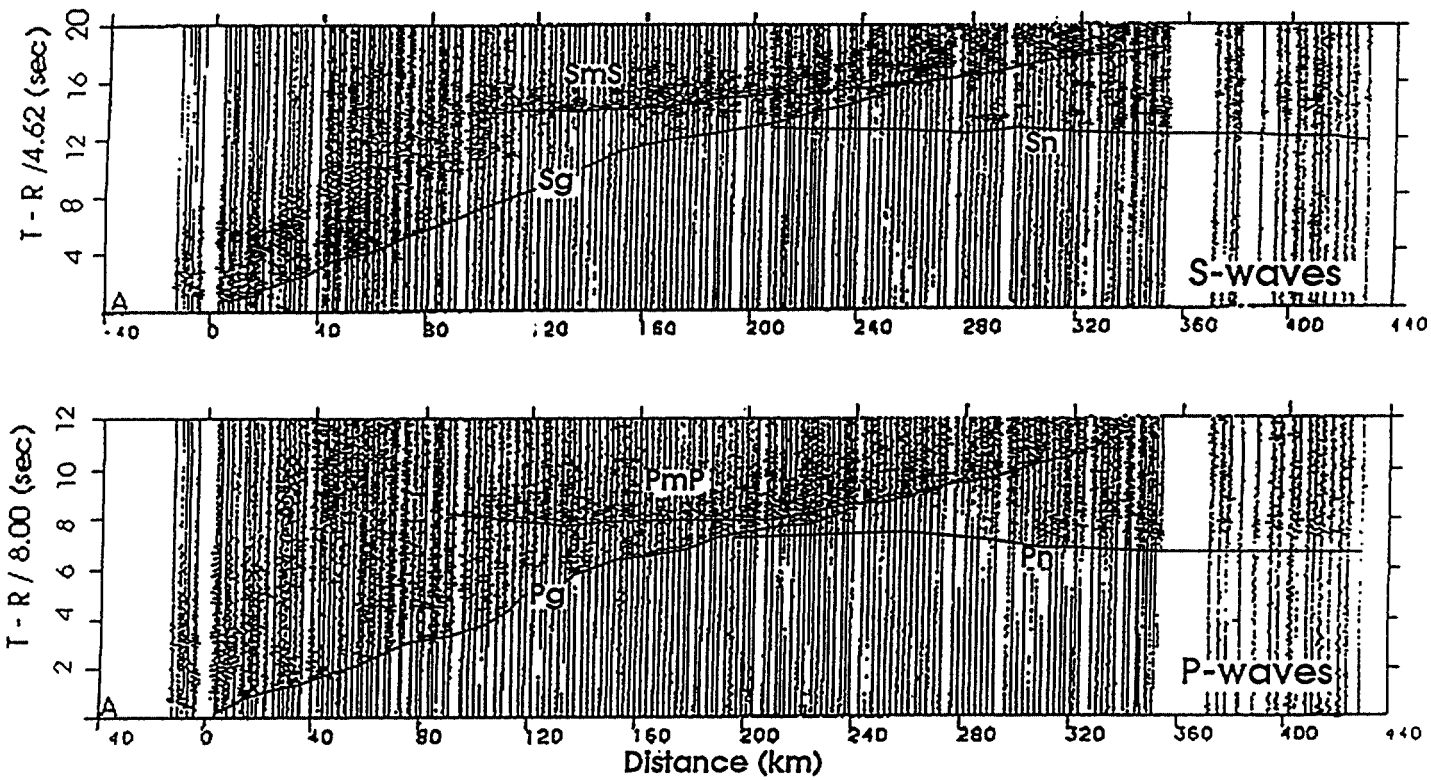

Figure 16: Trace-normalized record sections of S- (top) and P-waves (bottom) recorded on POLAR DSS profile from shot point A (adapted from Luosto et al., 1989). A bandpass filter of 2-6 Hz and 2-15 Hz was applied to the records of the S- and P-waves, respectively.

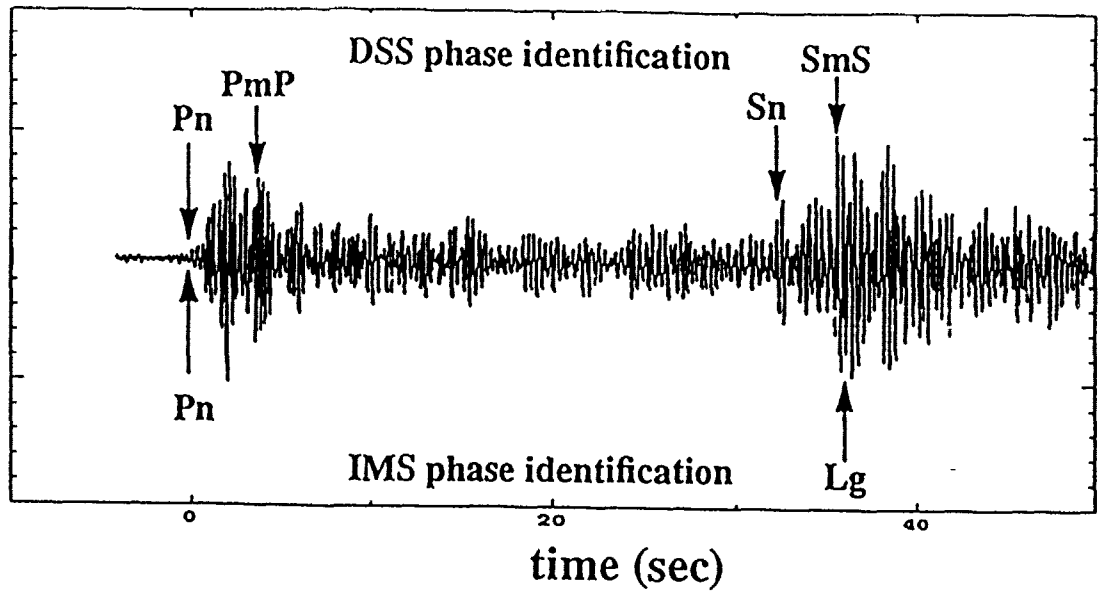

Figure 17: *Comparison of the IMS and DSS phase identifications on a coherent beam (bandpass filtered from 2 to 8 Hz) of a Kiruna mine blast recorded at the ARCESS array on 04/01/91.*

SmS, but are typical for reflected waves from mid-crustal boundaries in the Baltic shield (Luosto *et al.*, 1989; Hauser and Stangl, 1990). These arrivals can be seen on the DSS profile in Figure 16 (top) at distances less than 100 km.

Figure 19 shows that the predominant frequencies of the phase identified as *Lg* by the IMS decreases with distance from 8-10 Hz at 100 km to 2-4 Hz at 400 km. Beyond 400 km, the frequency content is 1-3 Hz, which is more typical of *Lg* energy. Since the recorded events with only a few exceptions have similar magnitudes, variations in the dominant frequency are probably not due to systematic differences in the source size. High frequencies such as those observed at distances less than 400 km are atypical for *Lg*-waves and support a *SmS* interpretation.

Our analysis indicates that the first intensive phases recorded in the northern Baltic shield within the *S*-wave group between 100-400 km are *SmS*-waves, and the high amplitude phases recorded at distances greater than 400-500 km are *Lg*-waves. This contention that between 100 and 400 km epicentral distance the first large amplitude *S*-phase is, in reality, *SmS* rather than *Lg* may cause confusion for those interested in arrival names, but is irrelevant to the issue of event location if the *Lg* travel-time curve in the IMS is a good fit to the

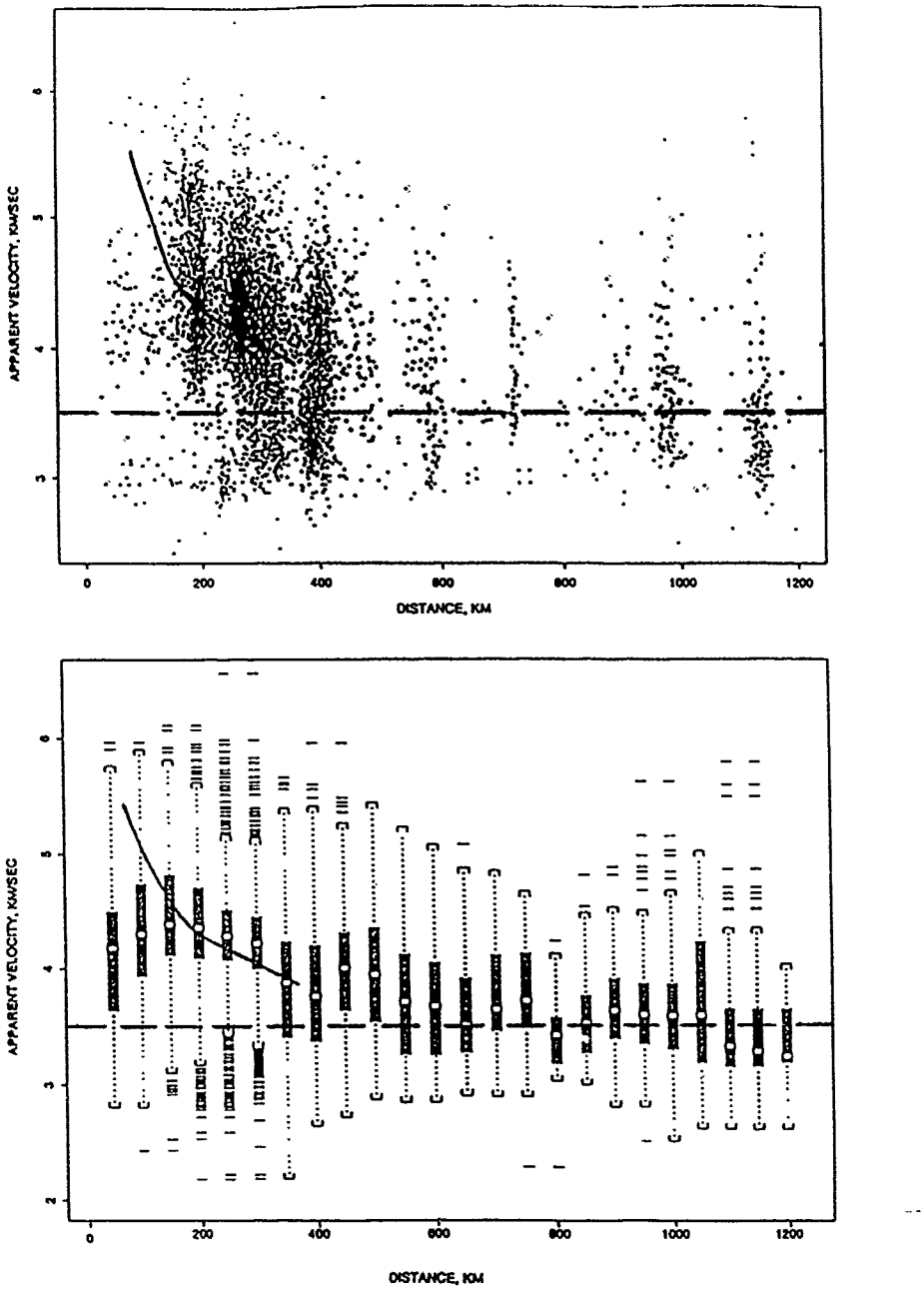

Figure 18: *Top: Lg apparent velocity vs. distance from the ARCESS array according to f-k analysis of the IMS data (dots). Bottom: box plots of the same data. Boxes were calculated for 100 km distance windows with 50 km overlaps. The horizontal white line in the interior of the each box is the median of the data. The height of the dark box is the difference between the third quartile of the data and the first quartile. The dotted vertical lines extend to the extreme values of the data, and thin horizontal lines are outliers. Top and bottom: solid line is the SmS apparent velocity curve inferred from the POLAR DSS profile observations; dashed horizontal line is 3.5 km/sec (Lg-wave group velocity).*

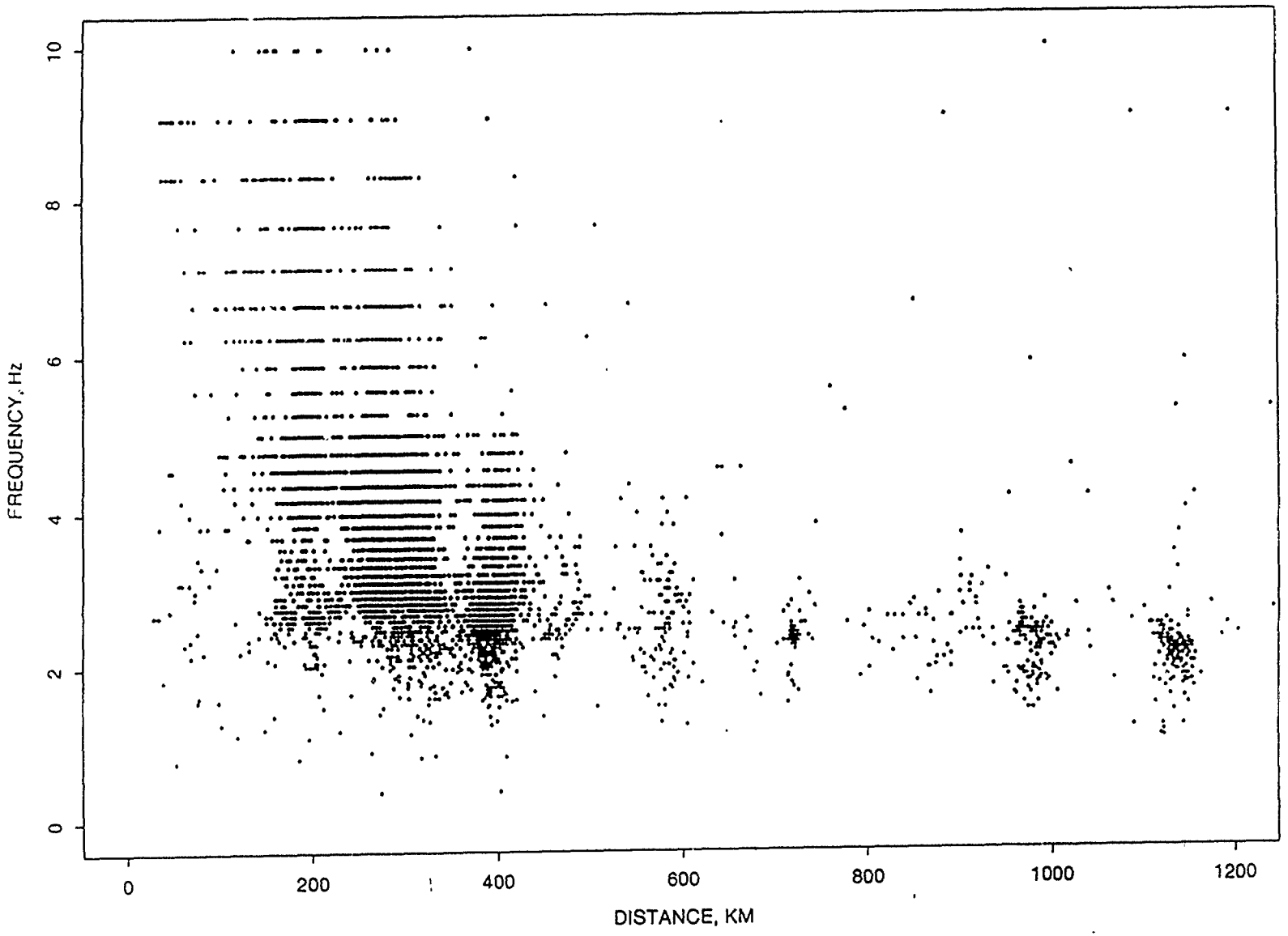

Figure 19: *Lg frequency vs. distance from IMS data.*

SmS observations. To demonstrate that it is not, we compared the *Lg* reference travel-time curve from the IMS bulletin with the *SmS* composite travel-time curve (Figure 20) constructed by smoothing DSS observations along the POLAR profile (Luosto et al., 1989). The standard deviation of the observed *SmS* travel-times relative to the average curve is ±0.47 sec.

Figure 20 shows that the *Lg/SmS* cross-over point is located near 220 km. The *Lg* travel-time curve being used for IMS locations is about five seconds early or late compared to the DSS observations at the *SmS* curve extremities. Based on this curve, we predict that events between 100 and 220 km distance from the array station will have IMS locations biased away from the array, and that events between 220 and 400 km from the array will have locations biased towards the array. Comparing single array locations from ARCESS for mine explosions within the northern Baltic shield with well known locations (A. Suteau-Henson, personal communication, 1992) shows that events located at distances greater than the *Lg/SmS* cross-over point, including the Kiruna mine, have a distance bias towards ARCESS and that events located at distances less than the *Lg/SmS* cross-over point have a distance bias away from ARCESS. For ARCESS locations of the Kiruna mine blasts, renaming *"Lg"* as *SmS*, and using *Pn* and *SmS* arrival times and travel-time curves inferred from the Polar DSS observations, the distance bias is eliminated.

Discussion and Conclusions

The IMS must incorporate regional knowledge of travel-time variations and phase identifications to improve its event location capability. This information is contained in numerous long-range seismic profiles and data from events with well-known locations and origin times.

In this report, we have used regional knowledge from DSS profiles to show how IMS locations can be improved, especially for one-array locations. The *Lg* travel-time curve currently used by the IMS for ARCESS locations is not a good fit to the *SmS*-wave arrivals observed in DSS profiles at ranges of 100 to 400 km. IMS mis-locations of mining events with well-known origins confirm that the arrivals detected by the IMS in this distance range as *Lg* are consistent with *SmS* travel-times. The major recommendation of this study is to replace the *Lg* travel-time curve (currently defined in the IMS at all distances) with an *SmS* curve based on DSS observations between 100 and 400 km for the Baltic Shield. The upper *SmS* distance range (400 km) will depend on the Moho depth and the earth crust velocity structure, and thus, will differ by area.

Having recommended that *SmS* should be used instead of *Lg* from 100 to 400 km, we also recommend that the *Lg* travel-time curve begin at around 400 km. *Lg* should not be

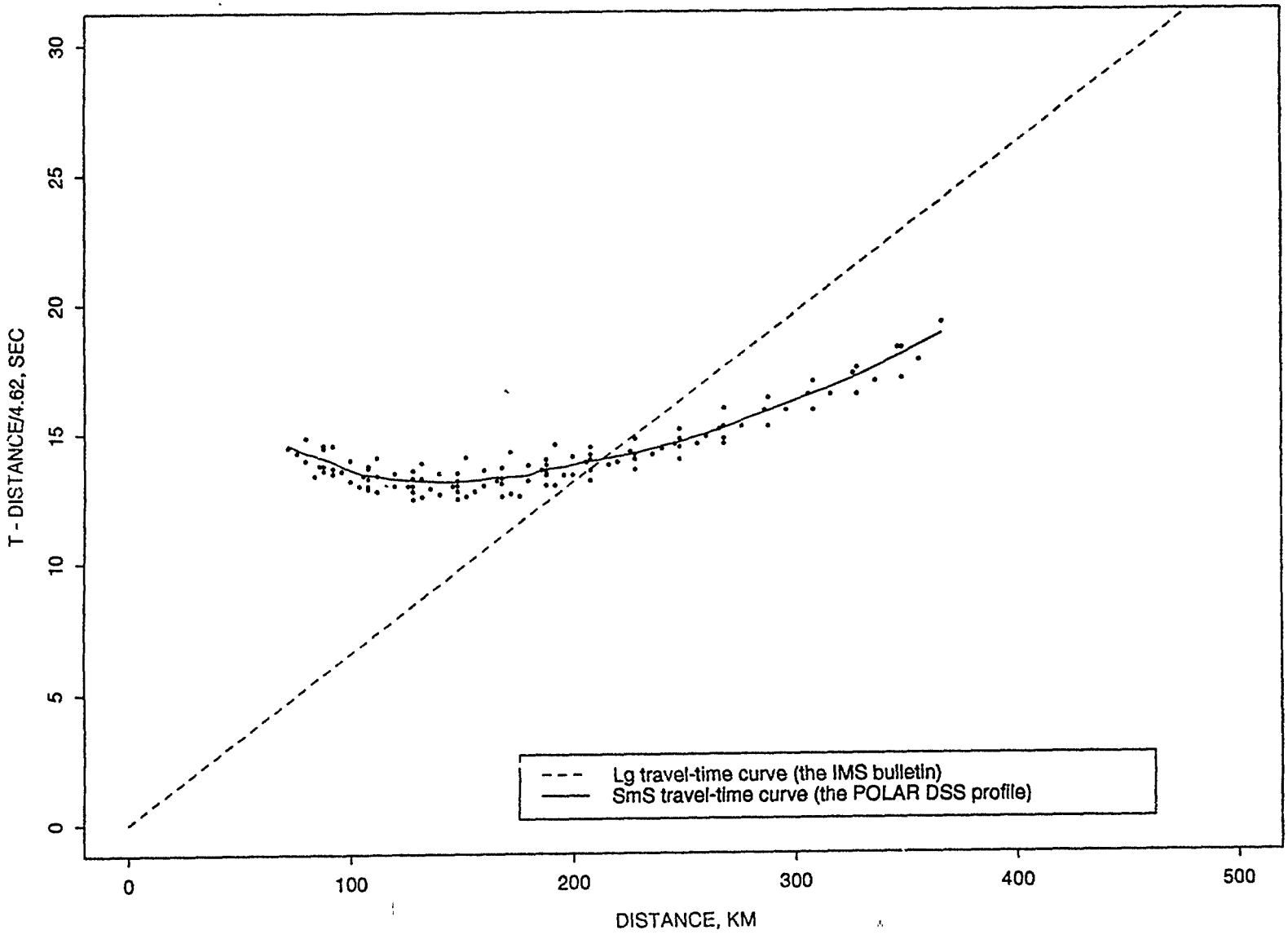

Figure 20: *Comparison of travel-time curves for Lg- and SmS-waves. Lg reference travel-time curve is adapted from the IMS bulletin, and SmS composite travel-time curve is inferred from observations along the POLAR DSS profile.*

defined between 0 and 100 km. *Sg* is more appropriate in this distance range. The intensive *PmP*-wave can also be helpful for event locations within the distance range from 100 to 400 km.

The characteristics of regional phases (phase velocity, frequency, arrival time, etc.) can be used to help identify them in the IMS, but because they are regionally variable, regional knowledge of the characteristics is necessary for automatic identification. This knowledge is contained in DSS observations and can be used as an aid to phase identification.

Acknowledgments

The author is grateful to Carl Romney and Jerry Carter for many fruitful discussions and helpfulness during this work. Lori Grant, Florence Riviére-Barbier, and Anne Suteau-Henson helped to perform the IMS data processing, and their contribution to this study is gratefully acknowledged.

References

Bache, T.C., S.R. Bratt, J. Wang, R.M. Fung, C. Kobryn, and J.M. Given (1990). The Intelligent Monitoring System, *Bull. Seism. Soc. Am.* **80**, 1833-1851.

Blandford, R.R. (1981). Seismic discrimination problems at regional distances, in *Identification of Seismic Sources - Earthquake or Underground Explosion*, D. Reider Publishing Company, Holland, 695-740.

Guggisberg, B. (1986). Eine zweidimensionale refraktionsseismische interpretation der Geschwindigkeits - Tiefen - Struktur des oberen Erdmantels unter dem Fennoskandischen schild (Projekt FENNOLORA), *Diss. ETH Nr. 7945*, Zurich, 199.

Hauser F. and R. Stangl (1990). The structure of the crust and lithosphere in Fennoscandia derived from a joint interpretation of *P*- and *S*-wave data of the FENNOLORA refraction seismic profile, in *Proceedings of the sixth workshop on the European geotraverse project*, 71-92.

Kennett B.L.N. (1992a). The distance dependance of regional discriminants. *Papers presented at 14th annual PL/DARPA seismic research symposium*, 233-238.

Kennett B.L.N. (1992b). Phase identification and location for regional and teleseismic events. *Papers presented at 14th annual PL/DARPA seismic research symposium*, 239-244.

Luosto, U., E.R. Flueh, C.-E. Lund and working group (1989). The crustal structure along the POLAR profile from seismic refraction investigations, *Tectonophysics* 162, 51-85.

Ryaboy, V. (1992). Implications of DSS Observations within Scandinavia and Northwestern Russia for IMS Data Processing, in Research at the Center for Seismic Studies, PL-TR-92-2117(II), 47-102.

Stangl, R. (1990). Die struktur der lithosphare in Schweden, abgeleitet aus einer gemeinsameninterpretation der P- und S- wellen registrierungen auf dem FENNOLORA profil. *Phd. Thesis*, University of Karlsruhe, 154.

Suteau-Henson, A. (1991). Three-component analysis of regional phases at NORESS and ARCESS: polarization and phase identification, *Bull. Seism. Soc. Am.* **81**, 2419-2440.

Suteau-Henson, A., V.Z. Ryaboy, F. Riviére-Barbier, H. Israelsson, and J.A. Carter (1992). Analysis of IMS locations of mine blasts and RMS *Lg* magnitudes in Scandinavia, in *Papers presented at 14th annual PL/DARPA seismic research symposium*, 401-407.

Vogfjord, K.S., Ben Yan and C.A. Langston (1991). Composition of short-period regional phases inferred from Fennoscandian array data, in *Papers presented at 13th annual PL/DARPA seismic research symposium*, 474-479.

Vogfjord, K.S. and C.A. Langston (1992). Short-period regional phases from Fennoscandian arrays, *Papers presented at 14th annual PL/DARPA seismic research symposium*, 450-456.

ML Magnitudes at the IMS Arrays Based on RMS Lg Amplitudes

Hans Israelsson

Introduction

Magnitudes based on RMS amplitudes of the *Lg* phase, introduced by Ringdal (1983) and subsequently studied for a number of cases, have proven to be a robust measure of the strength of underground nuclear explosions (see e.g., Hansen *et al.*, 1990). Determined and analyzed for large events (usually well above *mb(Lg)* of 5), such magnitudes not only correlate closely with yield of explosions with similar coupling, but are also usually remarkably consistent from station to station. The recent shift of focus in nuclear explosion seismology to events in the low magnitude regime, 2-4, raises the issue of whether *Lg* magnitudes maintain their robustness for small magnitude events.

In this report we get some insight into this issue; we calculate and analyze local magnitudes, *ML(Lg)*, based on RMS amplitudes obtained at local and regional epicentral distances, at the four IMS regional-arrays in Northern Europe (Bache et al., 1990). For the magnitude calculations, we adjust procedures developed and applied to recordings at regional and teleseismic distances for large Soviet explosions (Israelsson, 1992). The following questions form the subject of the analysis:

- What is the standard error of *ML(Lg)* from a mini-array?
- How does RMS *Lg* compare with STA/LTA *Lg* amplitudes (currently employed by the IMS; see Bache *et al.*, 1991) with regard to consistency and applicability?
- How does *ML(Lg)* relate to *mb(P)* and yield of mining explosions?

In addition, we discuss in a quantitative manner the effect on *ML(Lg)* of oceanic structures and other barriers along *Lg* propagation paths.

Definition of *Lg* RMS Amplitudes

The data in this study were retrieved from the database for the IMS system at the Center for Seismic Studies, and were limited to events in the period Nov 1990 to May 1992. The vast majority of the events were ripple fired mining explosions. Figure 21 shows the relative location of the four arrays: ARCESS, FINESA, GERESS, and NORESS. The Tornquist zone - a barrier blocking *Lg* waves - is also marked as a heavy dashed line. Figure 22 shows a section of typical recorded waveforms as a function of epicentral distance. The travel paths associated with these waveforms are outlined in Figure 21. The records in Figure 22, which were aligned manually on the first arrival *P* phase, show the development of

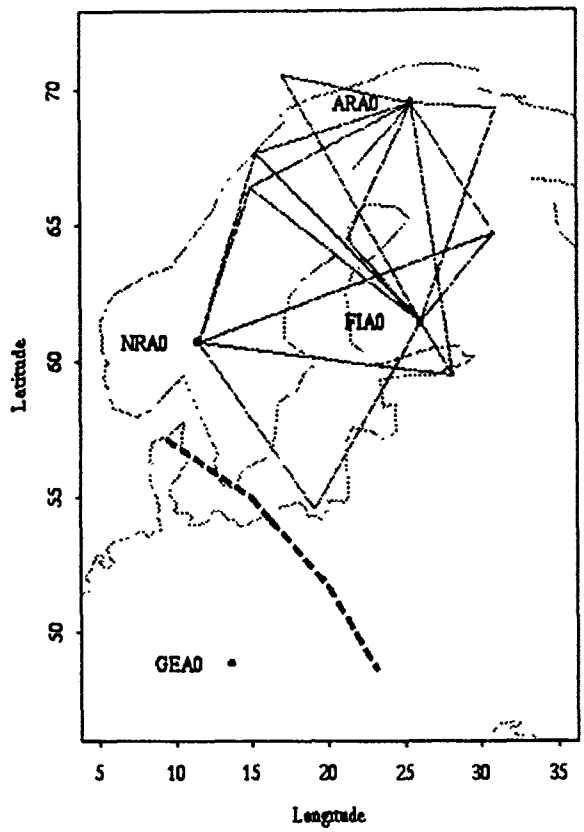

Figure 21: *The relative locations of the mini arrays and the travel paths for the waveforms of the record section in Figure 22.*

the *Sn* and *Lg* phases (in the group velocity window 3.10-3.65 km/s) typical of many Fennoscandian paths. *Lg* is, indeed, the most pronounced phase. At distances less than around 250 km, however, there is strong interference with *Sn*.

Although not apparent from the waveforms in Figure 22, there may sometimes also be interference in the coda of *Lg* with the *Rg* phase, which has a group velocity of typically around 3.0 km/s. *Rg* is recorded at distances primarily less than 250 km by the IMS stations (see Figure 23a). Hence, the time window over which RMS amplitudes of *Lg* and its coda is calculated should seek to avoid corruption by both *Sn* and *Rg* to the largest extent possible. For this purpose the RMS *Lg* amplitudes were calculated over the group velocity window 3.10-3.65 km/s (indicated in the record section of Figure 22). In some regions of Fennoscandia the Moho-reflected *SmS* with multiples may be prominent up to about 400 km in this velocity window, and may, therefore, further compound the corruption of *Lg* (Vogsfjord and Langston, 1990; Vogsfjord *et al.*, 1991).

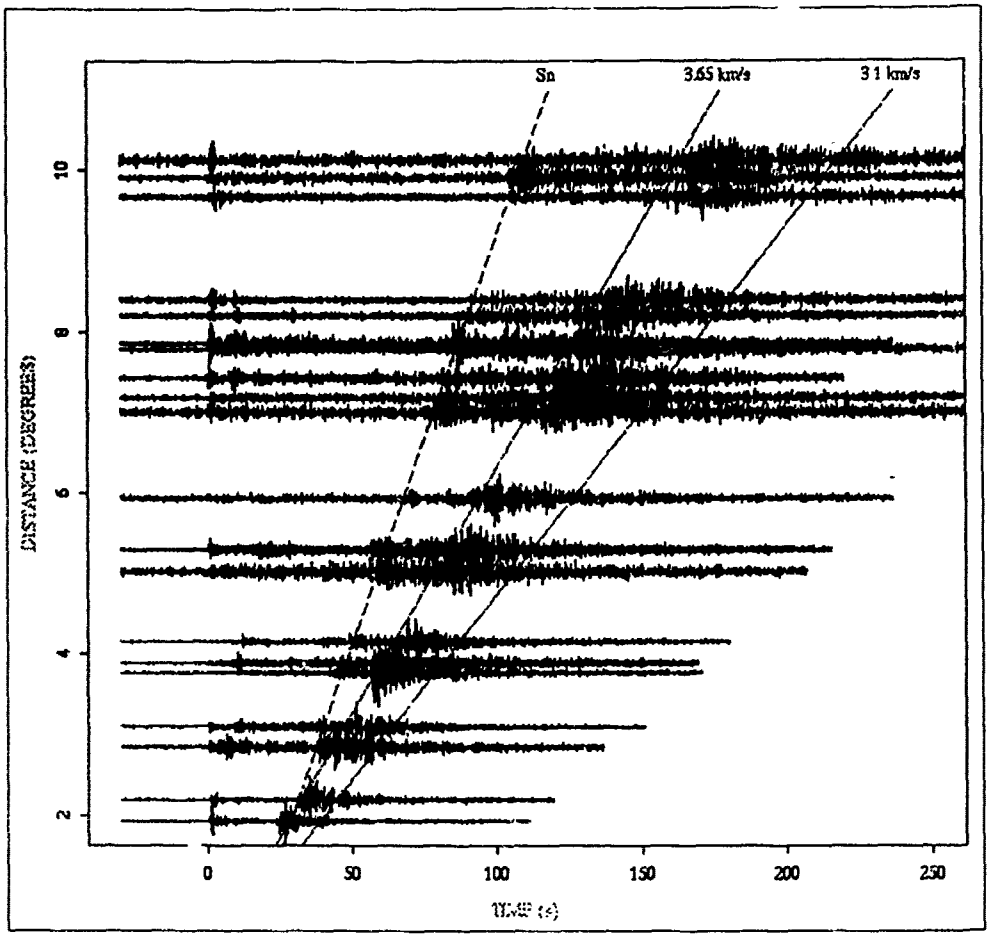

Figure 22: *Waveforms at the arrays for some paths in Fennoscandia (see Figure 21) plotted as a function of epicentral distance. The expected arrival time of Sn and the group velocities of 3.1 and 3.5 km/s are marked on the record section.*

The effect of interference with *Sn* and *Rg* near either end of the group velocity window can be reduced to some degree by band-pass filtering. The *Rg* phase has its dominant frequency usually around 1.0 Hz and it seldom exceeds 1.5 Hz for epicentral distances beyond 250 km (see Figure 23a). Furthermore, the average frequency of the *Sn* phase is usually higher than *Lg* as shown by the comparison in Figure 23b of the dominant frequencies (automatically measured by the IMS system on detecting beams) of *Sn* and *Lg* at the four arrays as a function of epicentral distance. The data in Figure 23a-b lead us to choose the frequency band 1.5-4.0 Hz for calculation of the RMS *Lg* amplitudes. This band differs only slightly from the 2-4 Hz band employed by the automatic processing of the IMS in its calculation of *Lg* amplitudes used for magnitude determinations (Bache *et*

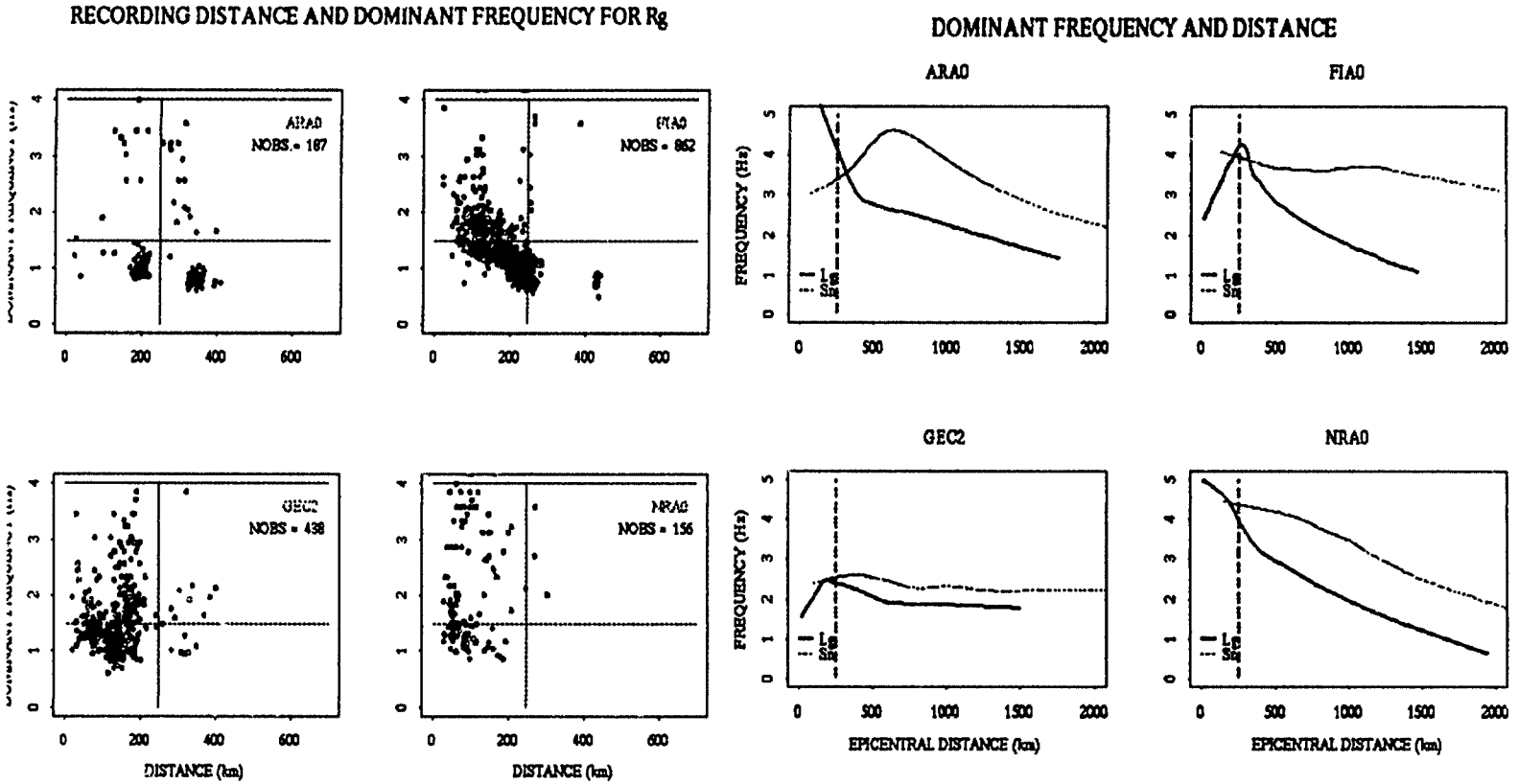

Figure 23: (a) Dominant frequency and epicentral distance of Rg phases identified by the IMS system during its operation from May 1991 to May 1992. The frequency band 1.5-4.0 Hz employed for the RMS amplitude calculations is indicated by the two horizontal lines and the 250 km epicentral distance is drawn as a vertical line in the diagrams. (b) Dominant frequency as a function of epicentral distance for the Sn and Lg phases at the four arrays. The curves represent smoothed averages of defining phases recorded over a period of one year (May 1991 - May 1992) with several thousand observations for most of the curves.

al.,1991). These automatically determined IMS amplitudes are really short-term averages, STA, corrected for long-term averages of the initial phase, LTA; both averages are measured on the incoherent, i.e., unsteered beam.

The length of the time window for RMS *Lg* varies linearly with distance, being about 12 and 48 s at 250 and 1000 km, respectively. The STA used by IMS is based on a 2 s window regardless of distance. The positioning of the group velocity window for a recording is determined by the origin time and location of the IMS. Consequently, errors in location and origin time may introduce errors in positioning the group velocity window, which in turn may result in erroneous RMS amplitudes. For recordings obtained at large distances this effect will most likely be negligible, whereas at shorter distances it may be more pronounced.

The RMS amplitudes, calculated for the bandpass filtered traces for each array element, were converted to ground motion using a constant calibration factor independent of frequency. Noise corrections, based on a noise sample of 60 s prior to the first arrival time, were also applied in accordance with the procedure by Ringdal and Hokland (1987). A minimum signal-to-noise ratio (i.e., RMS *Lg* amplitude uncorrected for noise/RMS amplitude for noise sample prior to first arrival) of 1.1 was required for RMS amplitudes to be calculated. Amplitudes of elements were rejected if the logarithmic value deviated by more than 0.3 magnitude unit, m.u., from the median value of the elements. Finally, if RMS amplitudes at more than 4 array elements had insufficient SNR or data were missing, no RMS amplitudes were defined for the array.

Stability of RMS *Lg* Amplitudes

In order to study the stability of the RMS *Lg* amplitudes of the array elements, we analyzed amplitudes from suites of closely spaced events assuming the logarithm of the RMS *Lg* amplitude, rms_{ij}, at element j for event i can be written as: $rms_{ij} = s_i + c_j + e_{ij}$. Here s_i represent the array average RMS amplitude on a logarithmic scale of event i, c_j the site amplification of array element j, and e_{ij} an error term with zero mean and standard deviation s_{ij}. We also impose the condition: $\Sigma c_j=0$, on the site amplifications.

The error terms, e_{ij}, or residuals: $rms_{ij} - s_i - c_j$, were approximately Gaussian (see Figure 24) with a standard deviation of about 0.05 m.u. Amplitudes at elements of an array that were closely spaced were also correlated as suggested by the data in Figure 25, which shows the correlation coefficient of the residuals as a function of the separation between array element pairs. The correlation drops rapidly with distance, and for a separation of 500 m or more there appears to be virtually no correlation. The standard deviation of the residuals seems to depend on several factors. First of all, it is a function of the SNR as

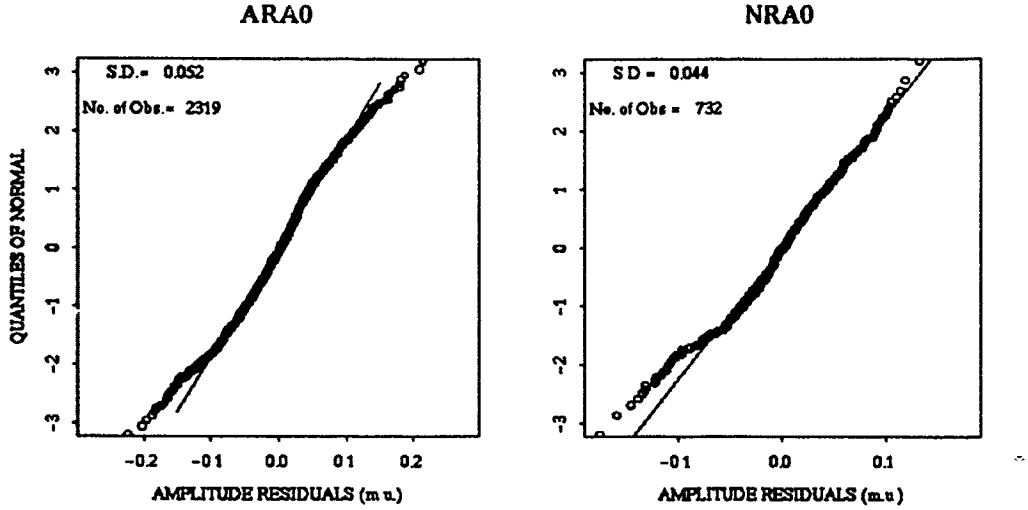

Figure 24: *Empirical distributions of the RMS amplitude residuals (on a logarithmic scale) at the elements of ARCESS (to the left, ARA0) and NORESS (to the right, NRA0) for a suite of mining events near latitude 67.64N and longitude 33.64E. The data are compared in Gaussian probability plots.*

indicated by the smoothed curves in Figure 26, which show a larger standard deviation for SNR below about 2.0. Interestingly enough, the residuals with very low SNR also appeared to be biased low. A comparison of the two standard deviation curves for ARCESS and NORESS in Figure 26 suggests that the standard deviation can be affected by the epicentral distance; the standard deviation for NORESS, at the larger epicentral distance (about 1300 km), is smaller than that for ARCESS (about 400 km) for similar SNR above 2.0. This can be expected as the length and positioning of the time window for the RMS amplitude calculations become more sensitive to location errors for data recorded at shorter distances.

Estimates for the site amplifications, c_j, obtained from suites of events in several different azimuths from a given array were quite similar. This apparent 'isotropy' of the *Lg* site amplifications is strikingly different from observations of teleseismic *P* waves, which, at least, at NORSAR have site amplifications that vary strongly with azimuth of approach. Averages of *cj*, shown in Figure 27 together with associated error bars, range over about 0.2 magnitude unit (m.u.) or more for a given array.

Figure 28 shows that the estimated site amplifications correlate closely with the relative seismic noise levels at the array elements. For NORESS, the only array for which the map-

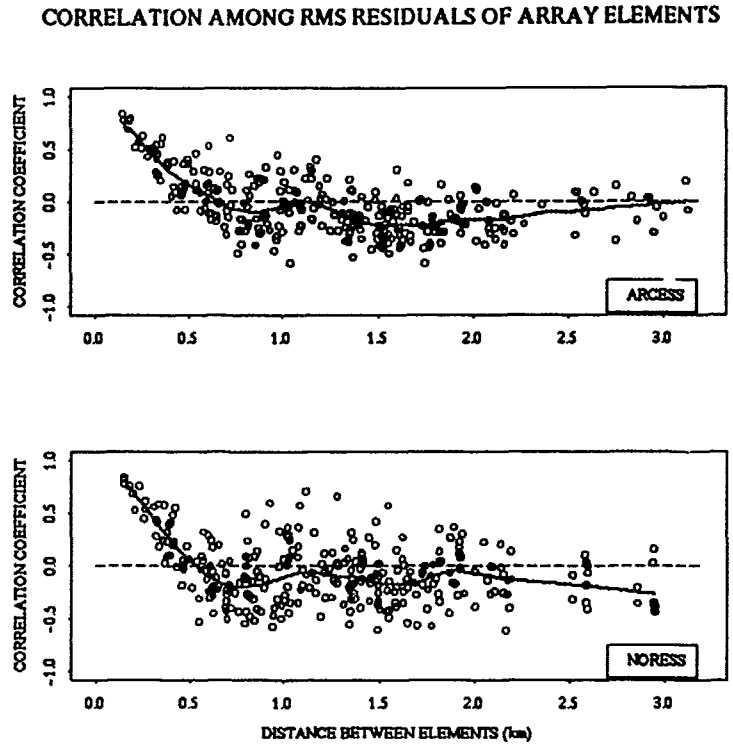

Figure 25: *The upper (for ARCESS) and lower (for NORESS) frames compare the correlation coefficients for Lg RMS amplitude residuals among array elements plotted as a function of distance between element pairs. The amplitudes were obtained for a suite of events near 67.64N and longitude 33.64E*

ping of the local surface geology was available (Mykkeltveit, 1987), the site amplifications also show correlation with surface structure (Figure 29). Array elements located in a narrow linear zone of gabbro - with density higher than the surrounding granite and rhyolite - have the smallest amplifications. The large amplifications of the two GERESS elements GEA0 and GEB2 is probably due to the fact that they are not sited on bedrock. The site amplifications at ARCESS and FINESA vary in a systematic fashion across the arrays with lower values in the Southeastern elements of the array.

For a given array, the term s_i, as defined by the simple additive model above, represents an average array amplitude on a logarithmic scale. The model assumes all rms_{ij} are independent and have equal standard deviation. An additive model weighted with the covariance matrix of the residuals would provide an estimate that takes into account the correlations of amplitudes at array elements that are closely spaced. For the sake of simplicity, we did

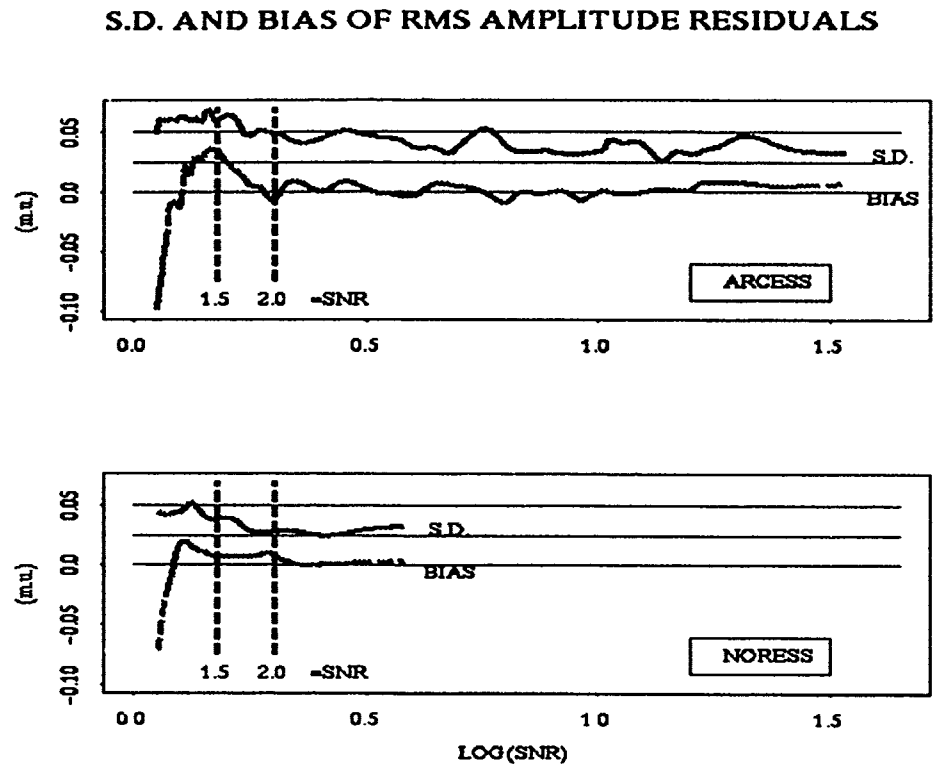

Figure 26: *Standard deviations and bias as a function of signal-to-noise ratio for RMS Lg amplitudes at array elements from a suite of events near latitude 67.64N and longitude 33.64E.*

not, however, correct for the correlation structure of the RMS amplitudes at the array elements in the calculations of s_i.

Definition of Array Magnitudes

In order to define a local magnitude for the array RMS amplitudes, we need to estimate their attenuation with epicentral distance, and to normalize to a reference magnitude scale. For the distance attenuation we fit array amplitudes, s_{ij}, for events, i, at the Fennoscandian arrays, j, to the following model: $s_{ij} = m_i + G(D_{ij}) - g\ log10(e)\ D_{ij} + b_j + e_{ij}$. The source term, m_i, represents the relative size of the event i, the geometrical spreading $G(D)=log10(D^{-1/3}\ sin(D)^{-1/2})$; g represents the spatial decay rate of non-elastic attenuation (Nuttli, 1973); b_j represents the average amplification at array j. As for the model in the previous section we imposed the condition: $\Sigma b_j=0$, on the array amplifications. We

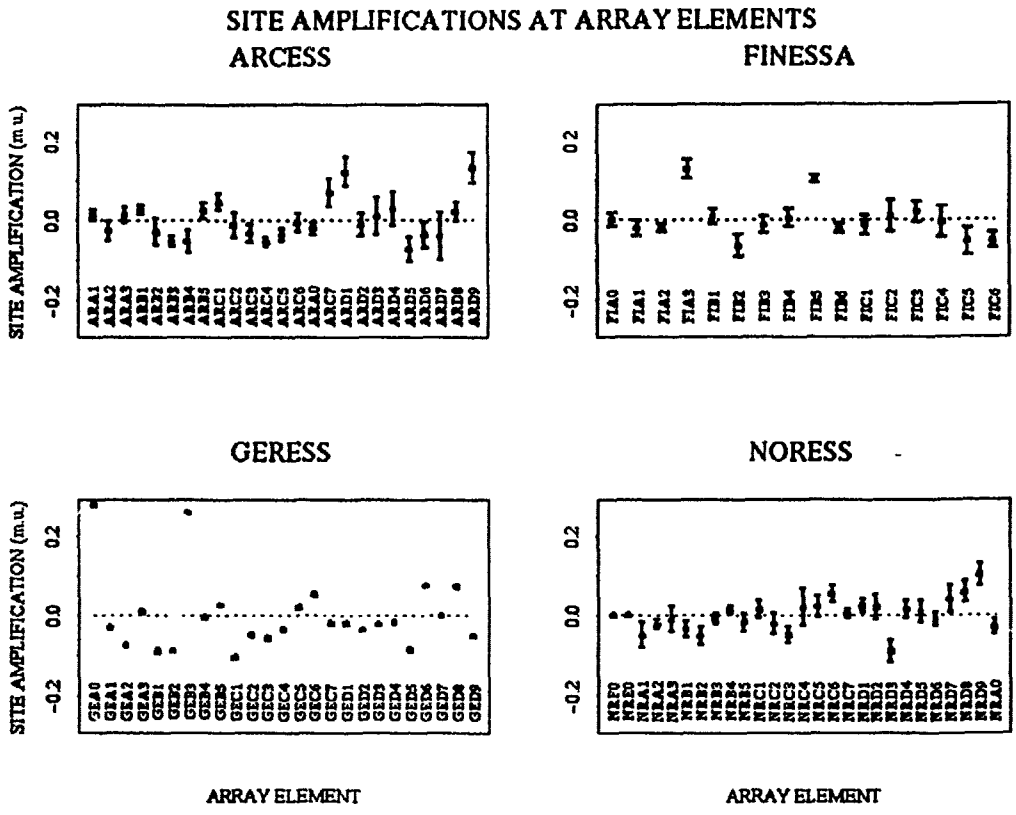

Figure 27: *Site amplifications at array elements of the four mini arrays. Error bars (not sufficient data for GERESS) indicate scatter in the estimates.*

estimated the source and amplification terms and the decay rate, g, with a standard least squares procedure using data for 52 mining explosions at 7 different locations in Fennoscandia and Western Russia. Only data at the Fennoscandian arrays were used, as there were only a small number of events with data common to GERESS.

The resulting g value of 0.00182 ± 0.00009 km^{-1} corresponds to a Q value of about 740 at 1.5 Hz and a group velocity of about 3.5 km/s for *Lg*. The attenuation of the RMS *Lg* amplitudes defined by the geometrical spreading and the non-elastic attenuation is almost identical to the attenuation curves derived by Bache *et al.* (1991) for *Lg* based on 1500 events.

The array amplifications b_j vary within about 0.1 m.u. with the largest value at ARCESS.

In order to bring the array amplitudes, s_{ij}, or equivalently, averages of rms_{ij} - c_j, corrected

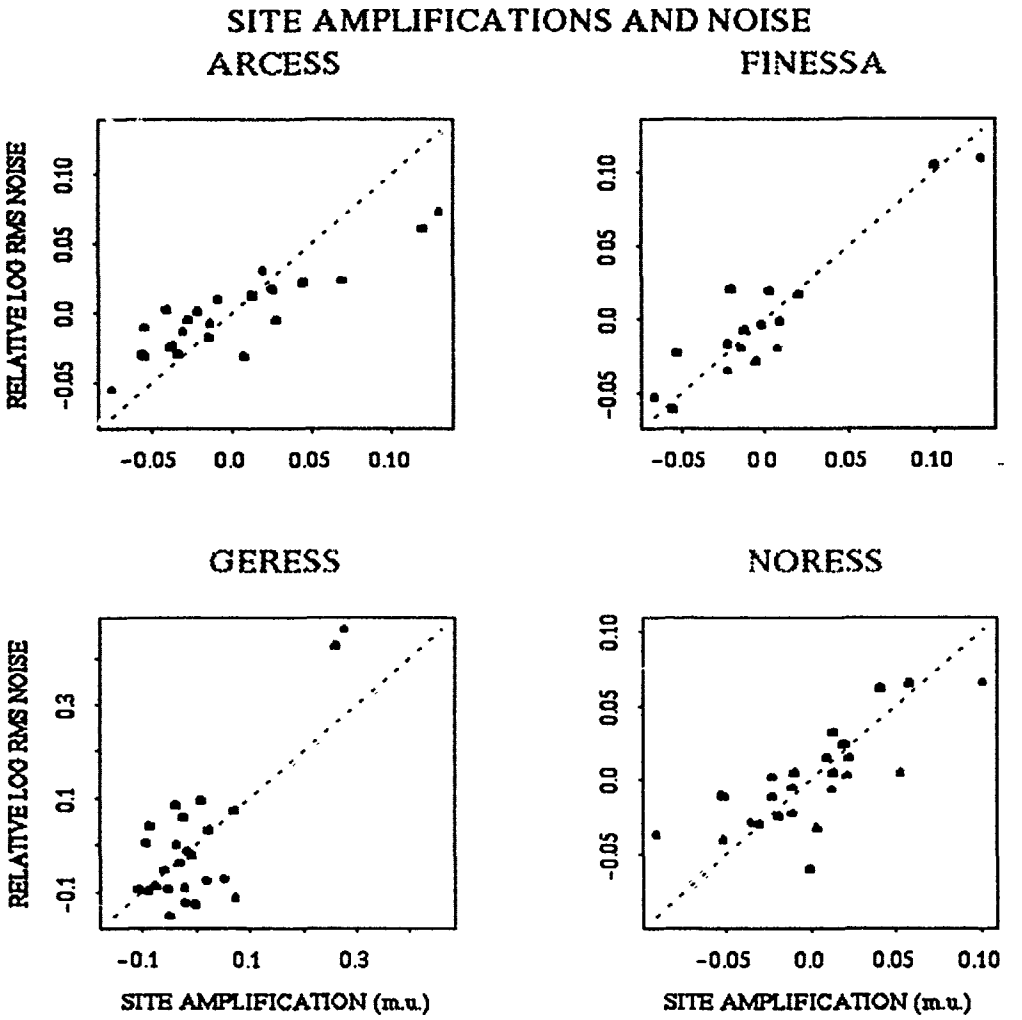

Figure 28: *Comparison of site amplifications and relative noise amplitudes at the array elements of the four arrays*

for distances, on a local magnitude scale we calculate a normalization constant a, so that the source terms, m_i, agree with the local magnitudes, ML, reported by the IMS, which in turn were normalized to the ML scale by Bath *et al.* (1976). Due to the lack of data for GERESS we assumed that the attenuation estimated for the Fennoscandian arrays was valid for GERESS as well, although the study by Sereno *et al.* (1992) and the crustal and upper mantle structures suggest a higher attenuation for paths to GERESS than across Fennoscandia (Guterach *et al.*, 1986).

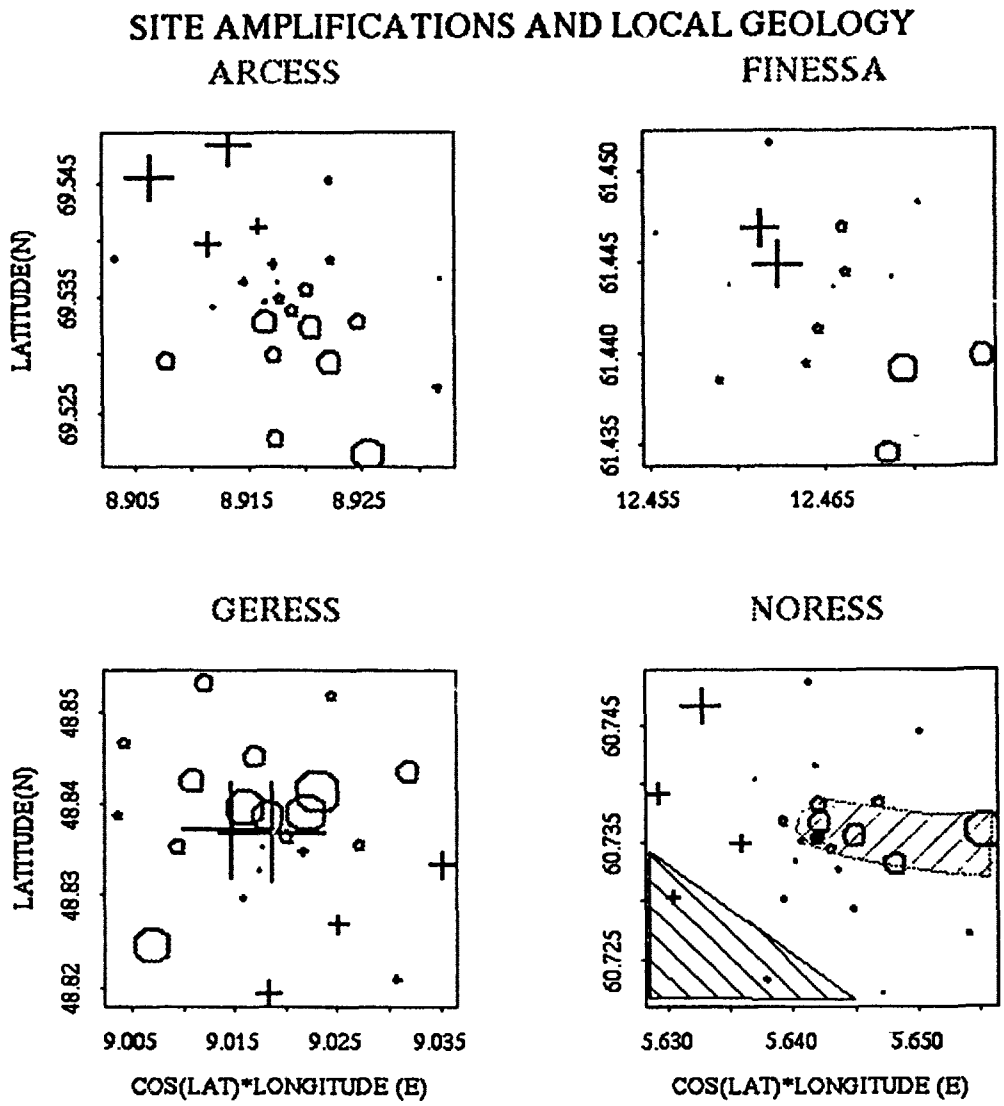

Figure 29: *Site amplifications plotted as a function of the relative location of the array elements. Plus signs and open circles are used for positive and negative site amplifications respectively. The diameter of a symbol is directly proportional to the modulus of the site amplification. The local surface geology according to Mykkeltveit (1987) is outlined for NORESS; the background of granite is interspersed by a triangular shaped rhyolite block in the SW part of the array and by a narrow linear zone of gabbro running from the central part of the array almost due east.*

Stability of Array Magnitudes

In earlier studies the stability of *mb(Lg)* based on RMS amplitudes of *Lg* has been demonstrated by pairwise comparisons of station magnitudes for suites of closely spaced events, i.e., for which the propagation paths are similar from event to event to the station pairs (Hansen *et al.*, 1990). Here, we made similar comparisons for suites of mining explosions in different parts of the operational area of the arrays. The results for eight such pairwise comparisons are summarized by the scatter diagrams in Figure 30 and by Table 8

Table 8: Stability of rms Lg magnitudes

Epicenter		Distance to array				NOBS	S.D.
Lat(N)	Lon(E)	ARA0	FIA0	GEA0	NRA0		
67.34	33.64	3.53	7.03			32	0.085
		3.53			11.80	30	0.096
			7.03		11.80	25	0.054
60.90	29.17	8.80	1.59			18	0.075
		8.80			8.16	22	0.069
			1.59		8.16	19	0.061
54.35	19.25		7.98		7.62	10	0.040
51.61	16.25			3.22	9.51	15	0.075

The events were selected on the basis of clustering of the IMS locations. For each case in Figure 30, amplitudes were calculated for events within 10 km of the epicenter given at the top of each scatter diagram. As the epicentral distances between each of the two stations and the events for a given case in Figure 30 were practically constant, array amplitudes (on a logarithmic scale) uncorrected for attenuation with distance were used instead of magnitudes in the comparisons. Apart from a few outlying data points, the station magnitudes are in good agreement. In addition to the number of observations, NOBS, a few other parameters are given in the top left corner of each scatter diagram. SIGMA and SLOPE represent the misfit error and slope of a straight line obtained on the assumption of equal error in the two station magnitudes, and S.D. is the standard error of the difference between the two array amplitudes divided by the square root of two. Outliers, marked with crosses, were omitted for the estimates of SIGMA, SLOPE, and S.D. The estimated misfit

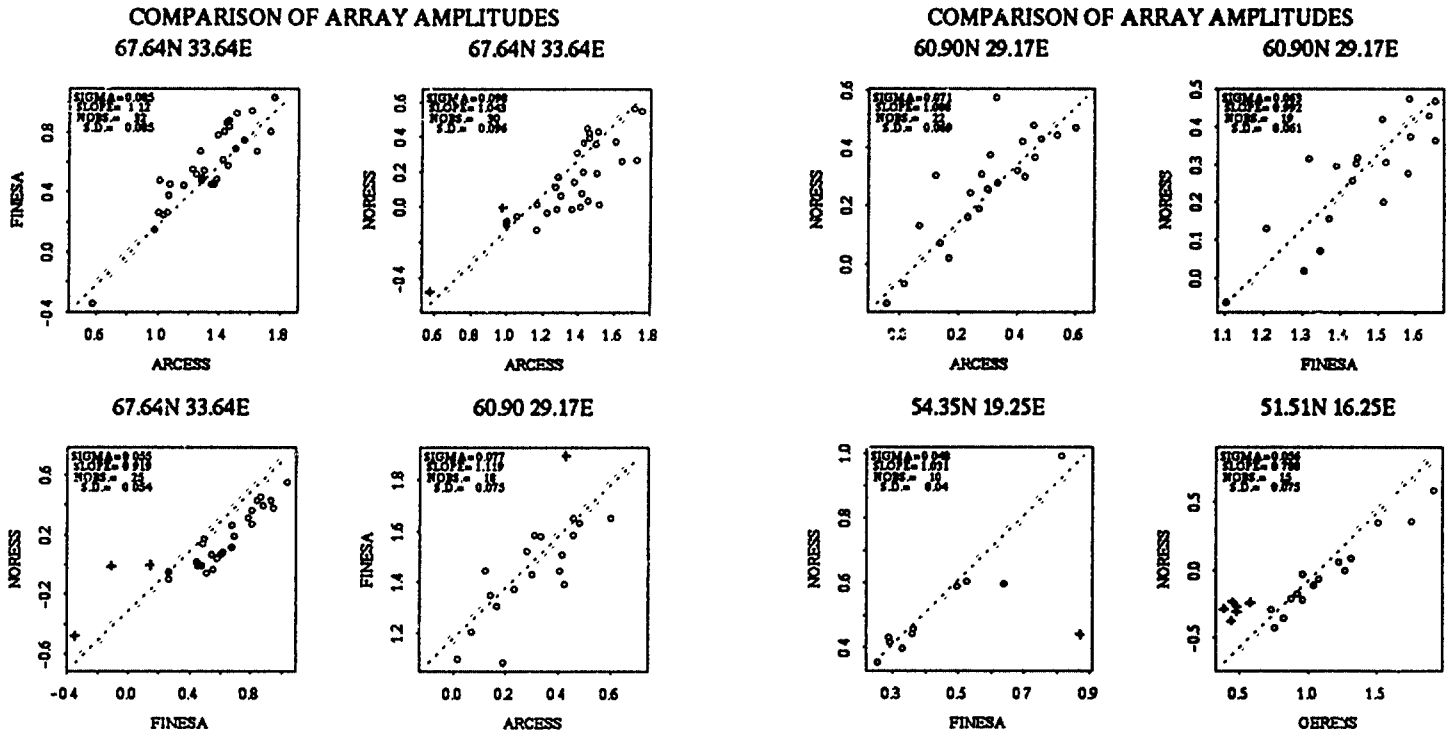

Figure 30: *Comparisons of array amplitudes for suites of closely spaced events. The approximate locations of the events are indicated above each scatter diagram. Outlying observations are marked with plus signs*

error is between 0.04 to 0.10 m.u. One data point has a discrepancy of more than 0.5 m.u. (for the 54.35 N and 19.25 E case). The other outlying data points can be associated with small amplitudes and hence poor SNR (cases 67.64 N, 33.64 E for FINESA and NORESS and 51.51 N 16.25 E for GERESS and NORESS). The summary in Table 8 suggests that the epicentral distances to the two arrays in a given comparison do not seem to have any dominant effect on the size of the misfit error for these particular suites of events.

In Figure 31 we compare the consistency of array magnitudes for events that are broadly distributed within the operational area of the arrays. The locations of the events in Figure 31 were all based on three or more IMS arrays. The pairwise comparisons are made for NORESS/ARCESS and NORESS/FINESA and for each case we give the number of observations, misfit error, slope, and standard error. In addition, the bias, defined as the median of the differences between array magnitudes, is given in the scatter diagrams of Figure 31. The geographical distributions of the events are shown on the maps to the right in the figure. Outlying data points are marked with asterisks both in the scatter diagrams and on the maps. Twelve of the 239 events with three or more array magnitudes having a range of at least 0.5 m.u. and 9 out of 384 events for which magnitudes could be computed for 2 arrays only, were identified as outliers. This corresponds to outlier rates of about 5% and 2% respectively. No clear geographical distribution can be seen for the outliers, although in the NORESS/FINESA case, the outliers are all located to the east of FINESA at large distances from NORESS. These events are often recorded with small amplitudes, and thus poor SNR, at NORESS. In spite of the broad geographical distribution, the array magnitudes show good agreement with misfit errors just above 0.1 m.u., which is somewhat larger than for suites of closely spaced events.

Although *Lg* is usually the dominant secondary phase for propagation paths confined to continental shield structures, it is frequently blocked for paths crossing significant tectonic boundaries. The Tornquist line which separates the 25-35 km thick crust of the Paleozoic Platform in Central and Western Europe from the 45-55 km thick crust of the East European platform (Guterach *et al.*, 1986) is an effective barrier for *Lg* waves from events recorded at NORESS (Kvaerna and Mykkeltveit, 1985; Gibowicz, 1987). In Figure 32 we compare *ML(Lg)* array magnitudes at NORESS and FINESA with those at GERESS for events on either side of the Tornquist line. The frames to the left compare the magnitude values and the frames to the right show the magnitude differences, GERESS-FINESA and GERESS-NORESS, as a function of location. Plus signs and open circles are used to indicate positive and negative values respectively; the diameter of the symbol is directly proportional to the modulus of the difference. Unfortunately only one of the events is located to the north of the Tornquist line. The events in Poland, south of the Tornquist line, have, with one exception, consistently larger magnitudes at GERESS. Magnitudes for events in

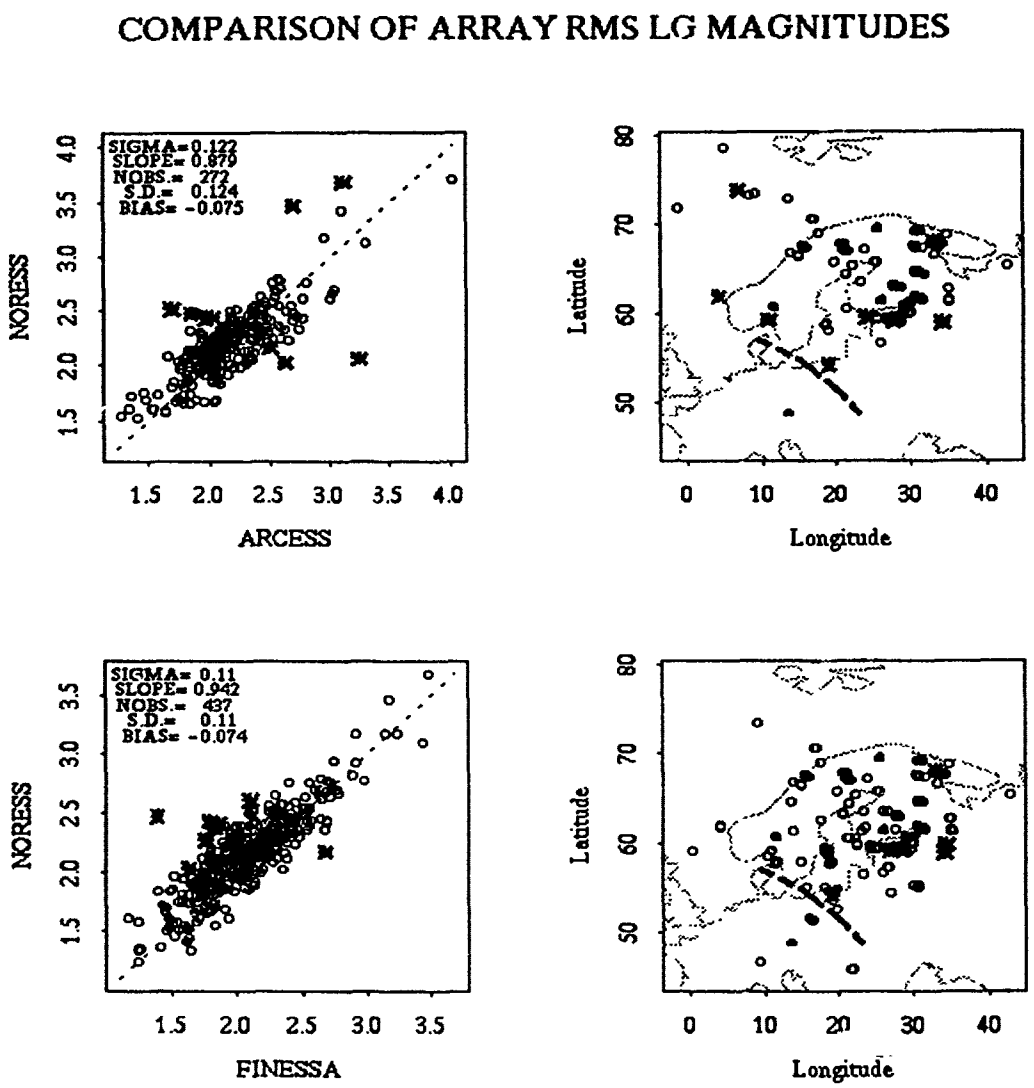

Figure 31: *Comparisons of array magnitudes, ML(Lg), for events widely distributed within the operational range of the arrays. Outlying observations are indicated - in both ML scatter diagrams and on the maps - as asterisks.*

Romania are consistently lower at GERESS compared to those at FINESA and NORESS. The *Lg* path to GERESS may in this case be subject to more blockage than paths to FINESA and NORESS by the major mountain belts of Central Europe. The comparison of the magnitudes in Figure 32, however, is complicated by the uncertainty in the amplitude distance curve applied here to the GERESS data. As emphasized above, this curve was obtained from paths to the Fennoscandian arrays and may underestimate the attenuation to

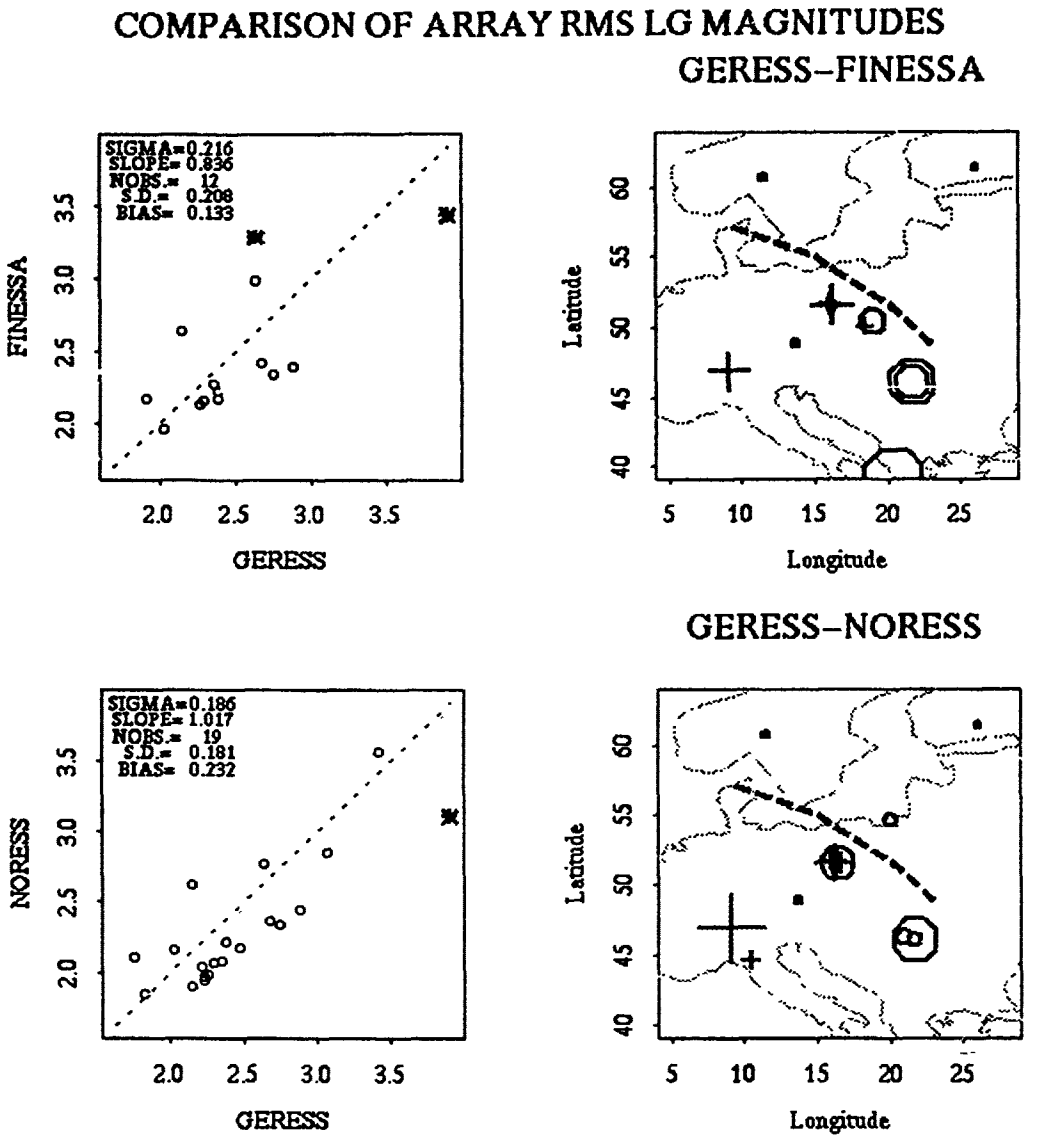

Figure 32: *Comparisons of GERESS array magnitudes with those at NORESS and FINESA. Outlying observations in the scatter diagrams are marked as asterisks. Magnitudes differences, ML(GERESS)-ML(FINESA) and ML(GERESS)-ML(NORESS), are shown on the maps to the right. Positive and negative values are represented by plus and open circles respectively, and the diameter of the symbols is directly proportional to the size of the residual.*

GERESS.

Finally, in Figure 33 we compare the consistency of *ML(Lg)* based on the RMS amplitudes and those defined by the short and long-term average amplitudes, STA/LTA, of the automatic IMS processing as described by Bache *et al.* (1991). The comparison is limited to FINESA and ARCESS events for which waveform data were available in the database to allow calculation of RMS amplitudes. The standard deviation of ML magnitudes is clearly smaller for RMS than for STA/LTA data. The larger scatter in the STA/LTA data may be explained by the fact that the STA/LTA magnitudes are based on a purely automatic procedure and *Lg* may, in some instances, have been mis-identified by the automatic system.

Array *ML(Lg)*, *mb(P)*, and Explosion Yields

It is of some interest to compare the local *ML(Lg)* magnitudes to the standard *mb(P)* scale. Body magnitudes determined by NEIS were the only *mb(P)* data (for 37 events) available for comparison. The NEIS magnitudes for these 37 events are typically based on 10 stations distributed at distances less than 30 degrees. The NEIS determinations are 25% trimmed mean values of station magnitudes. Furthermore, data for PKP arrivals or *P* arrivals recorded at distances less than 5 degrees are not included in the mean values. Since *mb(P)* is below 5.0 for most of the events, they are probably biased. Therefore we applied empirical bias corrections derived from differences of average and maximum likelihood magnitudes calculated by Ringdal (1986). In Figure 34 we compare the bias corrected NEIS *mb(P)* with *ML(Lg)* at GERESS and NORESS. There is significant scatter in the data and the *ML(Lg)* values are about 1 - 1.5 magnitude units smaller than those for *mb(P)*. There is also an indication in the data that $dML(Lg)/dmb(P) < 1$. This is to be expected due to the high-frequency band (1.5-4.0 Hz) used for *ML(Lg)* compared to dominant periods typically around or slightly less than 1 s for *mb(P)*. All events for GERESS in Figure 34 are continental and south of the Tornquist line. The distance correction used for GERESS *ML(Lg)* may exaggerate the actual differences in magnitudes between *mb(P)* and *ML(Lg)* as the attenuation for *Lg* phases recorded at GERESS appears to be larger than for paths to the Fennoscandian arrays (Sereno *et al.*, 1992). The events for NORESS are, with the exception of one event in Northern Norway, either oceanic, in the Atlantic, or south of the Tornquist line. Both oceanic paths and paths crossing the Tornquist line are likely to attenuate or block the *Lg* phase, and these effects may magnify the difference between *mb(P)* and *ML(Lg)* for NORESS.

As mentioned earlier, the vast majority of the events analyzed here are ripple fired explosions carried out for mining or other industrial purposes. Although efforts are under way to

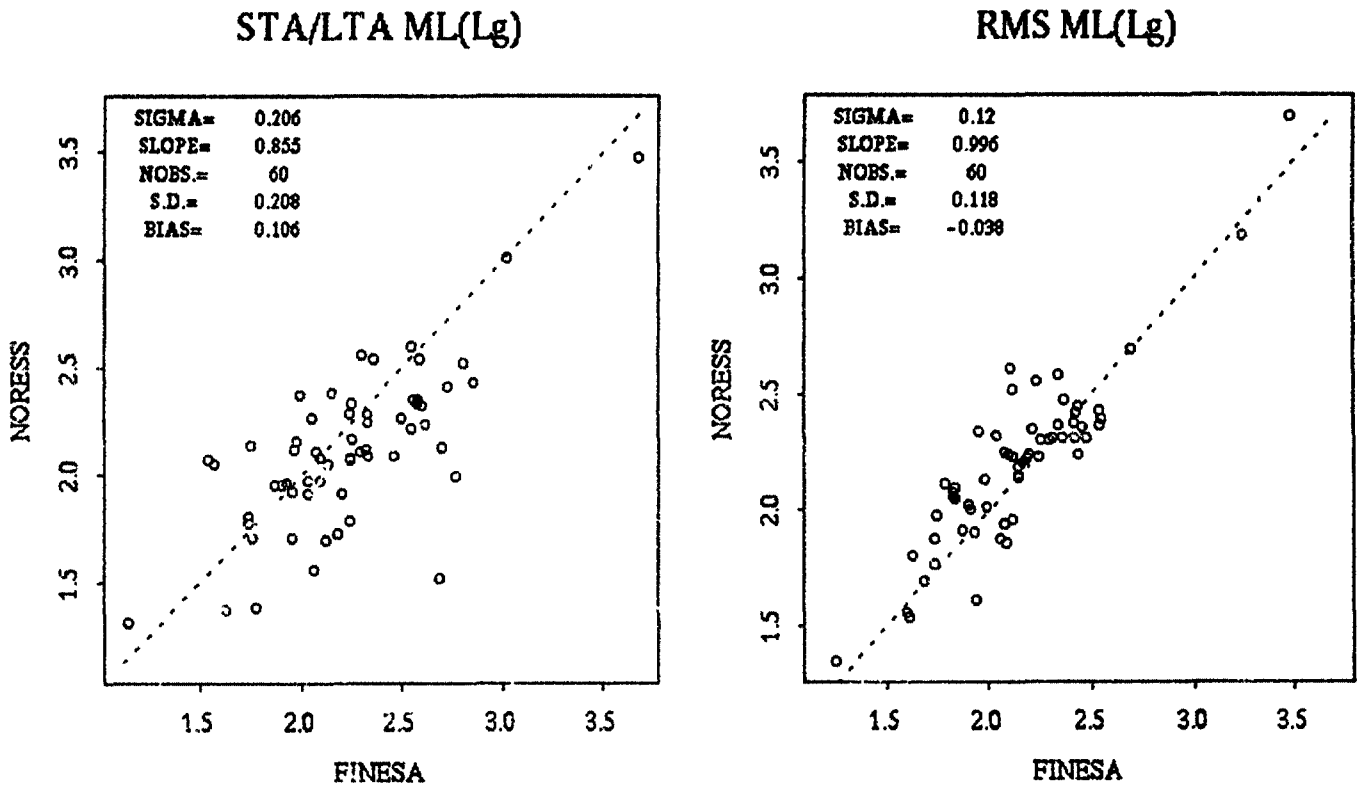

Figure 33: Comparison of the consistency of array magnitudes based on the short term/long term ratio of the Lg phase (to the left) and RMS amplitudes (to the right) for 67 common events.

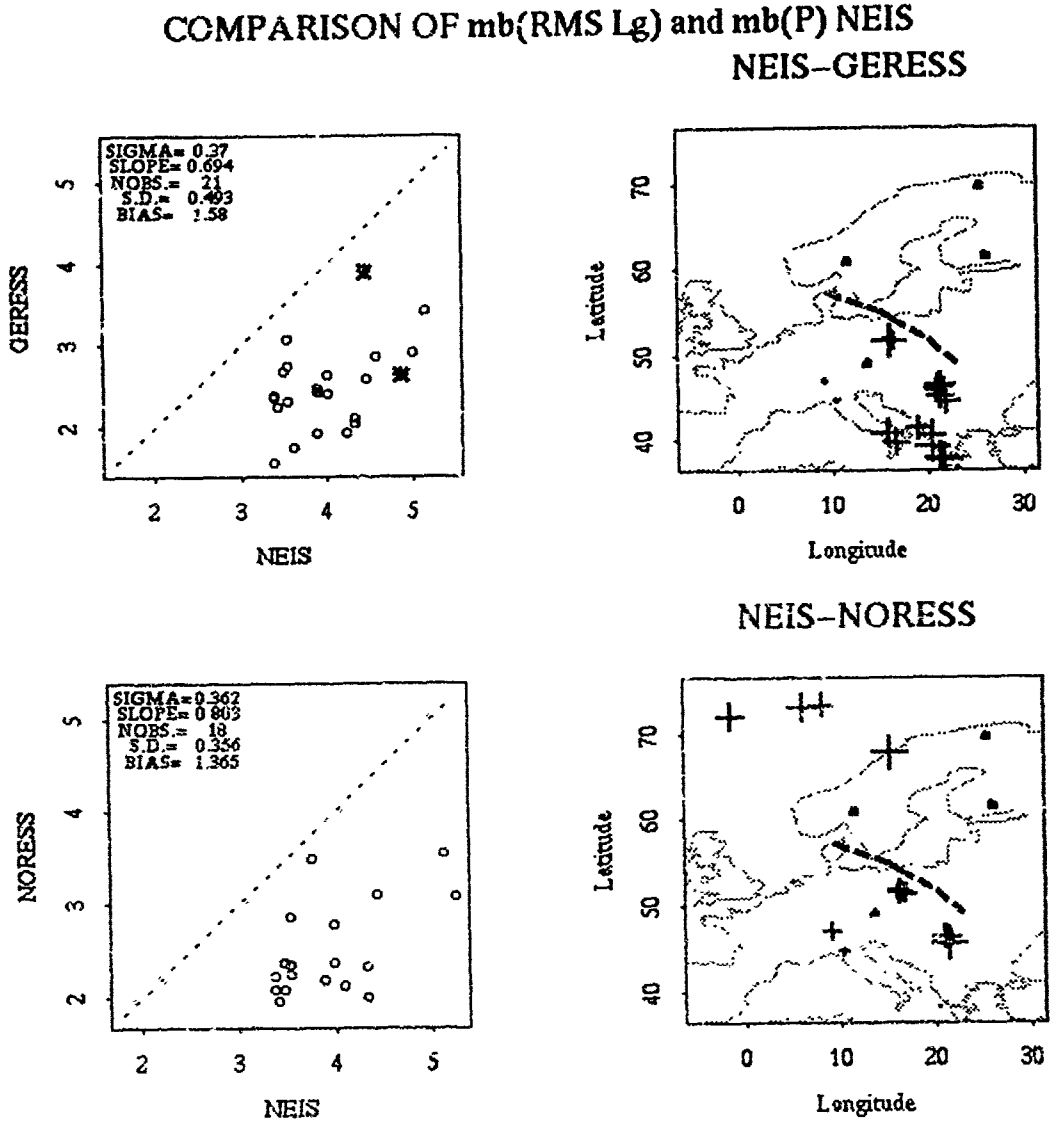

Figure 34: *Comparison of ML(Lg) at the arrays and mb(P) reported by NEIS.*

compile yield and other shot parameters for the explosions (Dahle *et al.* 1989; Grant and Coyne, 1992), such data are currently available only for a small number of events. In Figure 35 we compare the *ML(Lg)* at the three Fennoscandian arrays and the total tonnage of some explosions at the Kirunavaara mine in Northern Sweden based on information provided by Enback (personal communication, 1992). These explosions, that were comprehensive salvos, consisted of between 50 and 150 tons of slurry - a fluid explosive - distributed in holes with a 6.5 inch diameter. The explosive in the holes (between 0.5 to

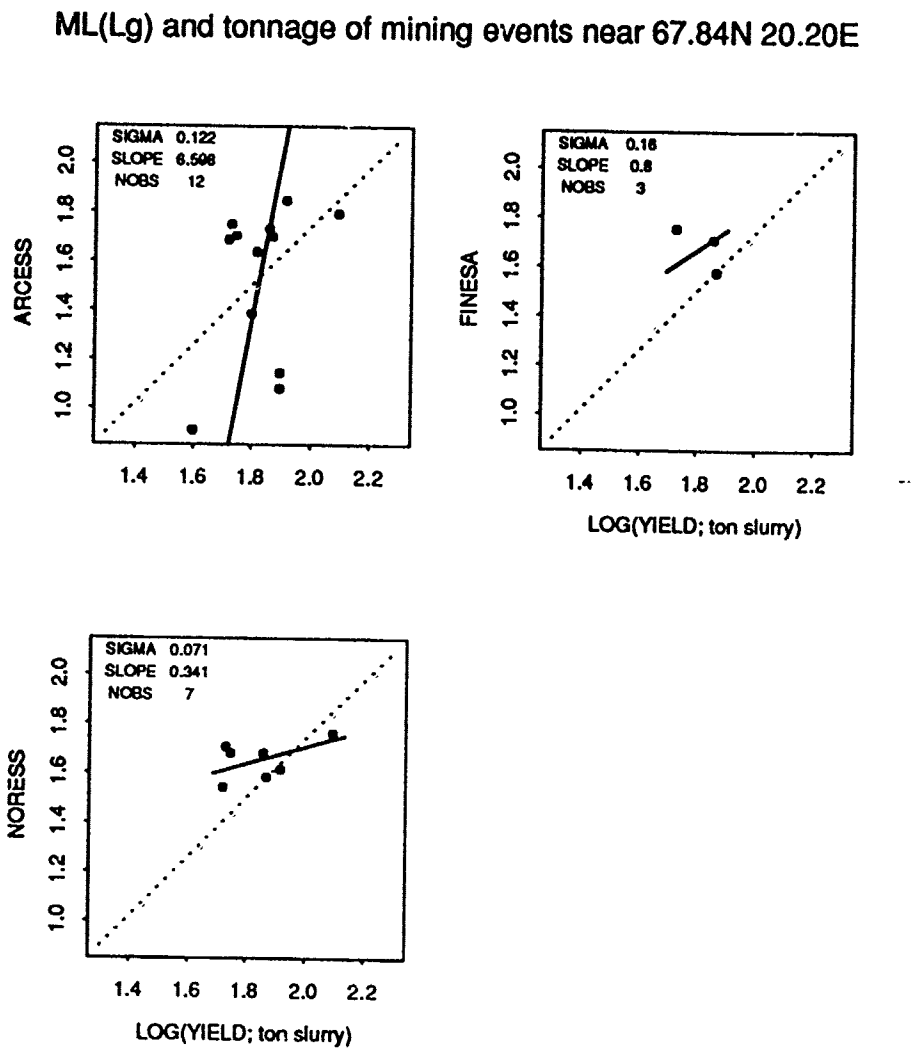

Figure 35: *Comparison of ML(Lg) and total tonnage of mine explosions at the Kiruna mine in Northern Sweden.*

about 3 tons in each hole) was set off sequentially with a delay typically between 25 and 30 ms. The wide scatter and large slope value for the ARCESS data may be due to the scatter and bias of the IMS locations. Suteau-Henson *et al.* (1992) have demonstrated a systematic bias in the IMS locations for events at the Kirunavaara mine due to mis-identification of the *Lg* phase. Scatter in the locations will cause scatter in the positioning of the

group velocity window (3.1-3.65 km/s) used for the RMS *Lg* amplitudes. The limited yield range (less than half a magnitude unit) renders confident estimates of the magnitude scaling with total explosion tonnage difficult. The data in Figure 35 suggest, however, that *ML(Lg)*=1.7 corresponds to about 75 tons of slurry.

IMS Network *ML(Lg)*

Until this point we have analyzed array *ML(Lg)* values separately, and although combining them into a network magnitude with averaging appears straightforward, a few issues have to be considered. A certain minimum signal-to-noise ratio of individual element magnitudes should be required in the formation of a network magnitude to minimize bias and reduce scatter. A weighting scheme can be applied with SNR values for this purpose. Sometimes there are large discrepancies among array *ML(Lg)* values. They may be caused by attenuation along oceanic paths or blockage by crustal anomalies along the path for *Lg*. Whatever the reason, such cases have to be dealt with. Here, we identify outliers as data for which the magnitude range of three or more arrays was 0.5 m.u. or larger. If all values agree, but are all based on *Lg* paths along oceanic or blocking structures, the network magnitude may underestimate the size of the event. Discrepancies among array magnitudes may also be caused by errors in the IMS locations, in particular for events at close distance to one or more of the arrays, such that other phases (*Sn* or *SmS*) or *S*-coda interfere in the group velocity window for the *Lg* RMS amplitude calculation. To minimize the effect of this kind of error, a time window in the late coda for arrays at distances less than 400 km may provide more robust results. Although the coda level would have smaller amplitudes than the *Lg* phase, the SNR might still be sufficient because of the close recording distance. However, the attenuation may be different from the *Lg* window for the late coda and a separate amplitude distance curve would then have to be developed.

Consequently, in order to be reliable, a network *ML(Lg)* should be based on consistent array magnitudes obtained at two or more arrays with recording distances beyond 400 km, and with paths which are not entirely oceanic or blocked paths. If we assume that the standard error of array magnitudes is 0.1 m.u. for events broadly distributed, a network average based on three independent array magnitudes meeting these requirements would thus have a standard error of 0.06 m.u. In other instances, a network *ML(Lg)* might be subject to larger scatter and bias.

Concluding Comments

In this study we have defined *ML(Lg)* magnitudes for the IMS arrays that can be calculated automatically for a given seismic event with origin time and epicenter determined by the IMS. For most of the events, the array *ML(Lg)* values were consistent, and for only a

small fraction of the events were the discrepancies between array *ML(Lg)* values larger than 0.5 m.u. The reasons for the outlying observations were not investigated, but they could be due to mis-locations in some instances. Indeed, discrepancies between automatically calculated array *ML(Lg)* values may be used as an indicator to flag possible mislocations of the automatic IMS system.

The standard errors of *ML(Lg)* for closely spaced events were estimated to 0.04 to 0.1 m.u., which is larger than the standard errors for *mb(Lg)* (0.03 m.u.) obtained for regional and teleseismic data at the large aperture NORSAR array and single stations (see e.g., Hansen *et al.*, 1990). The larger errors for *ML(Lg)* could be due to several factors: scatter in the IMS locations and origin times causing scatter in the positioning of the time window for *Lg*, and hence in the calculated RMS amplitude; the frequency band for the small events analyzed here emphasizing higher frequencies (1.5-4 Hz) compared the 0.6-3 Hz band used for large explosions; the shorter epicentral distances resulting in shorter time windows, which may add to the scatter in the calculated RMS amplitudes. Because of the unknown uncertainties of the IMS locations, the standard errors obtained here for *ML(Lg)* can, indeed, be considered as upper bounds.

Comparisons between *ML(Lg)* and *mb(P)*, determined by NEIS, for 37 events showed that the *ML(Lg)* values were generally 1 m.u. or more smaller than *mb(P)*, but there was very large scatter in the data. Firm conclusions are difficult to draw from this comparison because of the broad geographical distribution of the small sample of events, the unknown uncertainty of the *mb(P)* determinations, and the attenuation effects on the *Lg* wave traversing ocean and other blocking structures. The problem of relating *ML(Lg)* and *mb(P)* is further compounded by the difference in frequency bands employed for determining the two types of magnitudes.

References

Bache, T.C., Bratt, S.R., Wang, J., Fung, R.M., Kobryn, C., and J. Given (1990). The intelligent monitoring system, Bull. Seism. Soc. Am., 80, 1883-1851.

Bache, T.C., Bratt, S.R., Given, J.W., Schroeder, T.D., Swanger, H.J., and J. Wang (1991). The intelligent monitoring system version 2. NMRD Quarterly Technical Report #7, Science Applications International Corporation, Report 91/1137, San Diego, CA.

Bath, M., Kulhanek, O., Van Eck, T., and R. Wahlstrom (1976). Engineering analysis of ground motion in Sweden, Seismological Institute of Uppsala, Sweden, Report 5-76.

Dahle, A., A. Alsaker, and S. Mykkeltveit (1989) Establishment of a mining explosion data base, in NORSAR Semiannual Technical Summary, 1 April - 30 September, 1989, NORSAR Sci. Rept. No. 1 89/90, NTNF/NORSAR, Kjeller, Norway

Gibowicz, S.J. (1987). NORESS capabilities for detection and location of mining tremors in the Lubin area in Poland, in NORSAR Semiannual Technical Summary, 1 October 86-31 March 1987, NORSAR Sci. Rept. No. 2 86/87, NTNF/NORSAR, Kjeller, Norway.

Grant, L. and J. Coyne (1992). Ground Truth data for Seismic Discrimination, in Proceedings of the 14th Annual DARPA/AFPL Seismic Research Symposium. (Eds. J. Lewkowicz and J. McPhetres), Phillips Laboratory, Hanscom AFG, MA.

Guterach, A., Grad, M. Materzok, R., and E. Perchuc (1986). Deep structure of the earth's crust in the contact zone of the paleozoican precambrian platforms in Poland (Tornquist-Teisseyre Zone), Tectonophysics, 128, 251-279.

Hansen, R., Ringdal, F., and P.G. Richards (1990). The stability of RMS *Lg* measurements, and their potential for accurate estimation of the yields of Soviet underground explosions Bull. Seism. Soc. Am., 80, 2106-2126.

Israelsson, H. (1992). *Lg* as a Yield Estimator in Eurasia, Final Report: Volume I, PL-TR-92-2117 (I), Center for Seismic Studies, Arlington, VA.

Kvaerna, T. and S. Mykkeltveit (1985). Propagation characteristics of regional phases recorded at NORSAR, in NORSAR Semiannual Technical Summary, 1 April - 30 September 1985, NORSAR Sci. Rept. No.1 85/86, NTNF/NORSAR, Kjeller, Norway.

Mykkeltveit (1987). Local geology of the regional array sites in Norway, in NORSAR Semiannual Technical Summary, 1 April -30 September, 1987,NORSAR Sci. Rept. No. 1 87/88, NTNF/NORSAR, Kjeller, Norway.

Nuttli, O.W. (1973). Seismic wave attenuation and magnitude relations for eastern North America, J. Geophys. Res., 78, 876-885.

Ringdal, F. (1983). Magnitudes from *P* coda and *Lg* using NORSAR data, in NORSAR Semiannual Technical Summary, 1 October 82 - 31 March 1983, NORSAR Sci. Rept. No. 2 82/83, NTNF/NORSAR, Kjeller, Norway.

Ringdal, F. (1986). Study of magnitudes, seismicity, and earthquake detectability, Bull. Seism. Soc. Am., 76, 1641-1659.

Ringdal, F. and B.K. Hokland (1987). Magnitudes of large Semipalatinsk explosions using *P* coda and *Lg* measurements at NORSAR, in NORSAR Semiannual Technical Summary, 1 April - 30 September, 1987, NORSAR Sci. Rept. No. 1 87/88, NTNF/NORSAR, Kjeller, Norway.

Sereno, T.J., Swanger, H.J., Jenkins, R.D., Nagy, W.C., and D. Wahl (1992).Attenuation and travel-time characteristics of regional phases recorded at GERESS.

Suteau-Henson, A., Ryaboy, V.Z., Riviere-Barbier, F., Israelsson, H., and J.A. Carter, (1992). Analysis of IMS Locations of Mine Blasts and RMS *Lg* magnitudes in Scandinavia, in Proceedings of the 14th Annual DARPA/AFPL Seismic Research Symposium. (Eds. J. Lewkowicz and J. McPhetres), Phillips Laboratory, Hanscom AFG, MA.

Vogsfjord, K.S. and C.A. Langston (1990). Analysis of regional events recorded at NORESS, Bull. Seism. Soc. Am., 80, 2016-2031.

Vogsfjord, K.S., Yan, B., and C. A. Langston (1991). Composition of Short-Period Regional Phases Inferred from Fennoscandian Array Data, in Proceedings of the 13th Annual DARPA/AFPL Seismic Research Symposium. (Eds. J. Lewkowicz and J. McPhetres), Report PL-TR-91-2208, Phillips Laboratory, Hanscom AFG, MA.

Azimuth Variations at NORESS and ARCESS

Anne Suteau-Henson

Introduction

The purpose of this study is to investigate the variations in azimuth bias and scatter for regional phases at NORESS and ARCESS. The precision and accuracy of azimuth estimation using polarization of three-component (3-C) data and *f-k* analysis of vertical-component array data are evaluated as a function of azimuth from the array. At ARCESS, the clustering of events near known mines makes it possible to compare 3-C azimuth estimates to azimuths from mine locations. Data derived from the IMS automated processing and analyst review are used (Bache *et al.*, 1990). Our goal is to acquire region-specific knowledge that can be implemented in the IMS to improve automated locations. We also attempt to identify any correlation with propagation anomalies inferred from DSS observations (Ryaboy, 1992).

Azimuth Variations at NORESS

The Data Set

NORESS data, recorded between November 7 - 25, 1989 and January 16 - August 24, 1990, were selected for this study. The data set was constrained to 3-C signal-to-noise ratio (3-C SNR) above 2 and time of measurement within the four seconds following the analyst-reviewed arrival time to insure the quality of the polarization measurements for the data from the array of four 3-C elements (Suteau-Henson, 1990; 1991). Also, events mixed with interfering signals were excluded, when such information was available in the IMS database. The phase identification after analyst review was used as "ground-truth". A data set of 378 arrivals identified as *Pn* was selected from the IMS database for NORESS. The location of the corresponding events is displayed on the map of Figure 36.

Azimuth Bias and Scatter

The backazimuth from polarization ("3-C azimuth") was compared to the backazimuth from the IMS final event solution ("IMS azimuth"). For single-array locations, the latter represents a weighted average of *f-k* azimuths for defining phases (Bratt and Bache, 1988). Figure 37 (bottom) shows the azimuth difference (3-C minus IMS azimuth) for *Pn* as a function of azimuth. The scatter is reduced by selecting arrivals with 3-C SNR > 3, although this decreases the size of the data set. A small negative azimuth bias and significant scatter are observed east and south of NORESS. A large positive azimuth bias is

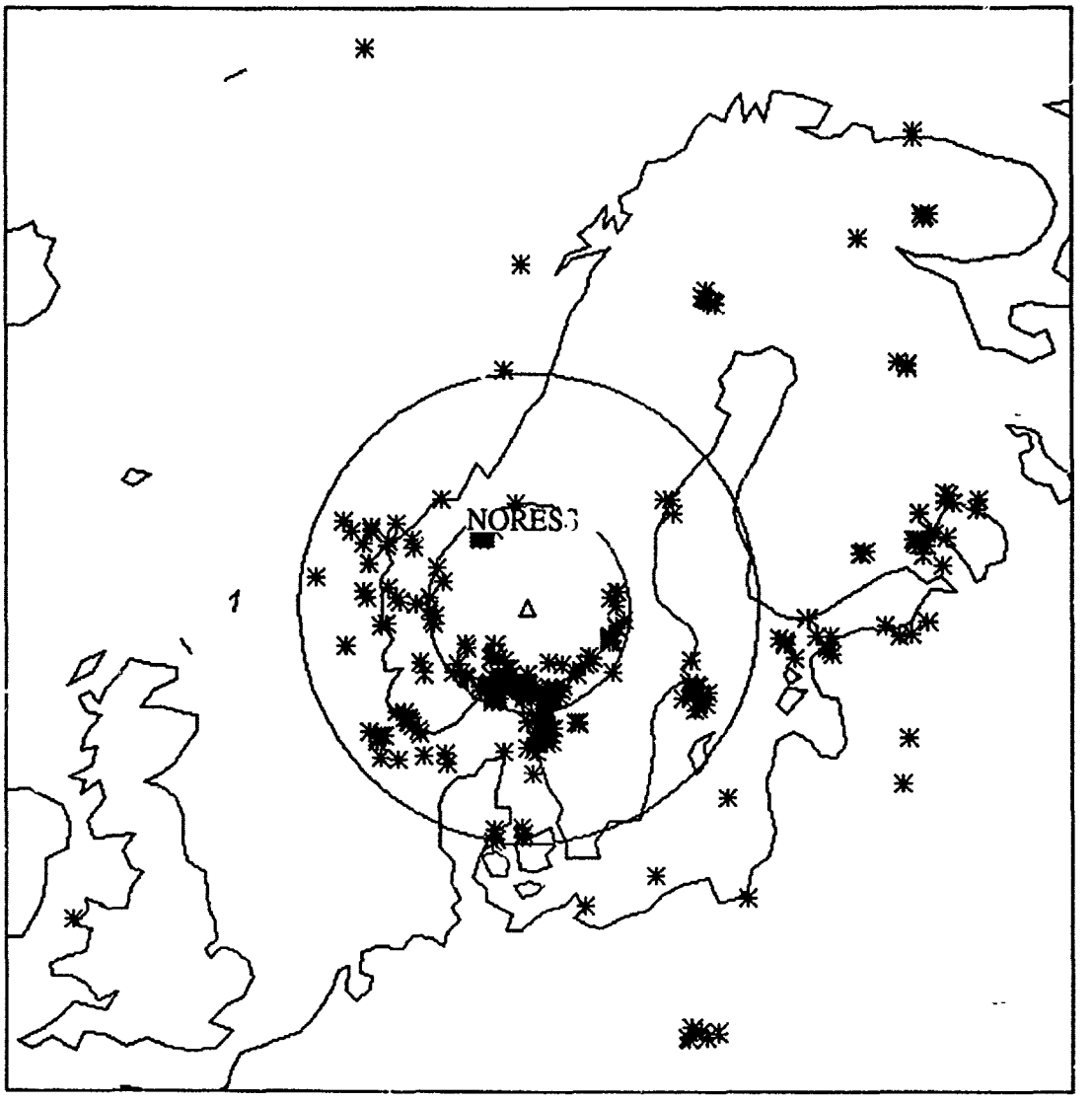

Figure 36: *Map showing the locations of events for which the Pn arrivals at NORESS were used in this study. The circles represent distances of 2.2 and 5° from the array.*

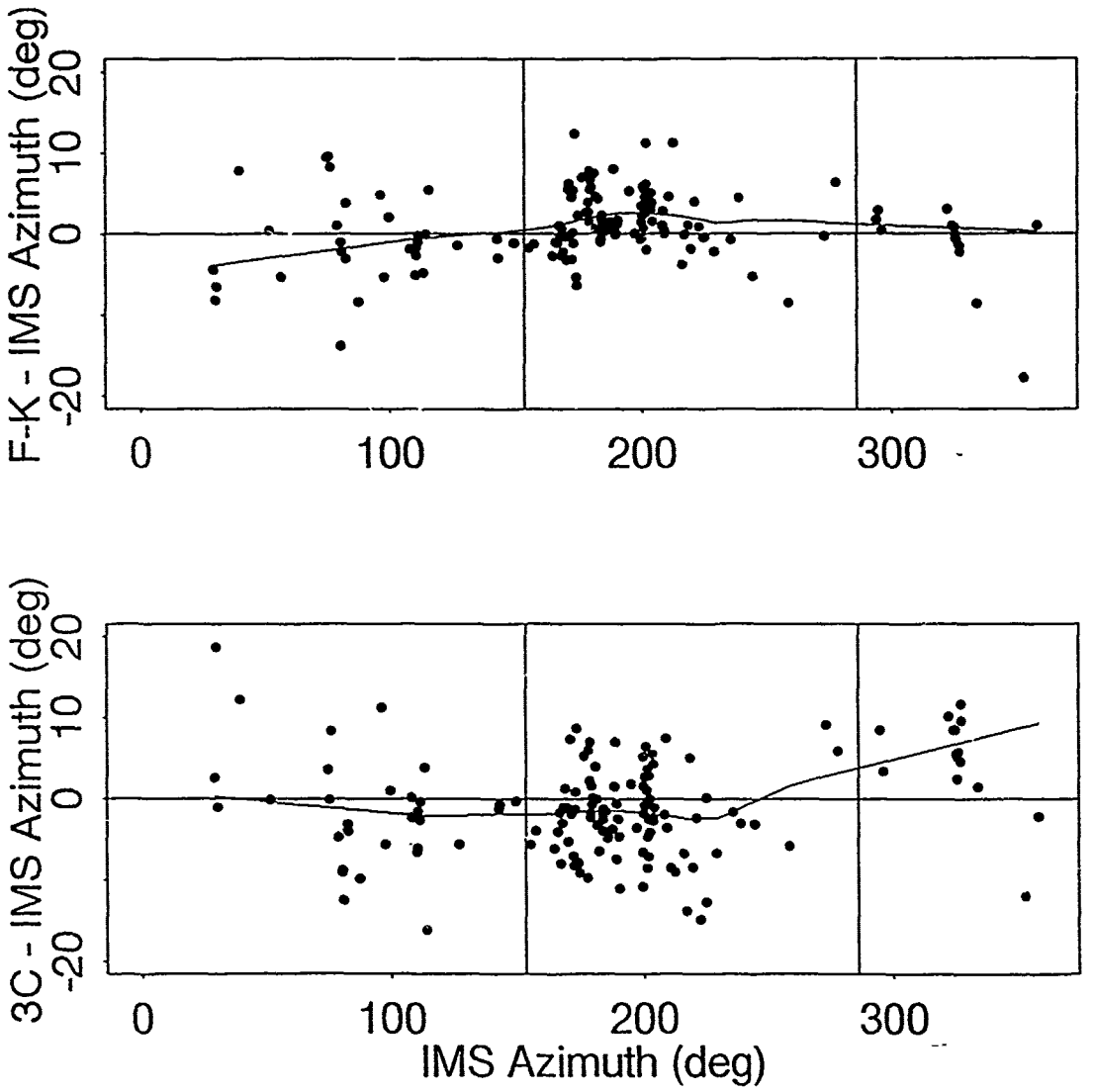

Figure 37: *The difference between estimated azimuth and azimuth fron IMS location is plotted as a function of azimuth for Pn arrivals at NORESS 3-C SNR > 3. Top: azimuths are estimated using f-k analysis of Pn waves; tom: azimuths are estimated using polarization of 3-C data. Only points azimuth difference less than 20 deg are shown (seven outliers were exclu The vertical lines represent the boundaries of a Pn travel-time ano (Ryaboy, 1992).*

observed in the northwest quadrant. According to Ryaboy (1992) a large area southwest of NORESS (approximately between 150 and 290° azimuth) has anomalous (early) *Pn* travel-times with respect to the standard model for Scandinavia. There appears to be a correlation between the large positive azimuth bias northwest of NORESS and the transition from early (south) to normal (north) travel-times. Thurber *et al.* (1992) attempt to establish similar correlations between *f-k* azimuth bias for *Pn* and *Pg* at the three scandinavian arrays and structure.

Figure 37 (top) shows the *f-k* azimuth difference as a function of IMS azimuth for *Pn* at NORESS with 3-C SNR > 3. Clearly, there are significant differences between the results from the two methods of estimation, especially south of the array and in the northwest quadrant. Events to the south have a positive *f-k* azimuth difference (mostly between 0 and 10°), while their 3-C azimuth difference is more scattered, with a small negative-bias. Also, the strong positive 3-C azimuth bias northwest of the array is not observed for *f-k* estimates, although more data are needed in that azimuth range to reach definite conclusions.

Azimuth Variations at ARCESS

The Data Set

Pn arrivals at ARCESS were selected from the IMS database for the same time period and with the same selection criteria as for NORESS resulting in a data set of 1198 arrivals. The IMS locations of the corresponding events at near-regional distance from ARCESS tend to cluster, and most of the clusters appear to be associated with known mines or mining areas (see Suteau-Henson, 1992). We identified twelve such clusters, and the azimuth and distance from ARCESS of the events within the various clusters are plotted in Figure 38. There is a possibility that some events have large enough location errors that they are wrongly assigned to a given cluster. In the following, we restrict our study to *Pn* arrivals with 3-C SNR > 3, to further limit the number of outliers, the amount of scatter, and the possibility of significant mislocation.

Azimuth Bias and Scatter

In Figure 39 the azimuth difference (3-C azimuth minus IMS azimuth) is plotted against the IMS azimuth for events with 3-C SNR > 3 for each of the twelve clusters. Events to the northeast show a positive bias, while the bias is negative south of the array. The amount of bias and scatter varies with each cluster. The bias is within ±10°, and the scatter varies from ±5° to ±10°.

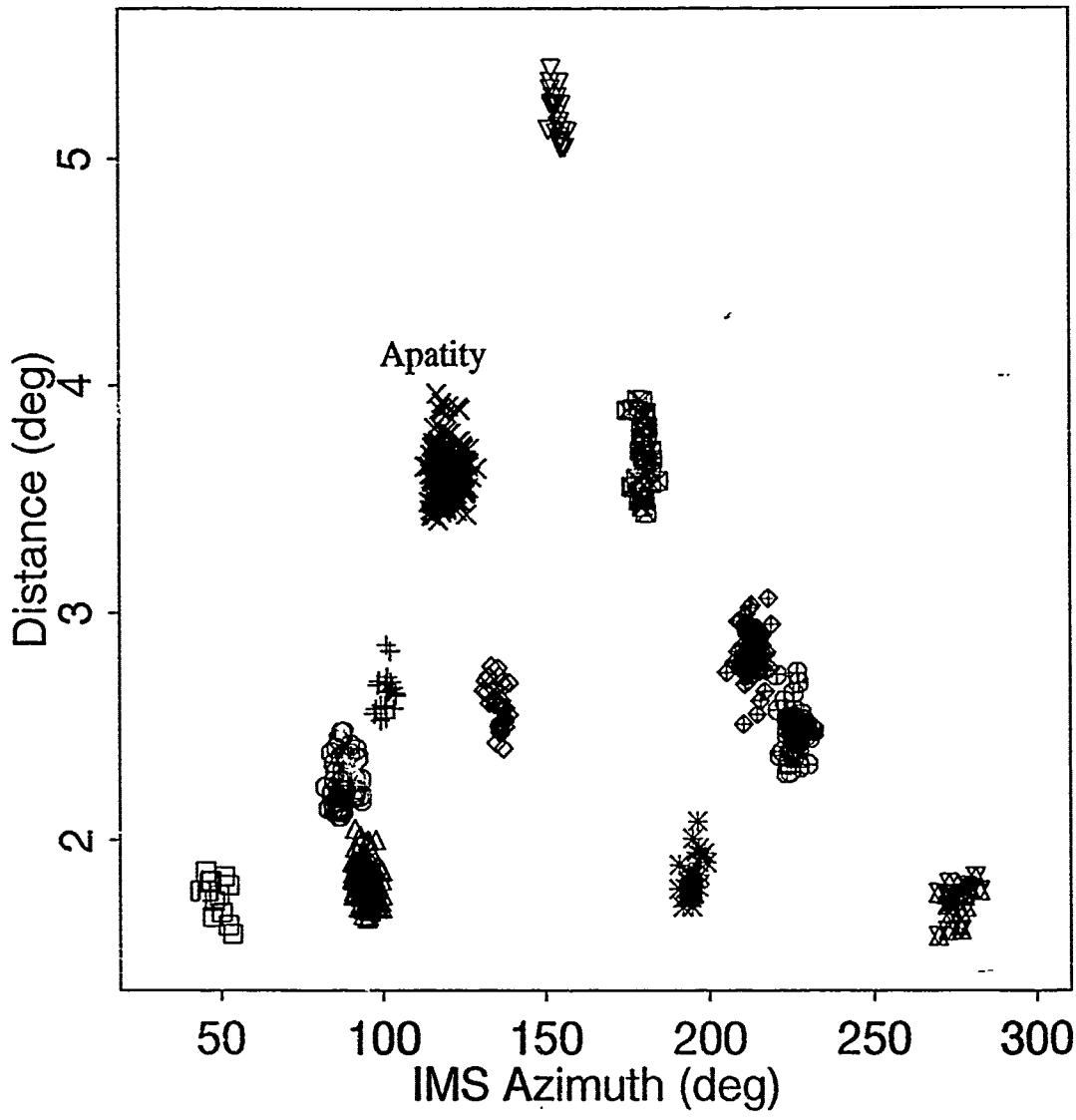

Figure 38: *Epicentral distance is plotted against azimuth (from the IMS location) for events in twelve event clusters at near-regional distance from ARCESS. Each cluster is assigned a different symbol.*

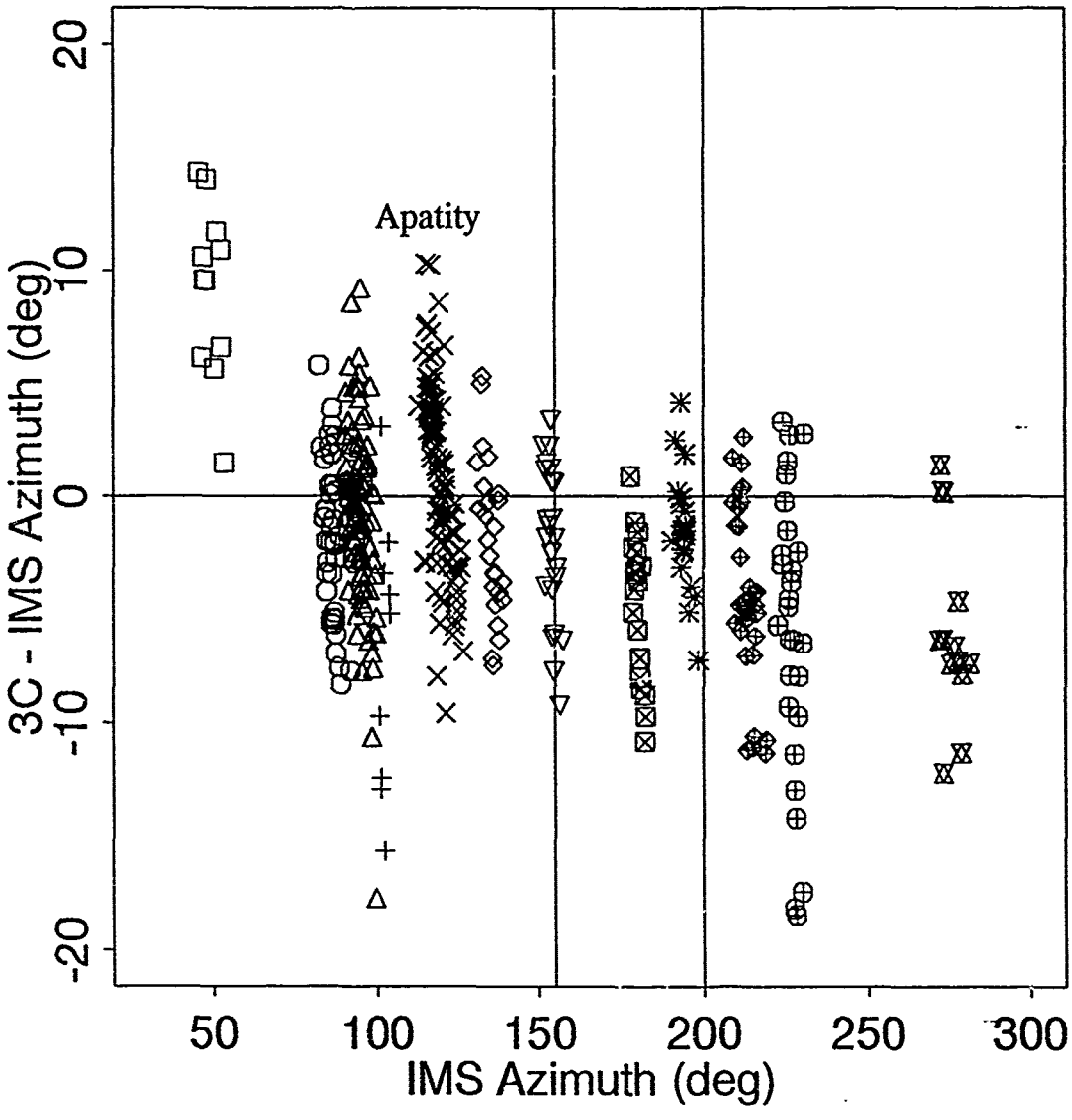

Figure 39: *The azimuth difference (3-C minus IMS azimuth) is plotted as a function of the IMS azimuth for Pn arrivals of events in twelve clusters at near-regional distance from ARCESS (see Fig. 38), with 3-C SNR > 3. A different symbol is used for each cluster. Only data points with a difference less than 20° are shown which excludes three outliers.*

Ten of the twelve clusters could be associated with a given mine or mining area. There often is some discrepancy between the location of the cluster and the mine(s) location, and this can be attributed to the inaccuracy of the IMS location and/or the mine(s) location. Mine locations from SPOT photos are accurately determined, although those used in the following may represent average locations for large mines. Since this study, more detailed locations from SPOT photos, DMA maps, and mining authorities have been made available (see Suteau-Henson, 1992). However, we cannot associate events with specific mines at this level of detail based solely on IMS locations.

For each of these ten clusters, it is possible to compare the 3-C azimuth with the azimuth of the corresponding mine (or the average over all mines associated with the cluster). The difference between 3-C and mine azimuths is shown in Figure 40 as a function of the IMS azimuth. The bias is as large as -10° for two of the clusters. More accurate mine locations might reduce this bias. The cluster indicated by an arrow is associated with a mine that has a SPOT photo location (SC17), and has a small negative bias, and a scatter of about ±5°. For other clusters, the scatter is less than ±10° and usually around ±5°.

The effect of SNR on the difference between 3-C and mine azimuths is investigated in Figure 41. Except for the last cluster to the right of the figure, raising the SNR from 2 to 4 does not significantly change the amount of bias, although it usually reduces the scatter, as expected.

Finally, we investigate the precision and accuracy of the azimuths from *f-k* analysis for various regional phases. For this purpose, a new data set was extracted from the IMS database, covering the period from March 4 to September 30, 1991. Arrivals with 3-C SNR > 2 were selected. Also, only "defining" phases were included, i.e., *Pn*, *Pg*, *Sn* or *Lg* whose *f-k* azimuths were used in event location (Bratt and Bache, 1988). For single-array solutions (most events in this data set) the *f-k* azimuths of defining phases are the only data used for azimuth estimation in the IMS. Figure 42 compares the *f-k* azimuths for each phase type to the IMS azimuths for the event cluster corresponding to the Apatity mining area in the Kola Peninsula. This cluster (marked with crosses in Fig. 38-41) has a very large number of events. Of particular interest is the *Pn f-k* azimuth. The figure shows that it is biased with respect to the IMS azimuth, but has a significantly smaller scatter. This property could be used to improve the precision of the location for events from this area, while a correction would be necessary to account for the systematic azimuth bias (see Suteau-Henson, 1992).

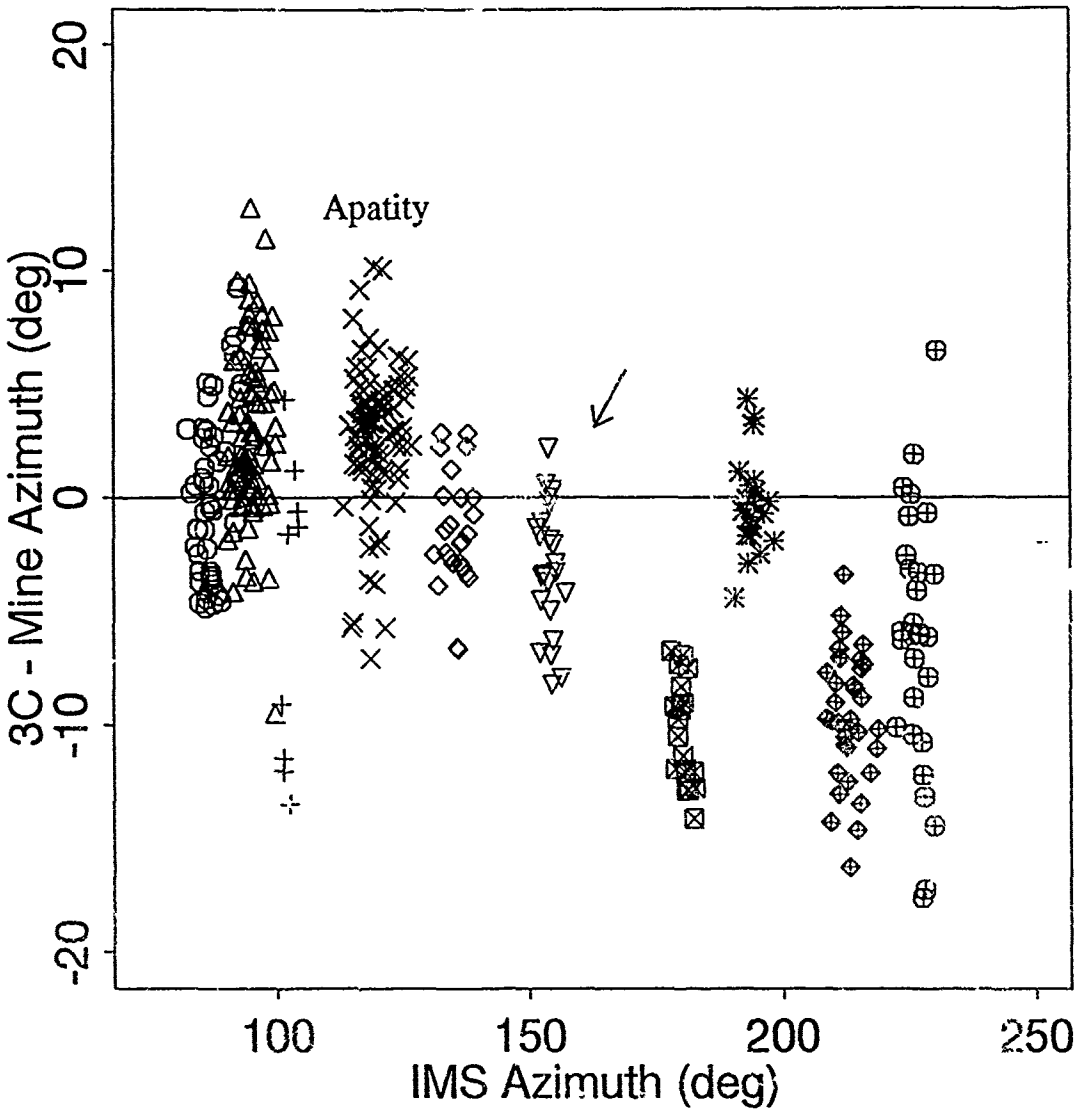

Figure 40: *The difference between the 3-C azimuth and the azimuth of the nearest known mine is plotted as a function of the IMS azimuth for Pn arrivals with 3-C SNR > 3 from events belonging to ten clusters at near-regional distance to ARCESS (see Fig. 38). Each cluster is represented by a different symbol. Only data points with azimuth difference less than 20° are shown.*

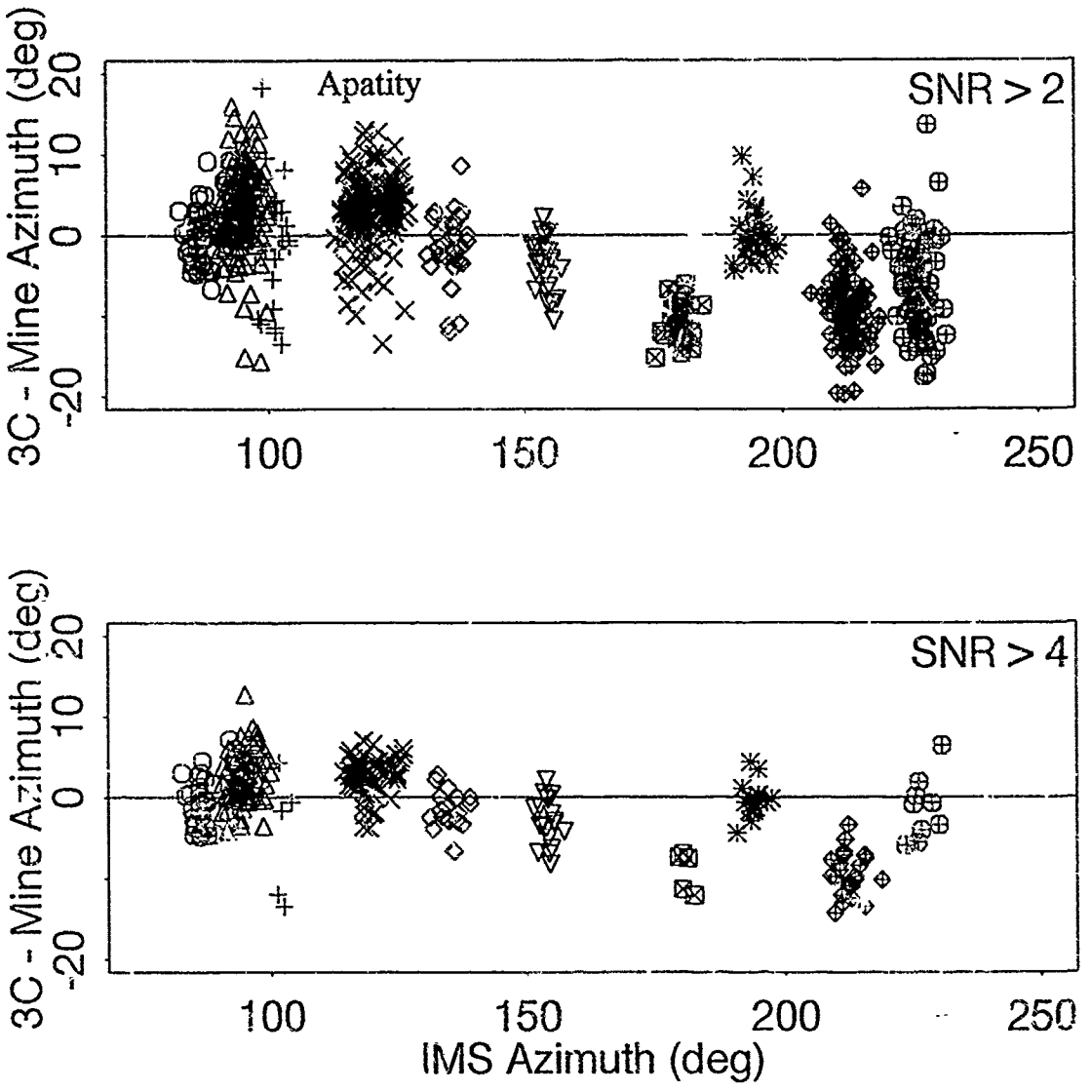

Figure 41: *For Pn arrivals from ten event clusters near ARCESS (see Fig. 38), the difference between 3-C and mine azimuth is plotted as a function of IMS azimuth for two values of the 3-C SNR threshold. Compare to Figure 40, where the threshold was set to 3.*

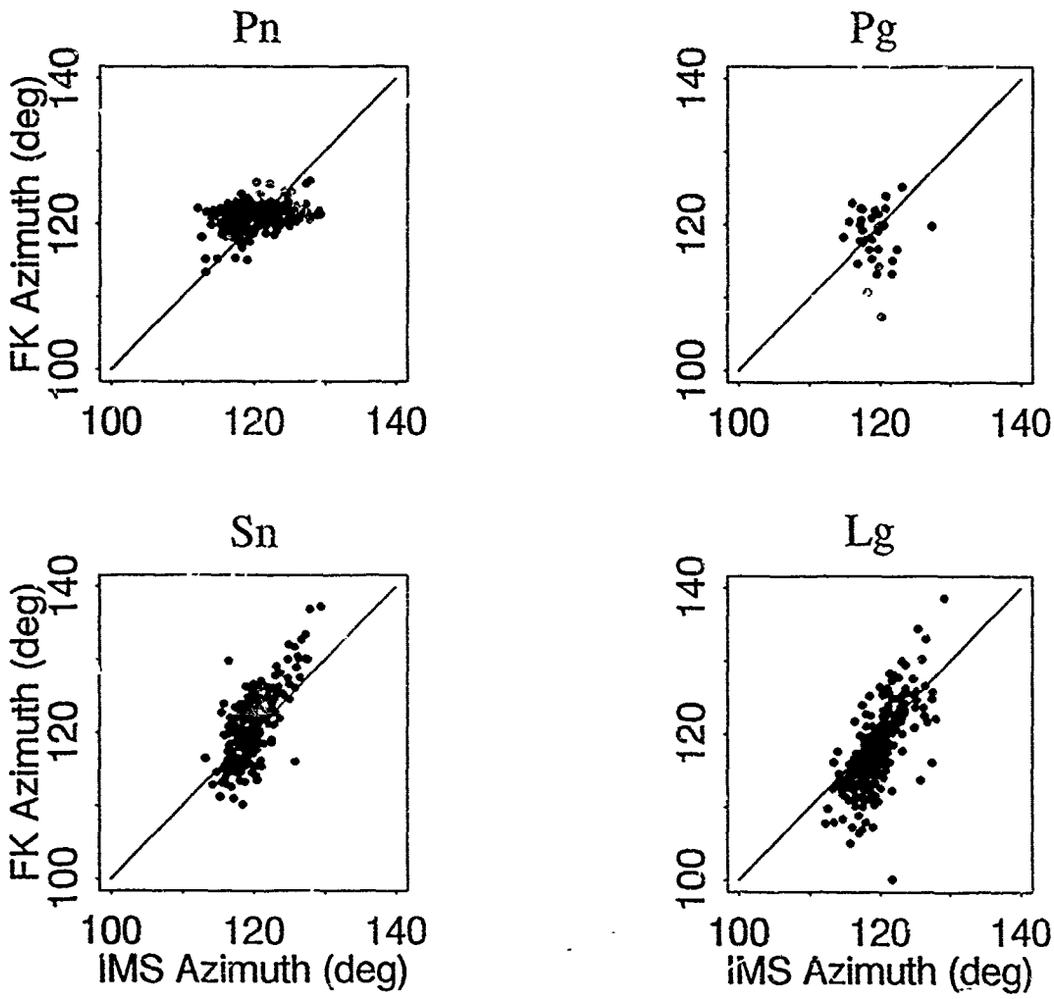

Figure 42: *The azimuth from f-k analysis is plotted against the IMS azimuth for defining regional phases of events from the Apatity mining area recorded at ARCESS. The 3-C SNR threshold is set at 2. The lines indicate equal f-k and IMS azimuths.*

Conclusions and Discussion

This study of the variation of azimuth bias and scatter at NORESS and ARCESS, based on data from several months of continuous IMS operation, has shown the following:

- The difference between the backazimuth from polarization of 3-C data and that from the IMS final event solution shows significant azimuthal variation, and some systematic trends can be observed in spite of large scatter at both arrays. Some of the bias appears to correlate with *Pn* propagation anomalies inferred from DSS profiles (Ryaboy, 1992). Variations in the difference between the backazimuth from *f-k* analysis for *Pn* and *Pg* and that from the IMS location is reported by Thurber *et al.* (1992), and they suggest that it can be explained by lateral heterogeneities.
- At ARCESS, we identified event clusters that appear to correspond to specific mines or mining areas. For such clusters, the scatter in the difference between 3-C and IMS azimuth is, as expected, a strong function of SNR. For *Pn* with 3-C SNR > 3, the scatter is ±5° to ±10°. The bias is as high as 10°. Similar observations are made for the difference between the 3-C azimuths and the azimuths inferred from the mine locations. As azimuth errors can result in significant mislocation, especially for single-array locations, our observations have important implications on location capabilities. Proper calibration appears feasible when enough data with "ground truth" locations are available.
- There may be significant differences in the azimuthal variations of 3-C and *f-k* azimuth estimates as shown for *Pn* at NORESS. They may be due to differences in contamination by other signals since different sensors, frequency bands, and time windows are used to obtain polarization and *f-k* measurements.
- For events from the Apatity mining area recorded at ARCESS, a comparison between *f-k* azimuth estimates for different regional phases and the IMS azimuth indicates significant variations in the accuracy and precision of the *f-k* estimates for the various phases. Such region-specific knowledge could be used to improve automated locations in the IMS (see Suteau-Henson, 1992).

In this study, we used phase identifications from the IMS analyst review. Some arrivals, however, may be misidentified. In particular, an arrival named "*Pn*" may actually be *Pg*, with the preceding *Pn* undetected because of low SNR. Such phase mis-identifications have been observed for earthquakes from western Norway (Baumgardt and Ziegler, 1988; Vogjford and Langston, 1991). Also, because of the limitations of automated processing, signal measurements (polarization, *f-k* spectrum) may be made at the time of another arrival sufficiently close in time, or there may be some contamination by signals from other arrivals. Because of these caveats, one must exercise some caution in interpreting

results of automated signal processing at regional distances. Phase mis-identifications can strongly affect incidence angle and distance estimation (see Ryaboy, 1992). However, their effect on azimuth estimation, while deserving further investigation, is not expected to be as important, although it may contribute to the azimuth scatter observed in this study.

References

Bache, T. C., S. R. Bratt, J. Wang, R. M. Fung, C. Kobryn, and J. W. Given (1990). "The Intelligent Monitoring System", *Bull. Seism. Soc. Am.* **80**, Part B, 1833-1851.

Baumgardt, D. R. and K. A. Ziegler (1988). "Spectral Evidence for Source Multiplicity in Explosions: Application to Regional Discrimination of Earthquakes and Explosions", *Bull. Seism. Soc. Am.* **78**, 1773-1795.

Bratt, S. R. and T. C. Bache (1988). "Locating events with a sparse network of regional arrays", *Bull. Seism. Soc. Am.* **78**, 780-798.

Ryaboy, V. Z. (1992). "Implications of DSS Observations within Scandinavia and Northwestern Russia for IMS Data Processing", in *Center for Seismic Studies Final Report* PL-TR-92-2117(II), October 1990 - March 1992, Hanscom Air Force Base, MA, 47-89.

Suteau-Henson, A. (1990). "Estimating Azimuth and Slowness From Three-Component and Array Stations", *Bull. Seism. Soc. Am.* **80**, Part B, 1987-1998.

Suteau-Henson, A. (1991). "Three-Component Analysis of Regional Phases at NORESS and ARCESS: Polarization and Phase Identification", *Bull. Seism. Soc. Am.* **81**, 2419-2440.

Suteau-Henson, A. (1992). "Improvement of Azimuth Estimation in the IMS", this report.

Thurber, C. H., C. G. Munson, and S. R. Bratt (1992). "Arrival Azimuth Bias at Fennoscandian Seismic Arrays", to be submitted to *Geophysical Journal International.*

Vogjford, K. S. and C. A. Langston (1991). "Analysis of Regional Events Recorded at NORESS", *Bull. Seism. Soc. Am.* **80**, 2016-2031.

Identification of Kola Peninsula Events

Florence Riviere-Barbier

Introduction

The Kola Peninsula is an area of intense mining activity. In addition to mining blasts, there is induced seismicity related to the large amount of rock being removed from the Khibiny Massif and natural seismicity occurring along faults located in the Kola-Finnmark zone (Norsar Sci. Rep. 1-91/92). The combination of industrial shots and natural seismicity makes the Kola Peninsula an ideal site to test discrimination methods.

A method of grouping seismic events based on cross-correlation values between pairs of waveform envelopes was described by Rivière-Barbier and Grant, (1992) in a study of mining events from Karelia. This report focuses on the application of that methodology to events from the Kola Peninsula. The 1992 paper featured events in the 165 km to 295 km distance range. In this study, the distance to the events has been extended to a range from about 175 km to 415 km. Naturally, the frequency content and signal-to-noise ratio (SNR) of the data are more limited in this case. The array is also different, data recorded at FINESA were used in the 1992 paper while in this report, the data were recorded at ARCESS.

Mine locations

The Kola Peninsula covers a very large area, so it has been divided into six different subareas, each of them including several mines. Table 9 defines the boundaries of each area, and the number of events within each area that were used for this study.

Table 9: Subareas extensions and number of studied events

Subarea	Latitude (°N)	Longitude (°E)	Number of events
I	69.00 - 70.00	30.00 - 32.00	72
II	68.50 - 69.50	32.00 - 36.00	62
III	67.30 - 67.799	33.00 - 35.00	168
IV	67.00 - 68.00	30.00 - 32.00	63
V	67.80 - 68.00 68.00 - 68.49	33.00 - 35.00 32.00 - 35.00	77
VI	67.00 - 68.00	32.00 - 33.00	31

Fifty mines were located in the Kola Peninsula using SPOT™ images. Four mines were located on DMA maps (SPOT™ photos covering this particular area were not available to us). Mine locations, their distances and their azimuths to ARCESS are given in Table 10

Table 10:

Subarea	Labels	Latitude	Longitude	Distance to ARCESS	Azimuth to ARCESS
I	SD1	69.597	30.049	177.39	85.63
	SD2	69.367	30.093	180.91	93.80
	SD3	69.368	30.134	182.49	93.69
	SD4	69.329	30.019	178.67	95.28
	SD5	69.435	30.531	197.11	90.89
	SD6	69.432	30.527	196.98	90.99
	SD7	69.398	30.614	200.79	91.97
	SD8	69.401	30.847	209.86	91.58
	SD9	69.409	30.953	213.90	91.22
II	SD10	69.410	32.135	260.08	89.97
	SD11	69.299	32.721	284.58	91.93
	SD12	69.276	32.811	288.49	92.32
	SD13	69.286	32.903	291.91	91.99
	SD14	69.256	33.106	300.38	92.38
	SD15	69.223	33.168	303.42	92.99
	SD16	69.070	35.008	378.56	93.41
	SD17	69.064	35.008	378.70	93.51
	SD18	68.932	34.938	379.42	95.78
	SD19	69.111	33.594	322.46	94.64
	SD20	69.093	33.482	318.54	95.16
	SD21	69.060	33.484	319.44	95.81
	SD22	69.034	33.506	320.97	96.27

Table 10:

Subarea	Labels	Latitude	Longitude	Distance to ARCESS	Azimuth to ARCESS
II	SD23	69.012	33.641	326.81	96.47
	SD24	69.013	32.939	299.55	97.72
	SD25	68.999	32.910	298.83	98.07
	SD26	68.997	32.871	297.38	98.19
	SD27	68.943	32.965	302.63	99.11
	SD28	68.930	33.096	308.09	99.09
	SD29	68.872	33.025	307.23	100.40
	SD30	68.792	33.133	314.15	101.72
	SD31	68.791	33.146	314.68	101.71
	SD32	68.700	33.125	317.31	103.49
III	SD33	68.268	33.403	347.49	110.29
	SD34	68.251	33.267	343.40	111.00
	SD35	68.120	33.400	355.35	112.66
	SD36	68.133	33.162	346.05	113.27
	SD37	68.112	32.986	340.96	114.23
	SD38	68.082	33.219	351.00	113.87
	SD39	68.040	33.229	353.80	114.49
	SD40	67.893	33.029	355.73	117.45
	SD41	67.803	32.781	353.06	119.76
	SD45	68.019	34.349	395.34	111.16
	SD46	68.006	34.697	408.77	110.32
	SD47	67.916	34.385	402.41	112.48
	SD48	67.926	34.486	405.50	112.03
	SD49	67.889	34.566	410.50	112.29
	SD50	67.895	34.615	411.93	112.07

Table 10:

Subarea	Labels	Latitude	Longitude	Distance to ARCESS	Azimuth to ARCESS
IV	SD42	67.759	32.824	357.45	120.22
	SD43	67.645	32.912	368.19	121.45
	SD44	67.607	33.486	390.10	119.69

Data

Four-hundred-forty-three events located in the Kola Peninsula between January 1, 1991 and September, 30 1991 by the Intelligent Monitoring System (IMS, Bache *et al.*, 1991) were studied. Figure 43 shows the location of the events in each of the six subareas. All events with a magnitude above 1.5 were selected within each subarea. If the data set was not large enough for a subarea (less than 30 events), the magnitude threshold was lowered to include events with magnitude above 1.0.

Recordings of most of these regional events four well-defined phases: *Pn*, *Pg*, *Sn*, and *Lg*. For some large events, an *Rg* phase could be seen even though the background noise had the same frequency content as the *Rg* phase (around 0.5 Hz). *Rg* was observed at distances up to 390 km.

Most of the events had magnitudes below 2.0 and low SNR for the signal recorded at ARCESS. Before processing, data were filtered between 2.0 and 16.0 Hz to improve the SNR. Unfortunately, this eliminated the *Rg* phase which was cited by Rivière-Barbier and Grant, (1992) as a determinant feature in their study of Karelian events. In this study, the benefits of improved SNR outweighed the benefits of using *Rg*.

Results of Event Classification

In the following sections, we describe the results of applying cluster analysis (Rivière-Barbier and Grant, 1992) to the events of each subarea. While we do not have "ground truth" to verify that the event groups correspond to specific mining sources, we present the evidence supporting the grouping in the form of event origin time histograms. Waveforms were also analyzed visually to confirm the groups defined on the cluster tree. Mines typically have a characteristic shooting time (e.g. Monday through Friday around noon) that is evident in the event groupings. Within our groups, there are usually a few events that do not fit the characteristic shooting tome. However, postponements and unusual shot times are not unheard of.

Subarea I

Figure 44 shows the distribution of 9 mines and the IMS locations of 72 events that were included in this area. The cluster analysis performed on this data set classified these events into five groups. Representatives of the groups are shown in Figure 45. Thirty-seven events among the 72 are exactly identical and group together. Twenty-three events were split into 4 smaller groups. The visual analysis did not allow to control the results of the grouping for two events because of their low SNR. The remaining 10 events were not classified because they were unique or they were mixed with another event.

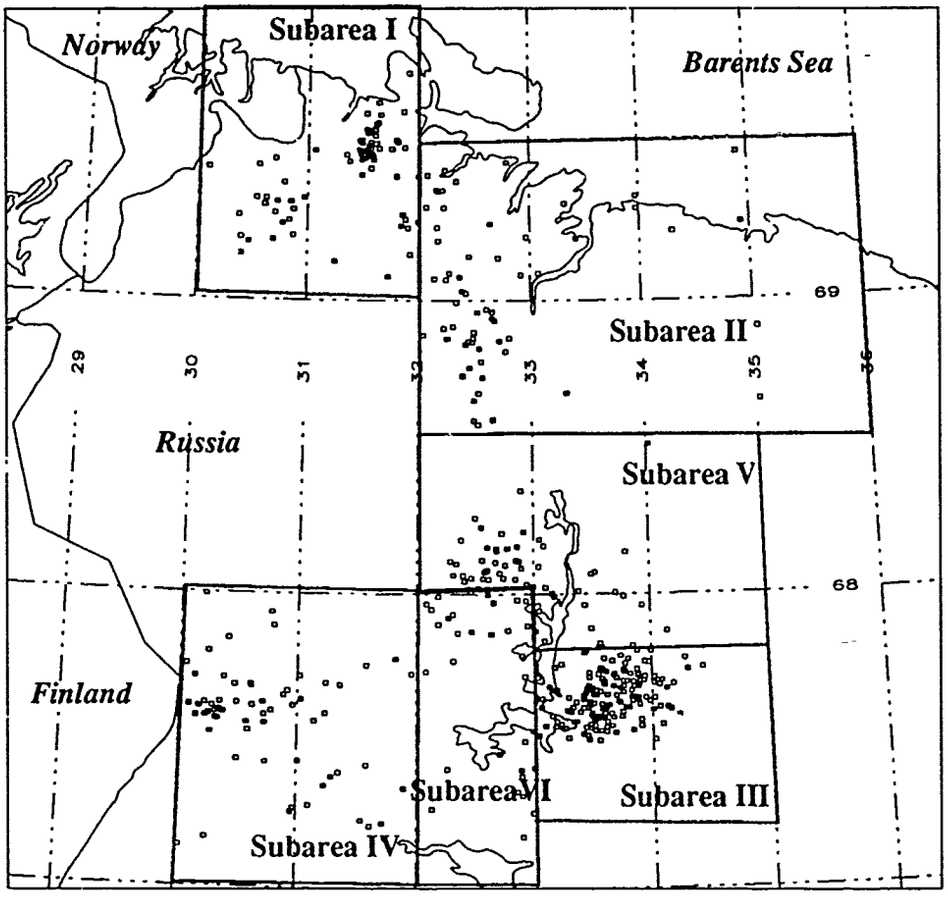

Figure 43: *IMS locations for 473 events from the Kola Peninsula. This large area has been subdivided into six subareas based on mine locations and event density.*

Figure 46 shows an histogram of the magnitudes for all the events located by the IMS in this particular area between January 1, 1991 and September 30, 1991. It clearly shows that most of the studied events have larger magnitude than the average and that they constitute a small subset of the total number of events. A mine whose events have magnitudes lower than 1.0, will not be "seen" in our analysis.

In Figure 47, the weekly distribution of the origin time is represented. The large majority of the studied events occurred Monday through Friday, a small number occurred on Saturday and none on Sunday. Again, the distribution of the studied event origin times does not

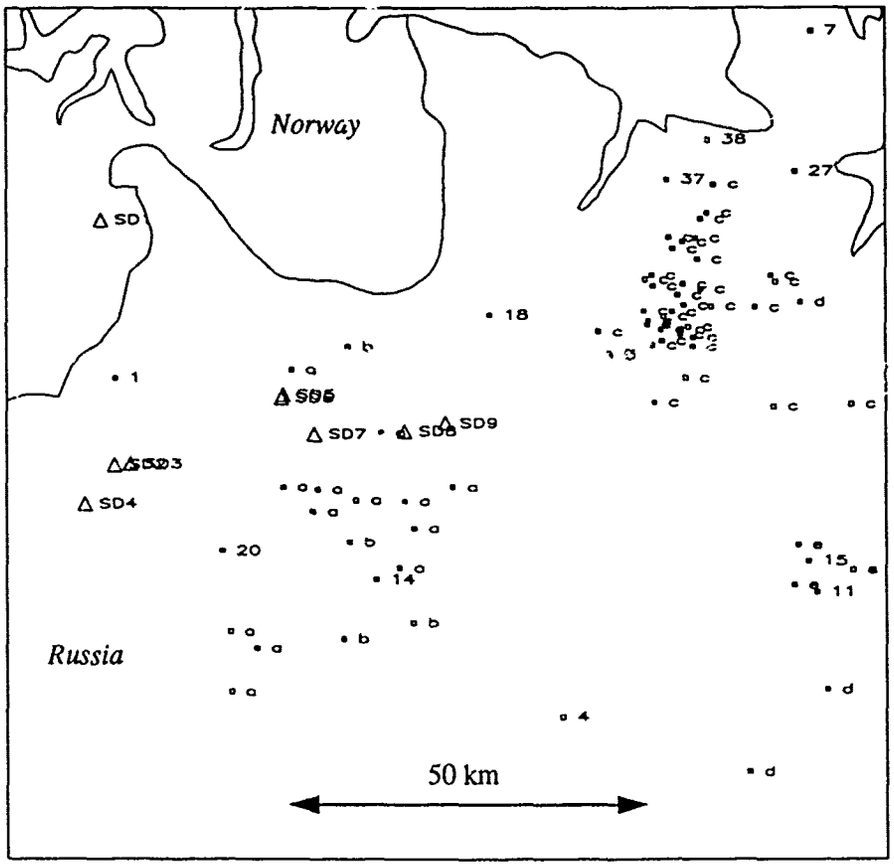

Figure 44: *Subarea I. This map shows the IMS locations for 72 events and SPOT locations for 9 mines. Different symbols are used to represent the events of each group. Number identify events that could not be classified.*

reflected the large amount of events occurring during the weekend which are characterized by smaller magnitudes.

In Figure 48, an histogram of the daily repartition of the origin time has been plotted for each group of events. This shows the origin time consistency among groups of events. The

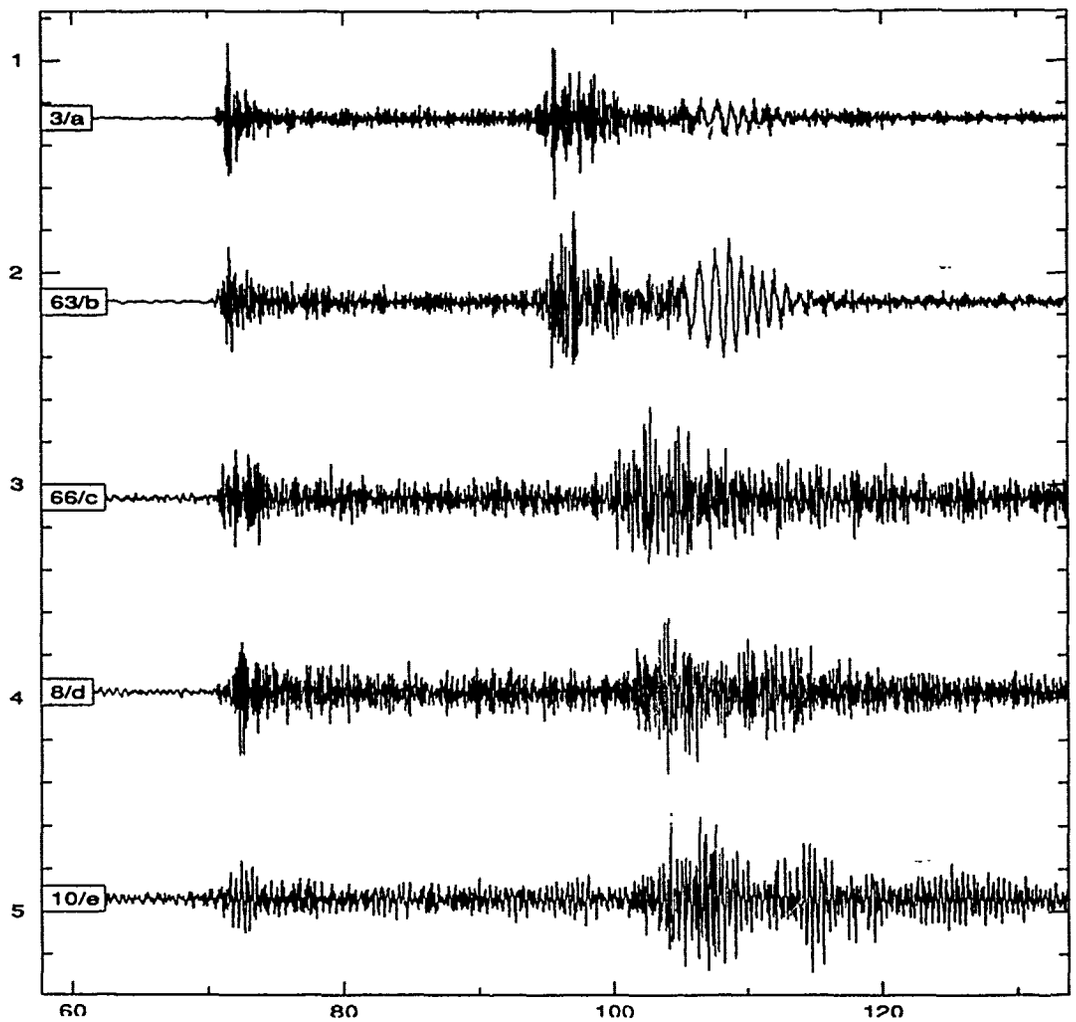

Figure 45: *Subarea I. The events where classified into five groups. One event representative of each group has been plotted. Signals from group "c", "d" and "e" have been filtered between 2 and 16 Hz. The Rg phase visible on the signals from groups "a" and "b" has been removed by the filtering on the other signals.*

largest group is characterized by two origin-time periods during the day while the other groups have narrower shot time windows. This support the idea that many of these events may be mine blasts. These consistent origin times in addition to the waveform peculiarities can be used in mine characterization.

Subarea II

Sixty-two events were studied in this area where 23 mines have been located (Figure 49). Most of the events are characterized by an emergent first arrival and a low SNR. Nevertheless, 8 different groups were differentiated, allowing the classification of 39 events (Figure 50). Five of the remaining events were not classified because of their low SNR. Four other events that were multiple events clustered together. Thirteen events were found to be unique, though many had the same *Lg-P* time as one of the eight groups. One event was

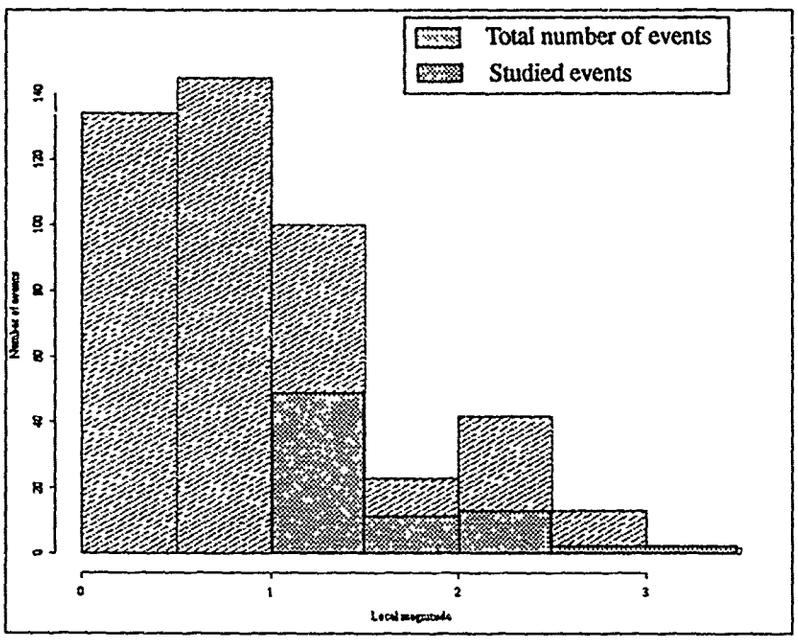

Figure 46: *Subarea I. Distribution of the magnitude for 459 events located by the IMS in subarea I. Superimposed is the magnitude of the events used in the study. More than 80% of the total number of the events have a magnitude between 0.0 and 1.5.*

clearly mislocated.

Their are several possible explanations for the discrepancy between the number of mines and the number of sources determined by cluster analysis: our data set does not include events from all mines, (limited data), and/or our method cannot distinguish between events from very closely spaced mines, (limitation of the method).

Over the period of time covered by the data set, only one event was reported close to mines SB16, SB17 and SB18. On SPOT photos, these three mines exhibit the same signs of activity as other mines that were associated with many events. We hypothesize that the blasts from mines SB16-18 are small and are therefore not recorded.

Assuming that these events are really correlated to the mines located in this area, the event locations are shifted toward the west relative to the mines (Figure 49). The events are consistently located closer to the array than they should be. In addition to the distance bias,

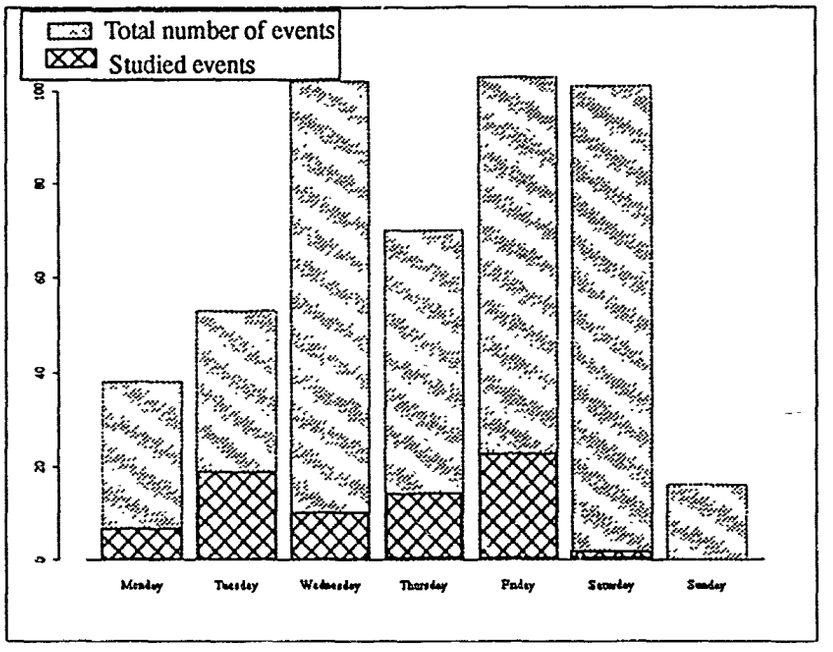

Figure 47: *Subarea I. Weekly distribution of the origin times based GMT origin time. The number of events occurring on Saturday or on Sunday is surprisingly high.*

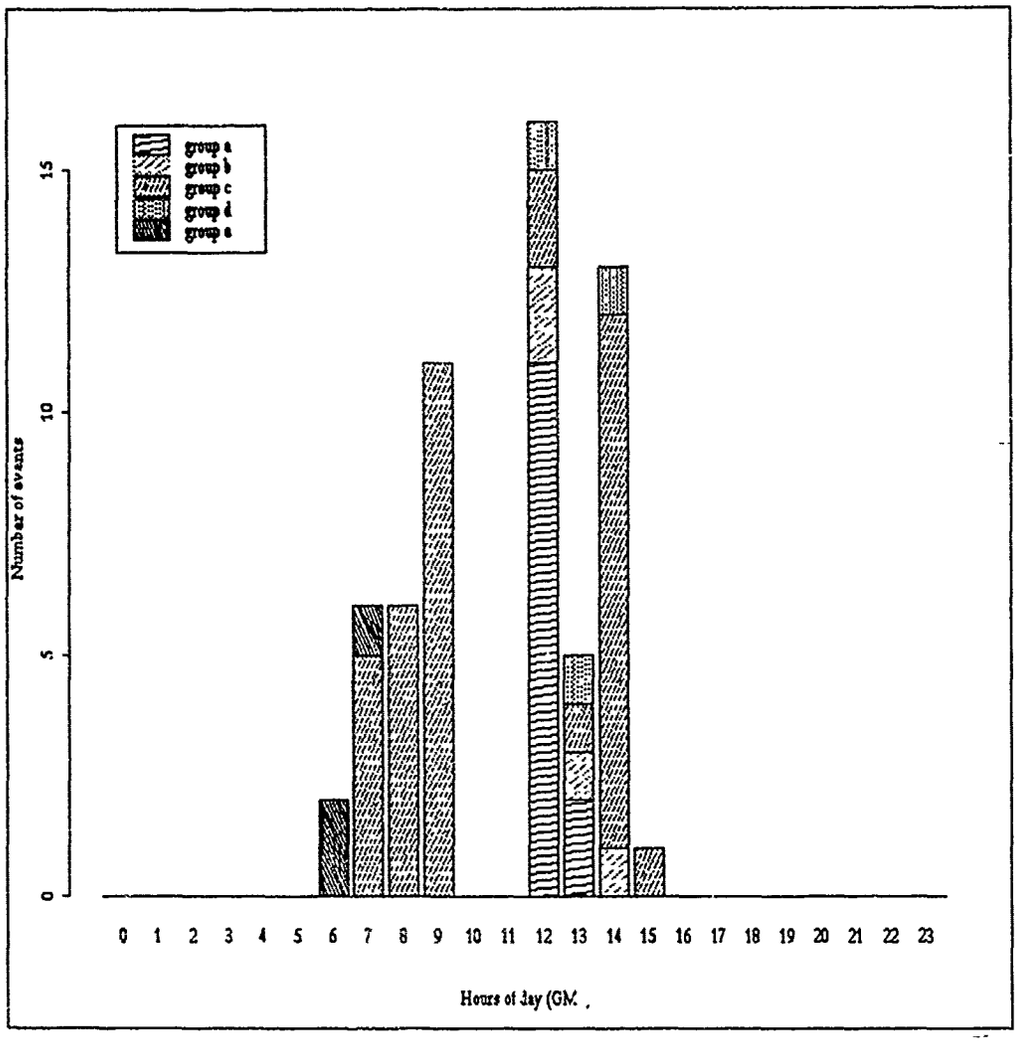

Figure 48: *Subarea I. Distribution of the origin time during the day for the five different groups. Events from group "c" seem to occur either in the morning or in the afternoon while events from the other groups occur in a narrow range of time.*

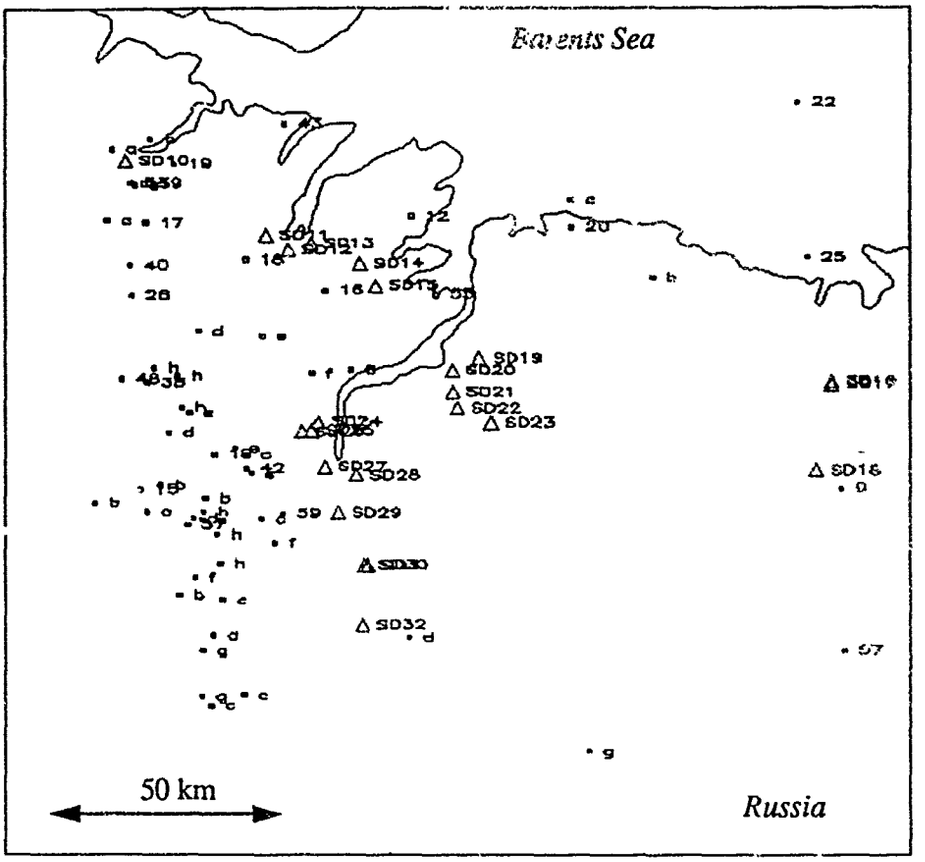

Figure 49: *Subarea II. IMS locations for 62 events and SPOT locations for 23 mines. Of the three events located off-shore, event 25 was not classified because of a low SNR, event 22 did not belong to any group and event 60 was classified in group "e".*

there is a large discrepancy between locations of events from the same group. Two events from group "b" and two events from group "e", with cross-correlation values greater than 0.7 for each pair of events were located more than 87 km and 55 km apart, respectively. This is largely the result of errors in the automatic event location for single array events by the IMS. Careful reanalysis of these events placed them closer together.

Figure 51 shows the distribution of the magnitudes for 161 events including the events from the studied data set located by the IMS. Less than 30 events whose waveforms were available had a magnitude larger than 1.5. In Figure 52, the distribution of the seismic

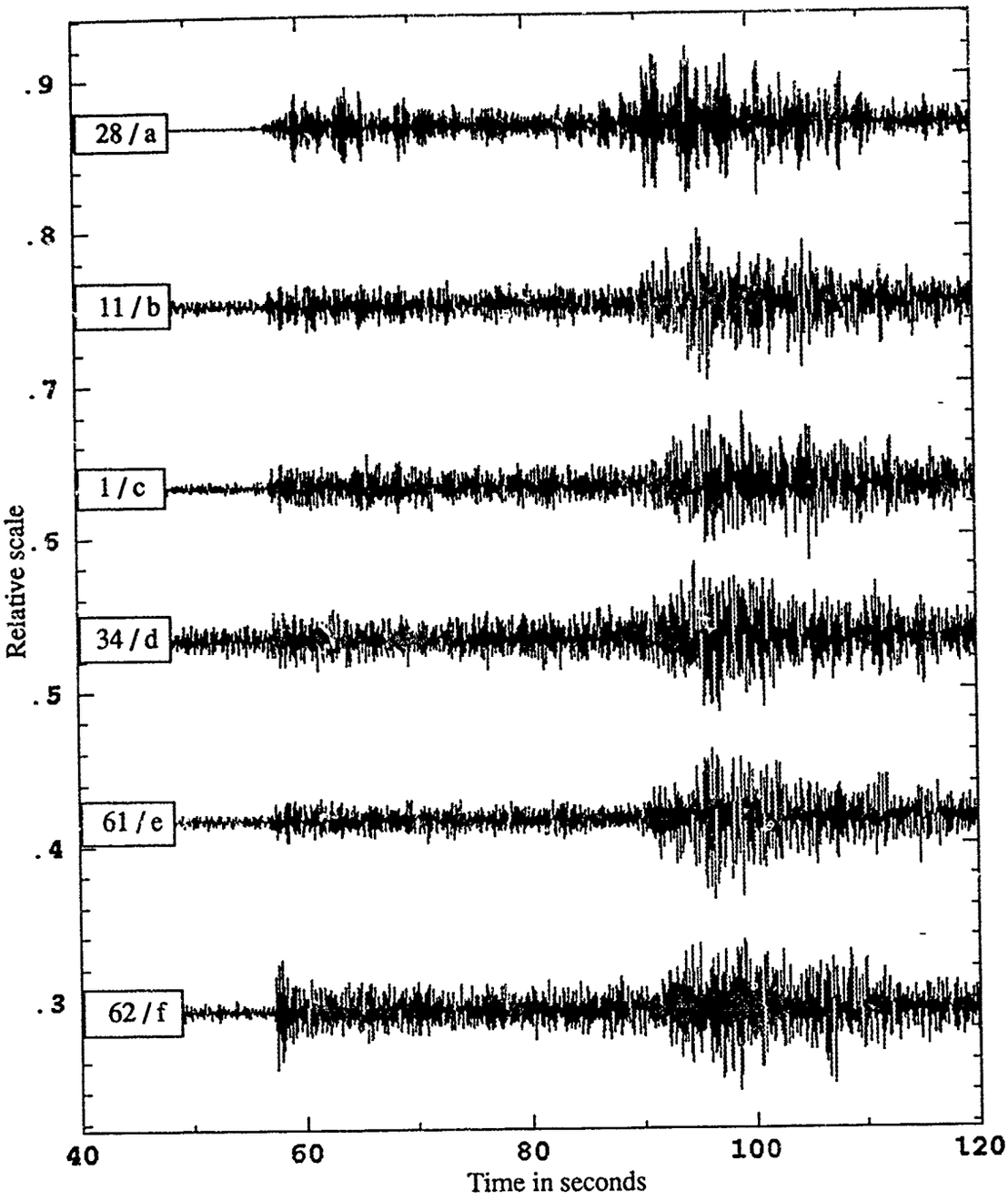

Figure 50: *Subarea II. Six events representative of each of the defined groups are plotted. They have been filtered between 2 and 16 Hz. The SNR is low for all events located in this subarea.*

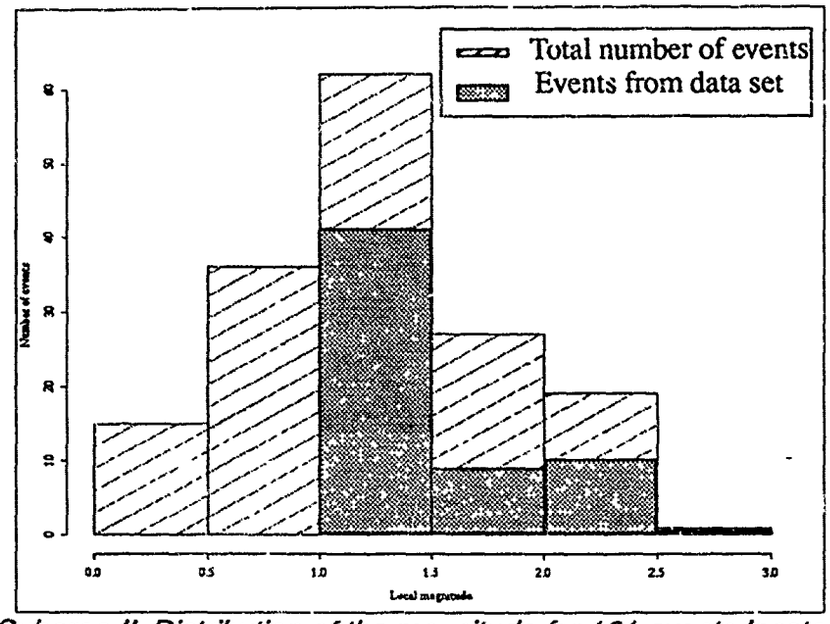

Figure 51: *Subarea II. Distribution of the magnitude for 161 events located in subarea II by the IMS between January 1, 1991 and September 30, 1991. Superimposed is the distribution of the magnitude for the studied events.*

activity as a function of day of week has been plotted for these 161 events. Only one event occurred on Saturday and very early in the morning. Figure 53 shows the daily distribution of the origin time day for each group of events. For three of these groups, origin times are confined to a small period of time during the day (e.g. early in the morning, around noon, in the afternoon). As already mentioned for the events in subarea I, the distribution of the origin times as a function of the hour of day could be an additional feature to characterize certain mines.

Subarea III (Apatity mine)

The Khibiny Massif is the most active area of the Kola Peninsula. More than 800 events were located by the IMS in the Khibiny Massif between January 1,1991 and September 30, 1991. Two-hundred-twenty-one events had a magnitude above 1.5, but waveforms were available for only 168 of them (Figure 54).

Information has been provided by Russian and Norwegian scientists about this particular mine. This information includes maps showing the location of the mining areas in the Khibiny Massif where five different districts (numbered i to v) were identified, a bulletin listing the events recorded at the Apatity seismic station, and a list of five events whose locations and sizes were known. Since the beginning of 1991, scientists running the Apa-

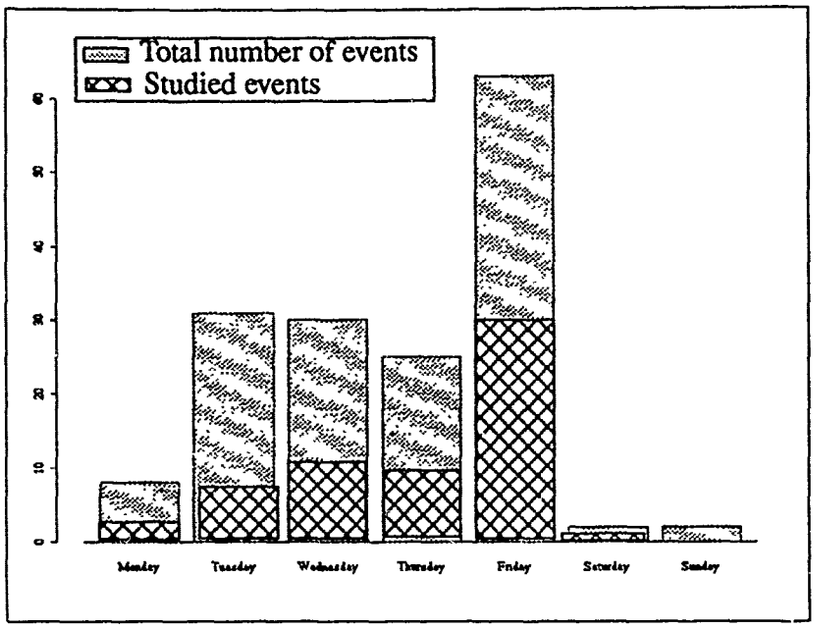

Figure 52: *Subarea II. Friday shows the highest level of seismic activity while Saturday and Sunday show a very low level as expected if these events are related to mining activities.*

tity seismic station have reported the origin district of the events by assigning them a number (**i** to **v**), and an event classification (explosion, earthquake or unknown).

Figures 55 to 57 show the forty events that were already classified by the Russian scientists according to their origin. Each mining area of the Khiniby Massif was represented except area **ii**. Events reportedly from the same part of the Massif showed a large variability in the recorded signal. This observation was confirmed by the results of the cluster analysis.

Five reference events are listed in the NORSAR report (NORSAR Sci. Rep. 1-91/92), each of them originating from one of the five different mining sections. Three of them (from mines **i**, **iii** and **v**) were located by the IMS, but only two had a signal length long enough to be processed using our method. The other two events (from mines **ii** and **iv**) were not identified by the IMS. Their sizes were 35 tons and 430 tons, respectively. The 35-ton event could have been missed because of a low SNR, but the 430-tons event was the largest of the reference events and it is not clear why it was not located by the IMS (probably due to a software failure). Only two events (from mines **iii** and **v**) whose sizes were 94 tons and 392 tons, respectively, were studied. The magnitude computed by the

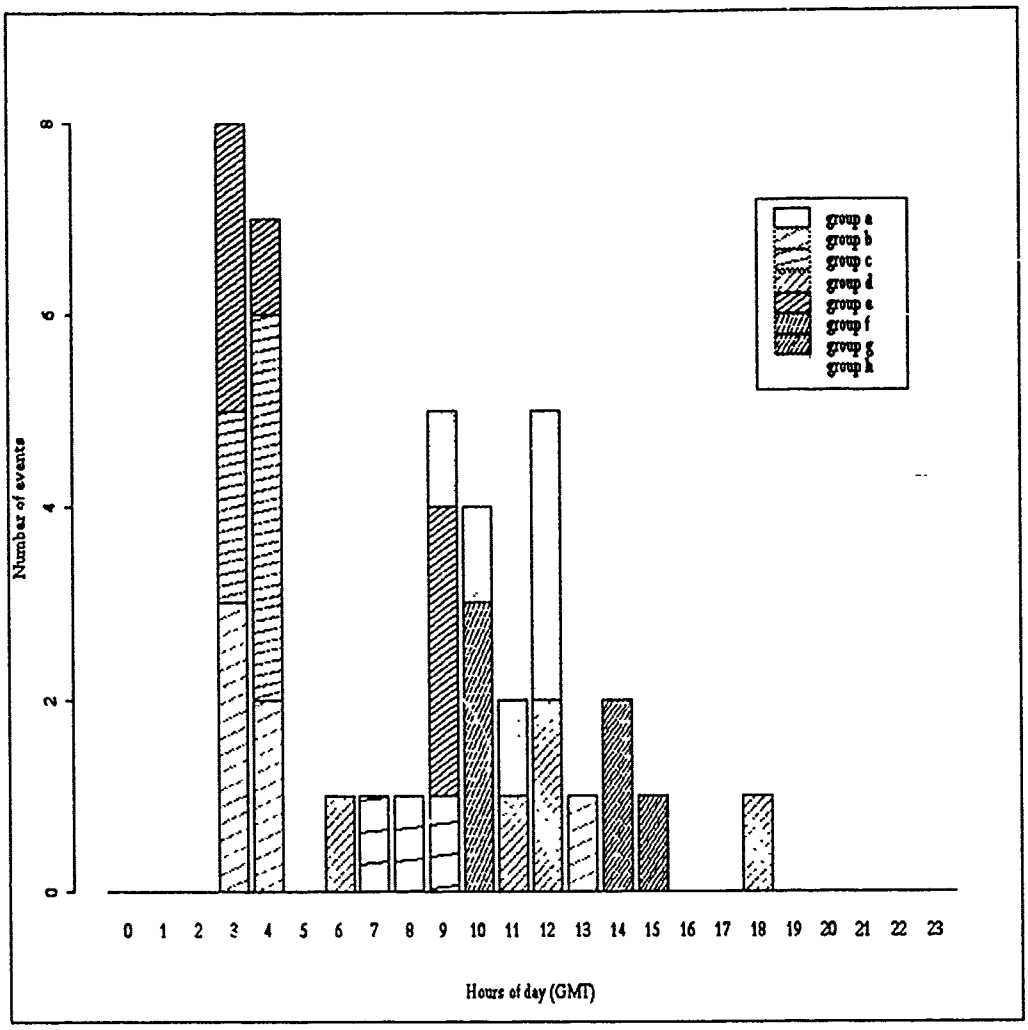

Figure 53: *Subarea II. Except for groups "c", "f" and "h", the origin times seem to occur randomly during the day and are more spread out over the entire day than for subarea I. Blasts start as early as 5:00 in the morning (local time), and end after 8:00 in the evening (local time).*

IMS was 2.45 for both of these events. Figure 57 shows signal recorded at ARCESS for both events. Amplitudes of the first arrival are nearly the same, which may explain the similar magnitude.

The interpretation of the results of the cluster analysis was difficult due to the number of events and the number of different kinds of signal. This large variability is reflected in the number of groups that could be defined using the cluster tree. One-hundred-ten events were distributed into 21 groups. Among the remaining events, 20 were mixed with another

event, 37 were unique, and 1 had a low SNR. It is interesting to notice that the events that are the most similar are usually close in time. For example, the four events belonging to group "f" occurred within 2 weeks.

In Figure 58, IMS locations are reported for events belonging to groups "a1", "f" and "h2". The maximum distance between the locations of two events belonging to the same group is as large as 25 km. Two events from group "a1" were reported in the Apatity bulletin as originating from mining area v.

Figure 59 shows the distribution of the magnitudes for 567 events located by the IMS in

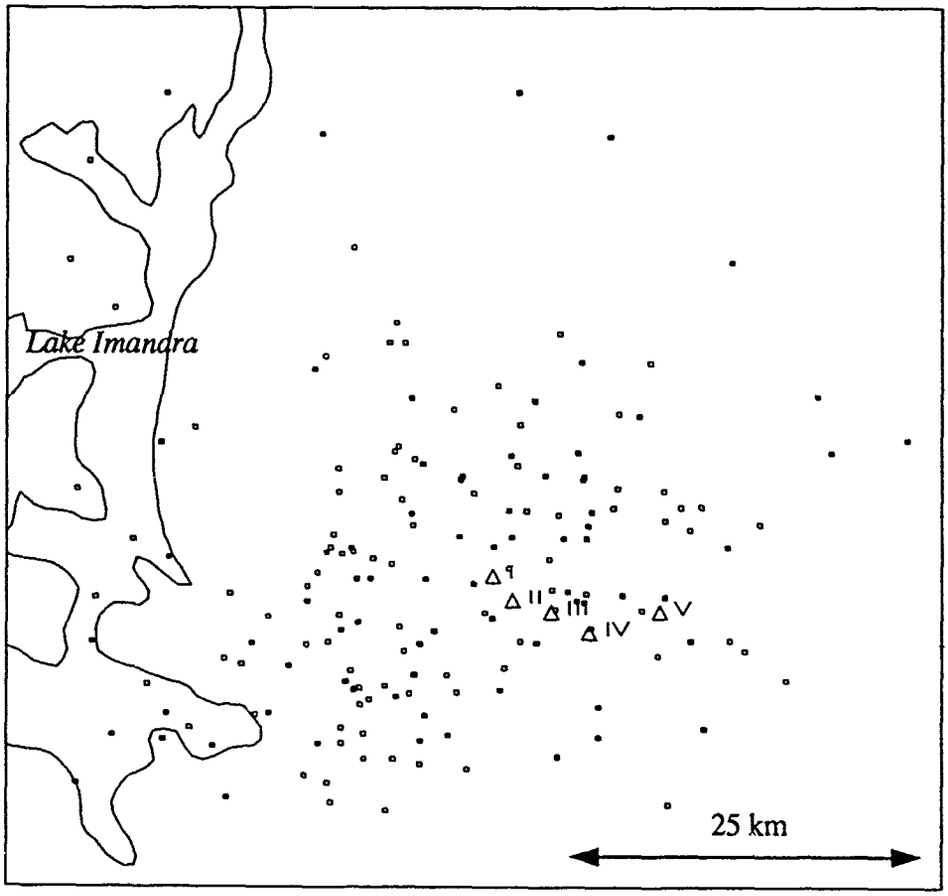

Figure 54: *Subarea III. Locations of 168 events (squares) from the Apatity mine in the Khibiny Massif. Five different mining sectors were identified (NORSAR report), the center of each sector is represented by a triangle.*

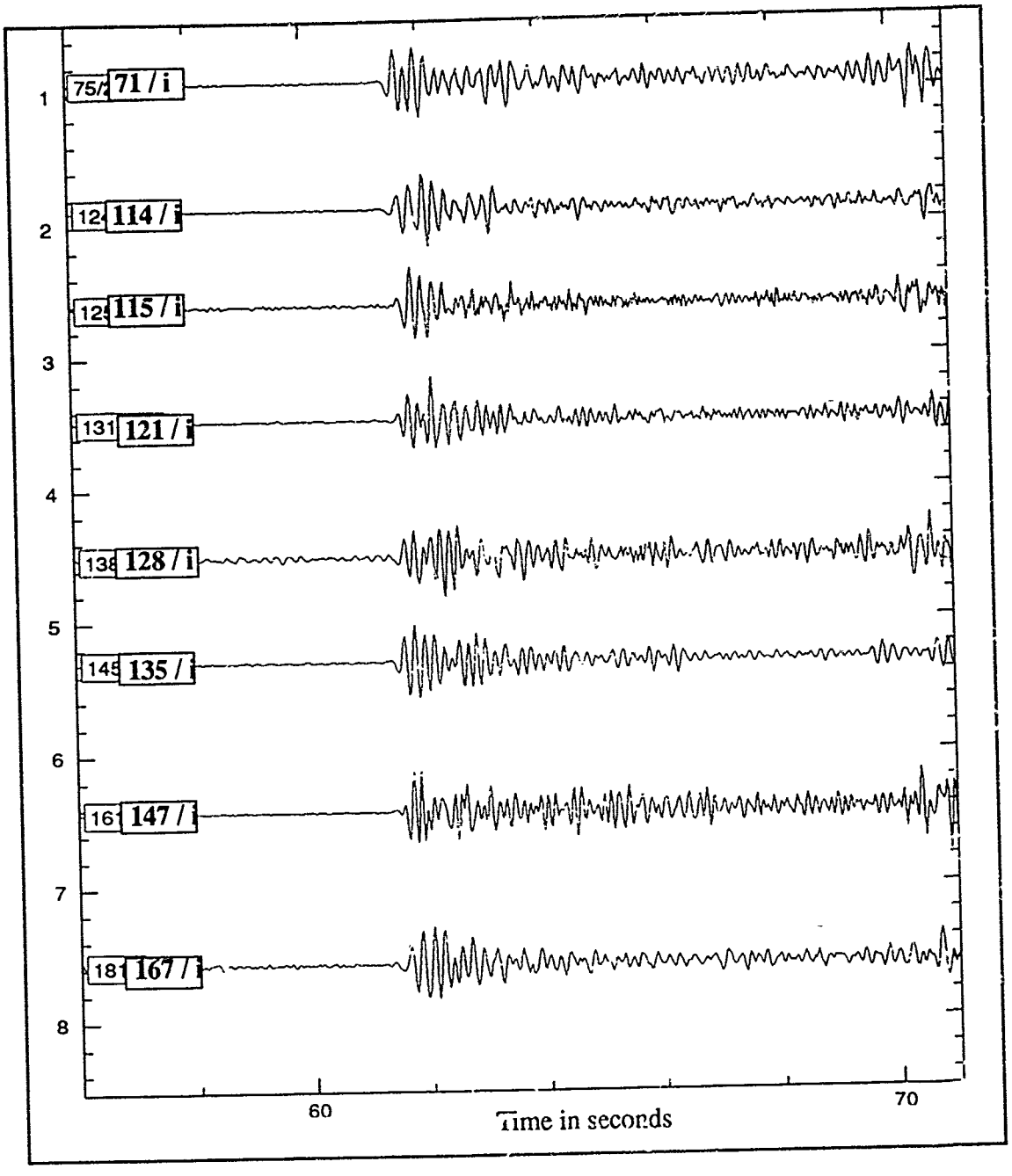

Figure 55: *Subarea III. Eight events from the data set were pre-classified as originating from the mining area I of the Khibiny Massif. Visually, they all have the same Lg-P time, but the shape of the first arrival is different from one event to another.*

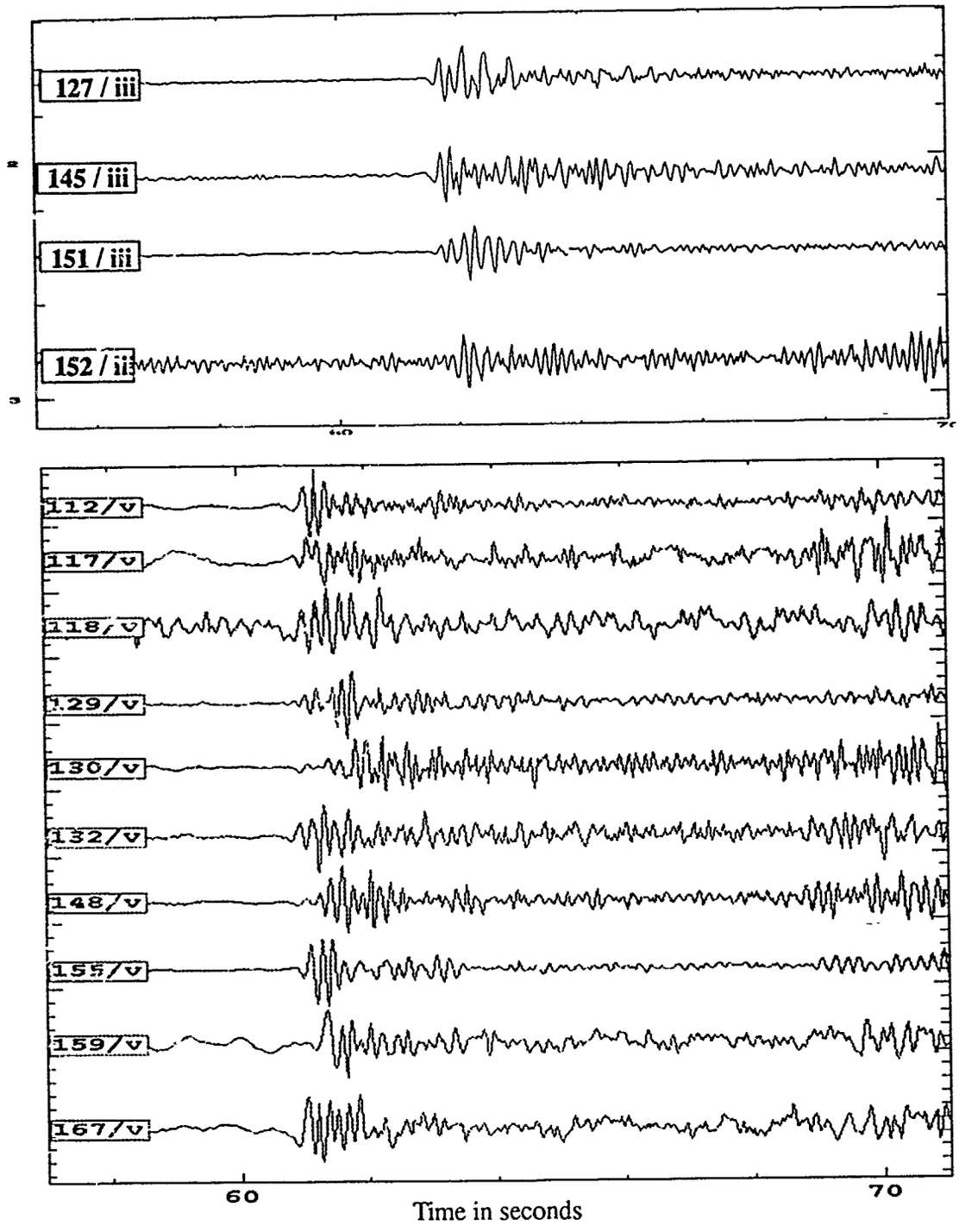

Figure 56: *Subarea III. Upper: First arrival for four events from mining area iii. Lower: First arrival for ten events from mining area v. In both cases, it is difficult to find particularities in the signals that would characterize the origin area.*

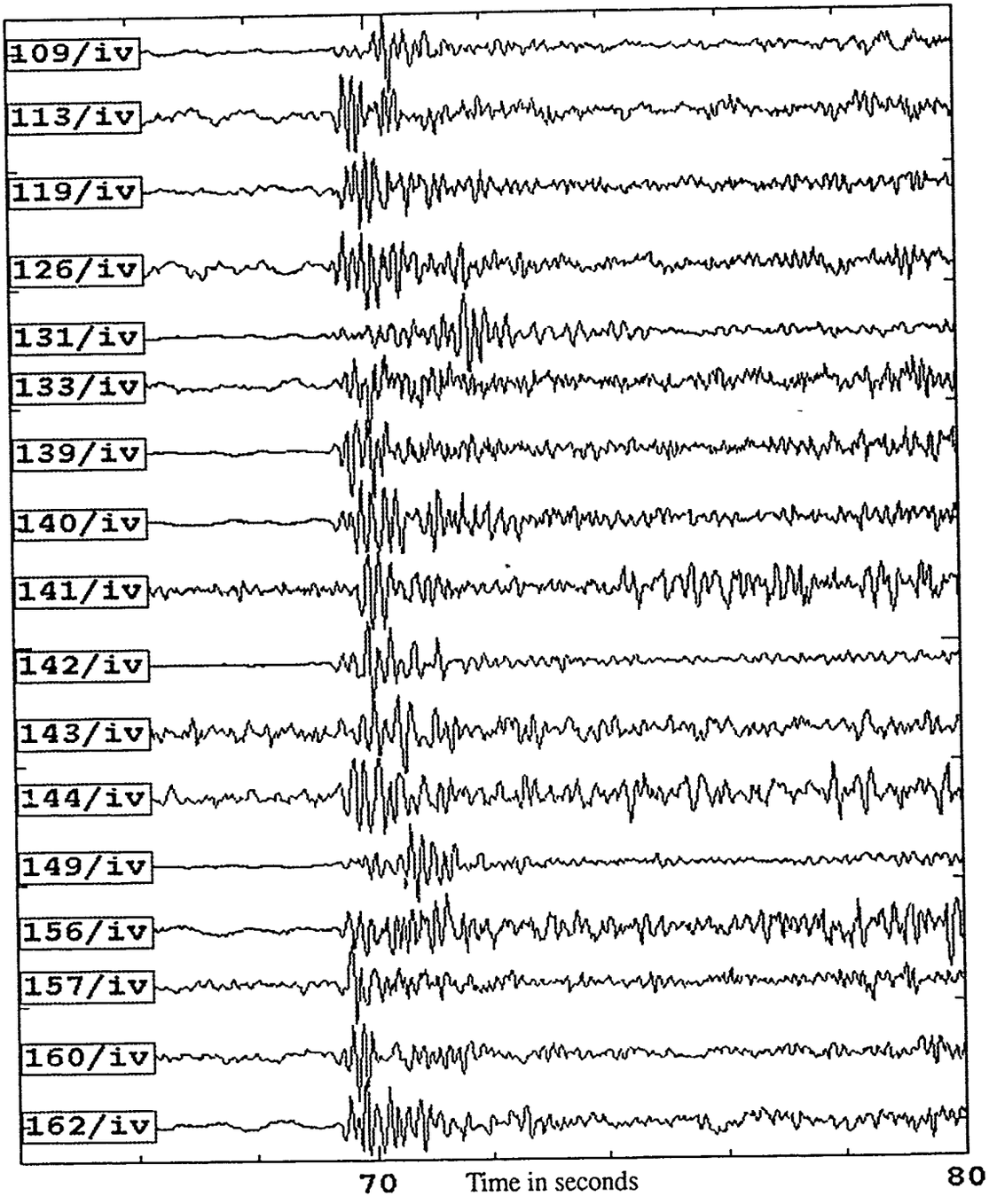

Figure 57: *Subarea III. Eighteen events of the data set occurred in mining area* ***iv*** *of the Khibiny Massif. Clear differences can been seen in the first arrival, which can be either emergent or impulsive, and also in the length of the wave train. The result of the cluster analysis disagreed with this classification.*

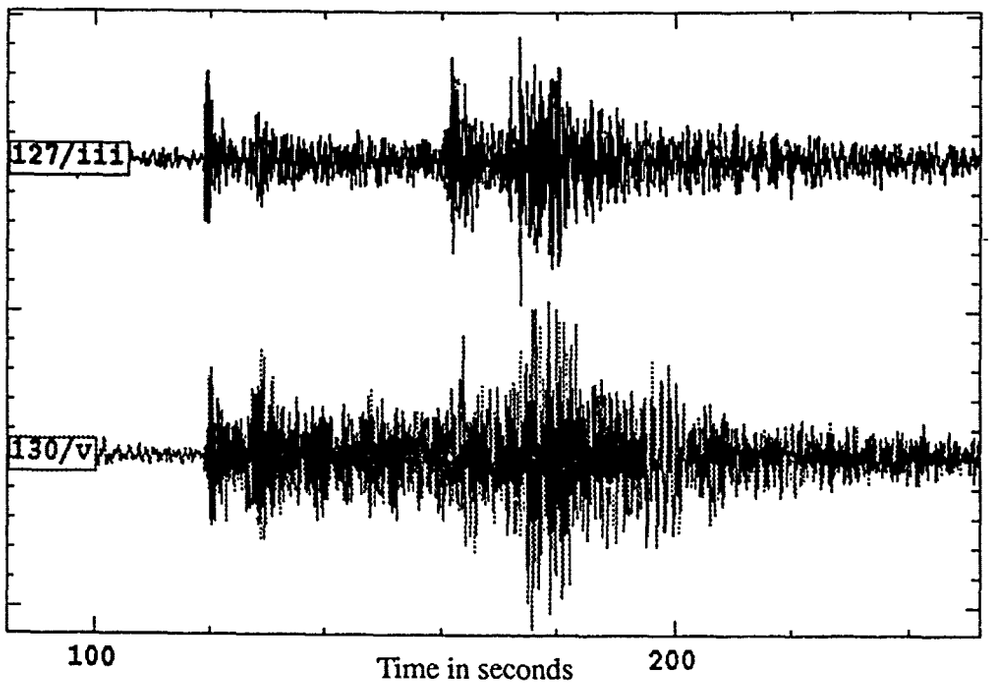

Figure 58: *Subarea III. Information about these two events are given in the NORSAR report. Their shot sizes are 94 tons and 392 tons, respectively. The local magnitude computed by the IMS was 2.45 for both events. The plot shows that the amplitudes of the first arrivals (plotted at the same scale) are about the same, while the amplitude of the Lg phase is clearly larger for the second event. Only the amplitude of the first arrival was used in the computation of the local magnitude.*

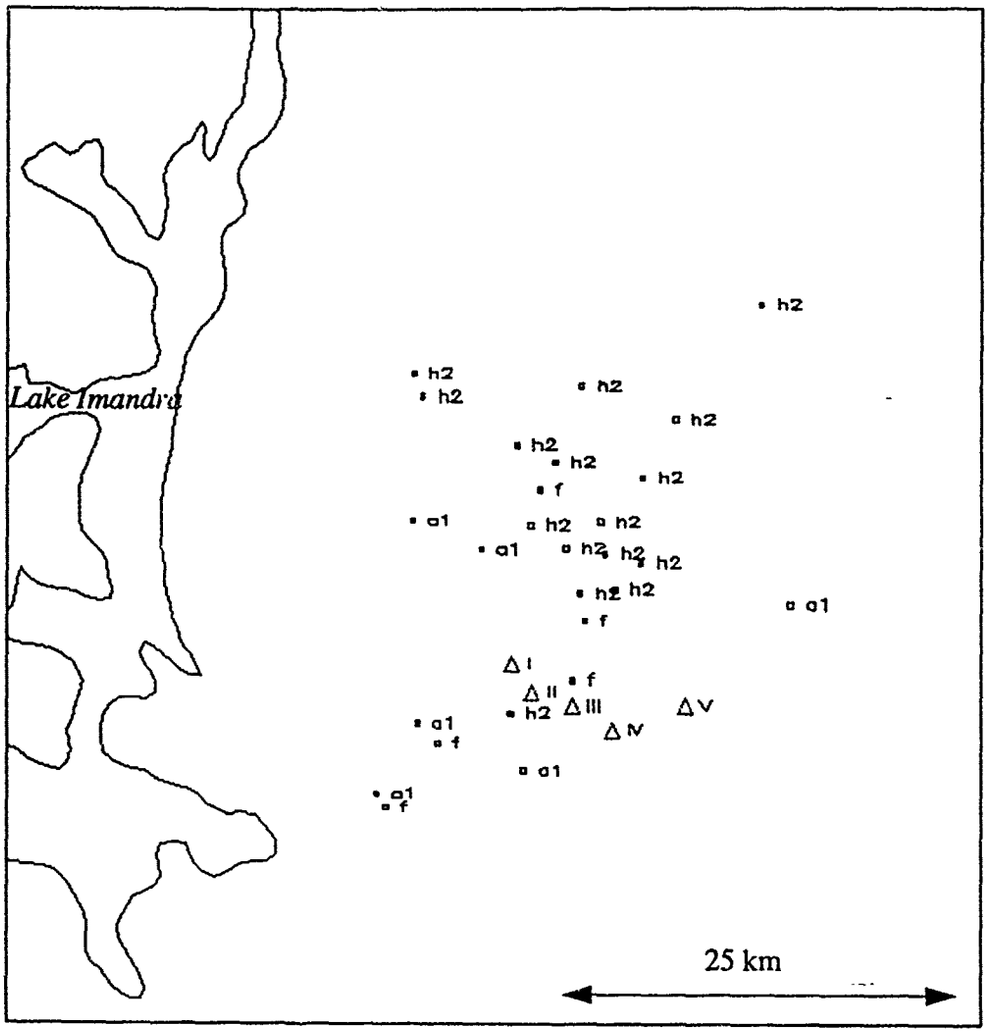

Figure 59: *Subarea III. Event locations for group "a1", "f", and "h2" (square). Locations of the five different mining areas of the Khiniby Massif are plotted (triangles). These locations were estimated from a map of the Khibiny Massif in the NORSAR report. Discrepancy between event locations within the same group can be as large as 25 km.*

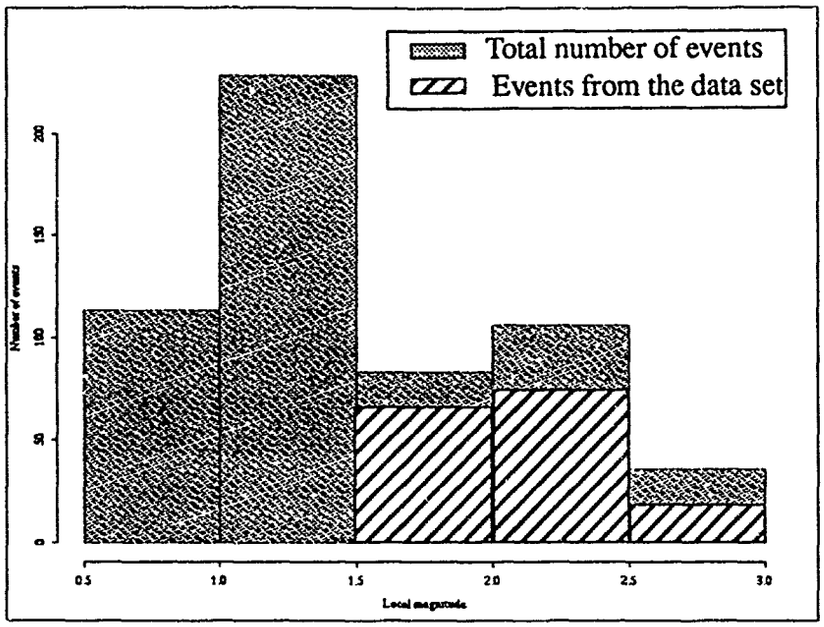

Figure 60: *Subarea III: Distribution of the local magnitude for 567 events located by the IMS in the Khibiny Massif. Superimposed is the distribution of the local magnitude for the set of events that was studied. A large majority of events have a magnitude below 1.5. The number of events with magnitudes between 2.0 and 3.0 is large with respect to the other mining areas in the Kola Peninsula.*

the Khibiny Massif between January 1,1991 and September 30, 1991. Half of the events occurring in this area have magnitude lower than 1.5, but in the same time, the largest events occurring in the Kola Peninsula (above 2.5) are concentrated in this area. *Figure 61* shows the daily distribution of the shots. Surprisingly, the origin times are evenly distributed over the week with a pick of activity on Friday. Half of the events occurring during the week-end are represented in our data set which implies that they have fairly large magnitudes. Figure 62 shows origin time during the day for each group of events and does not include events that were not classified. In contrast with subarea I and subarea II, these groups do not exhibit the origin time pattern that seems to characterize the other two mining areas.

Subarea IV

Sixty-three events were studied in this area (Figure 63). Several mines were found on DMA maps but their locations were not confirmed on SPOT images. Among these 63

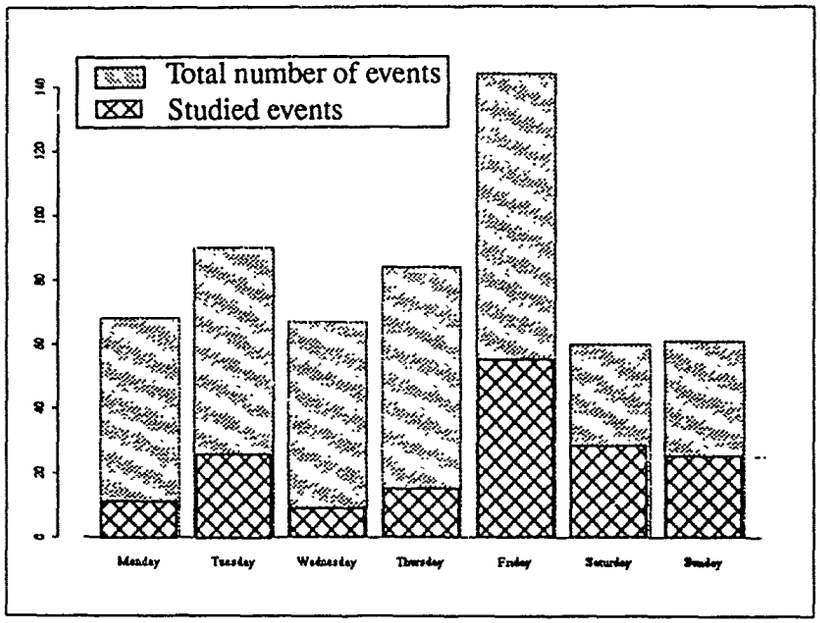

Figure 61: *Subarea III. Daily distribution of the origin times. The activity during the week-end is very high. As observed for subarea II, Friday has the largest number of events.*

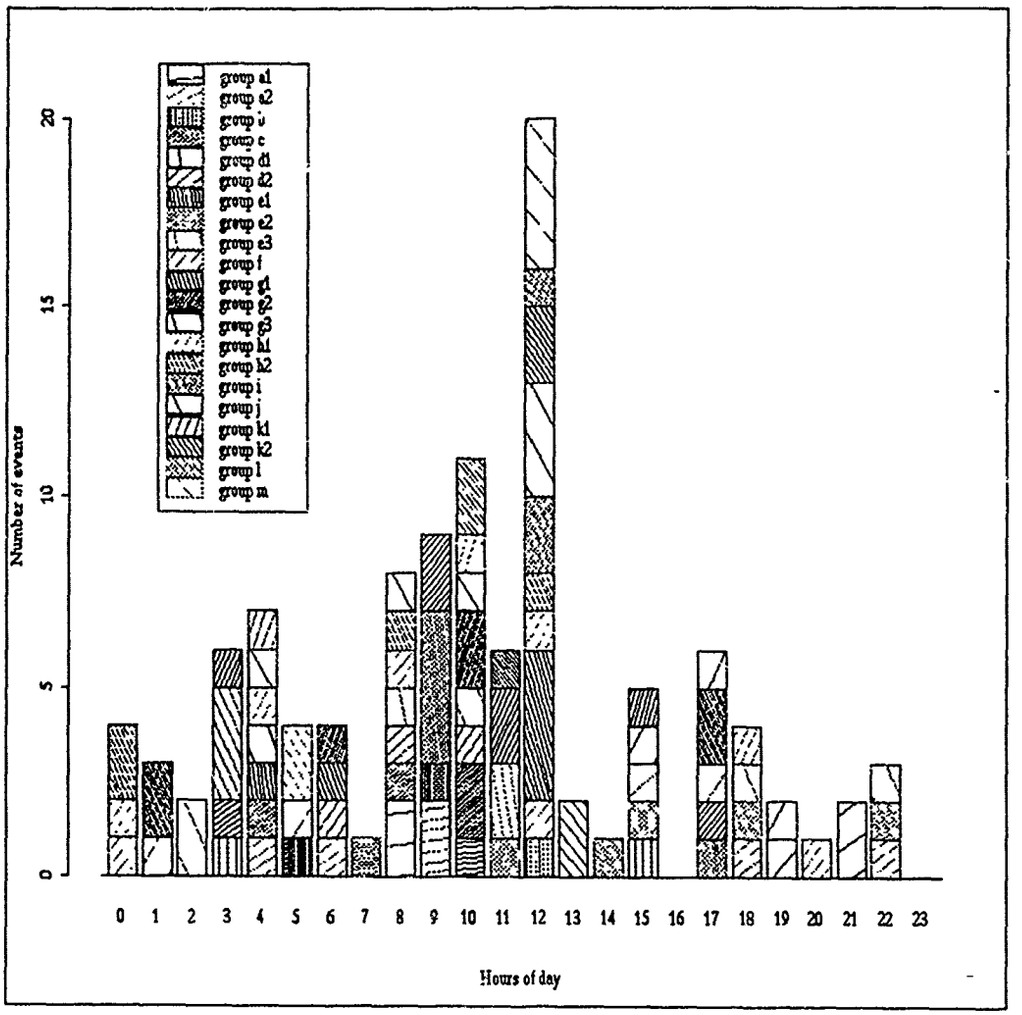

Figure 62: *Subarea III. Daily distribution of the origin times for the 168 studied events. Generally, shots from the same group take place at any time of the day. Some groups like "m" are more consistent, the origin times occurring between 12 pm and 3 pm (local time); while other groups like "h2" that show a very high level of similarity between events, have their origin times spread out over the entire day.*

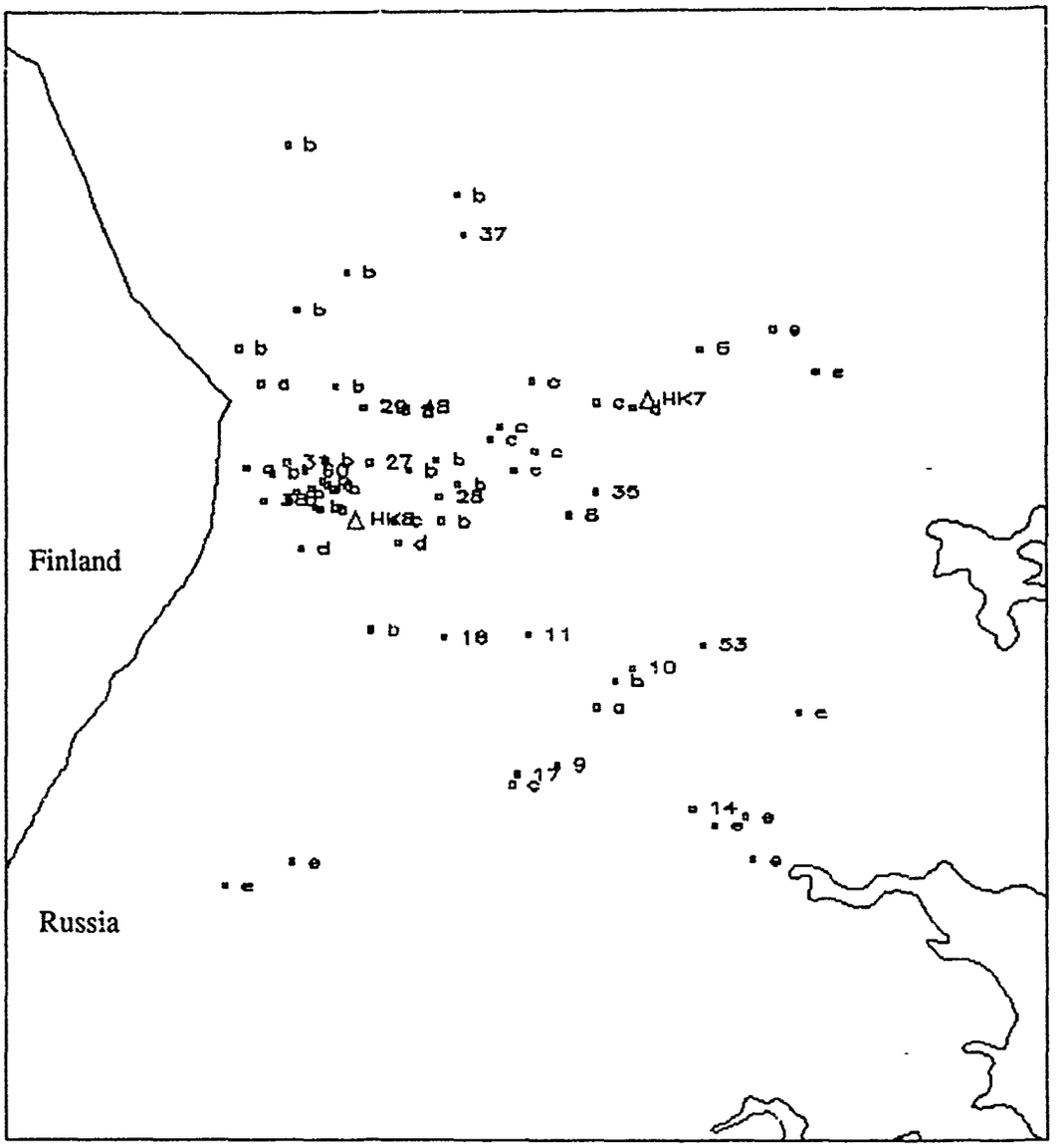

Figure 63: *Subarea IV. IMS locations of the 63 events (squares) that where located in subarea IV. The mine locations (triangles) were determined using a DMA map.*

events, 12 were multiple events that grouped together. The events were split into five groups (Figure 64) despite the fact that only four mines have been identified. The differ-

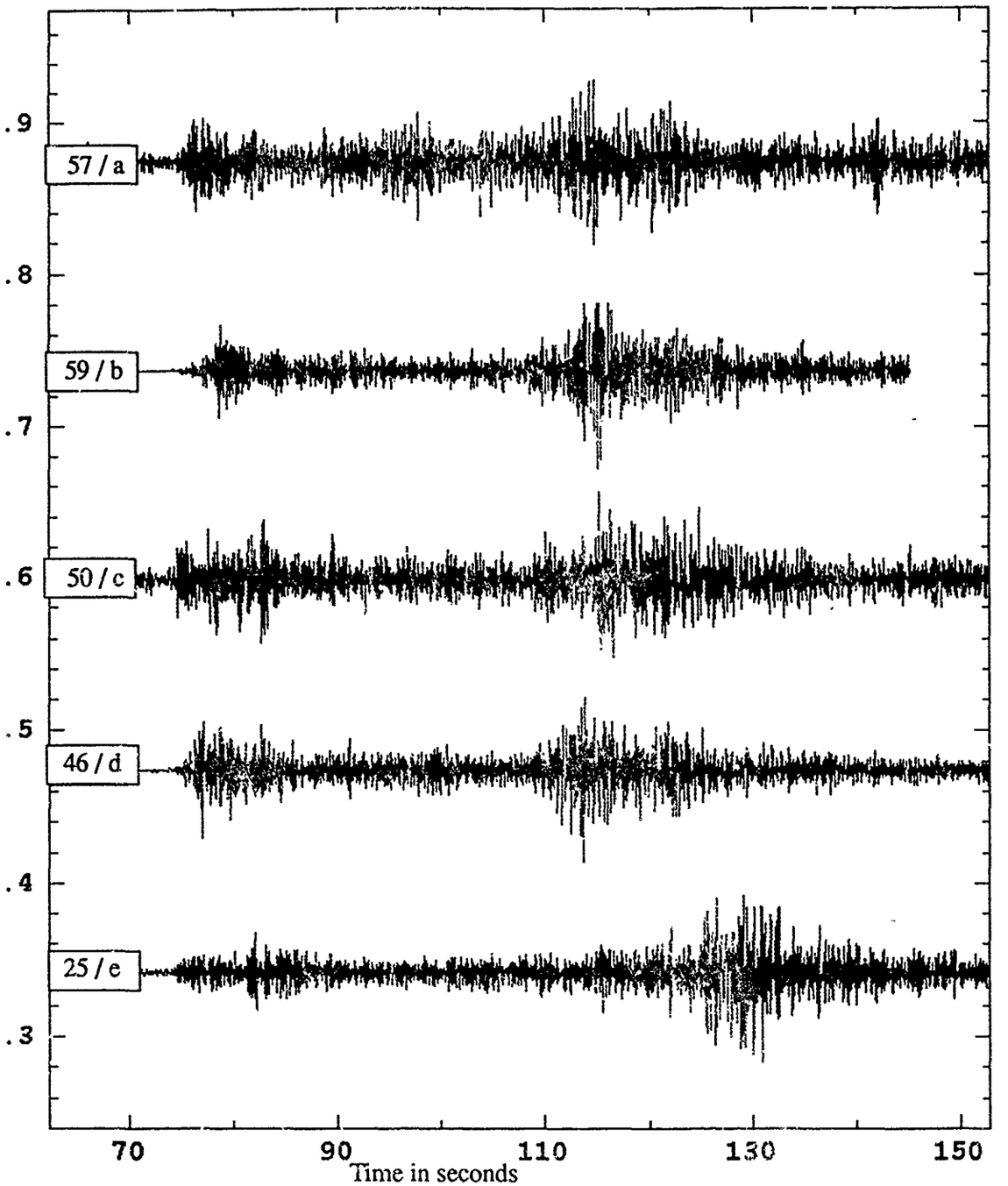

Figure 64: *Subarea IV. Five events have been plotted. Each of them is representative of one of the five groups that were defined. Events from group "e" are clearly further away. The events from subarea "d" show an emergent first arrival, often lost in the background noise for the lowest-magnitude events.*

ence in the *Lg-P* time between the first group and the last group is about 12 s. Most of the events are characterized by an emergent first arrival that is particularly difficult to identify.

Figure 65 shows the distribution of the magnitudes for 102 events located in this area by

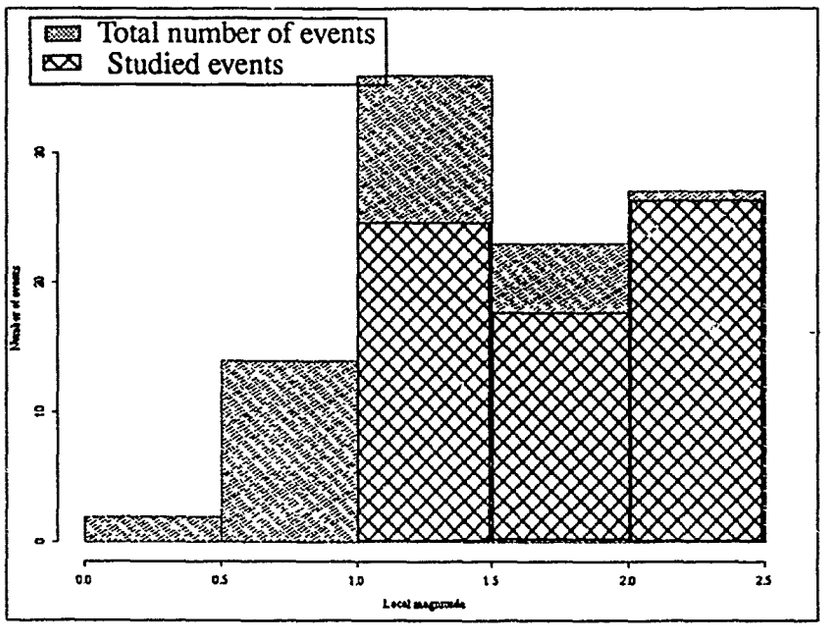

Figure 65: *Subarea IV. Distribution of the magnitudes for 102 events located in subarea IV by the IMS. Magnitudes for this subarea are higher, on average, than for the other subareas. Most of the events have magnitudes above 1.0 while it is the opposite for other subareas.*

the IMS. The magnitude histogram for this subarea is reversed with respect to the histograms for subarea I and subarea II. Most of the events in subarea IV have magnitude above 1.0 while it is the opposite for the events from subareas I and II. Nevertheless, SNRs are fairly low. The weekly distribution of the origin times is plotted in Figure 66. It shows that the highest seismic activity occurs unexpectedly on Saturday and that the activity on Sunday is not negligeable. The distribution of origin time during the day for each group of events is plotted on Figure 67. Origin times are concentrated in the middle of the day but none of the group shows a preferential time range. A low level of activity can be seen at 10 GMT (Noon, local time) while for subareas I, II and III, the seismic activity is high between 10 am and 11 GMT.

All off the features mentioned above: high magnitudes associated with low SNRs, high seismicity during the week-end, and emergent first arrival seems to indicate that the seis-

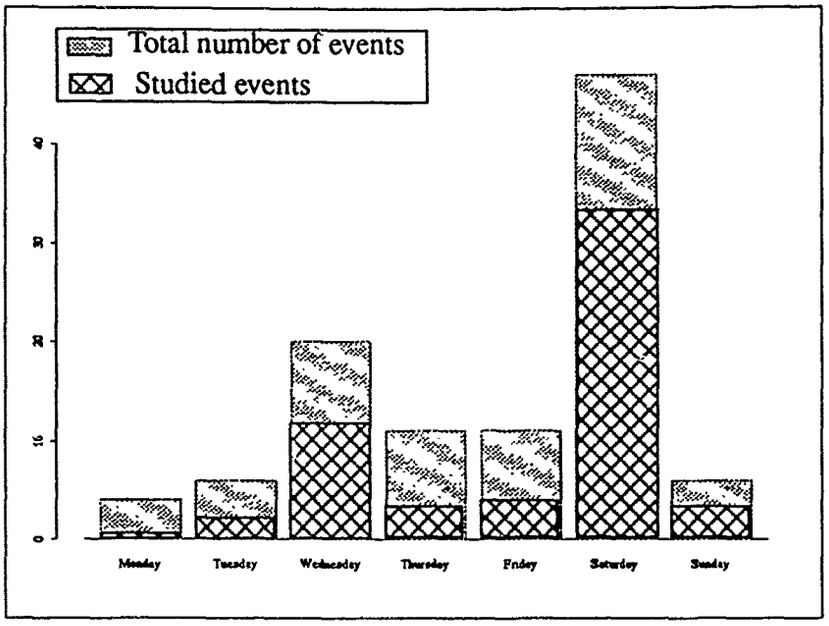

Figure 66: *Subarea IV. This weekly distribution of origin times shows that the highest activity occurs on Saturday and that the activity on Sunday is not neglegable.*

mic activity in this particular subarea is different from the seismic activity taking place in subareas I, II and III.

Subarea V

This subarea includes nine mines all located closed to Lake Imandra (Figure 68). Seventy-seven events from this area were studied. They were selected in such a way that the boundaries of the subarea did not include the Khibiny Massif which is a large mining area by itself (Apatity). Despite this selection basis, several events from Apatity were included in the data set because of the lack of accuracy in their locations. As with the events subarea II, the events are shifted toward the west with respect to the mines.

Most of the events could be classified into seven groups (Figure 69). The data set was split into two large groups at a low cross-correlation level, and this dichotomy was based on the difference between *Lg-P* times. On the left branch of the tree, the events (groups "d", "e", "f" and "g") were located further from the array. Some of them originated from Apatity. The other events (groups "a", "b" and "c") are clearly closer to the array. Within each of these two large subsets, the *Lg-P* times are fairly similar for each group.

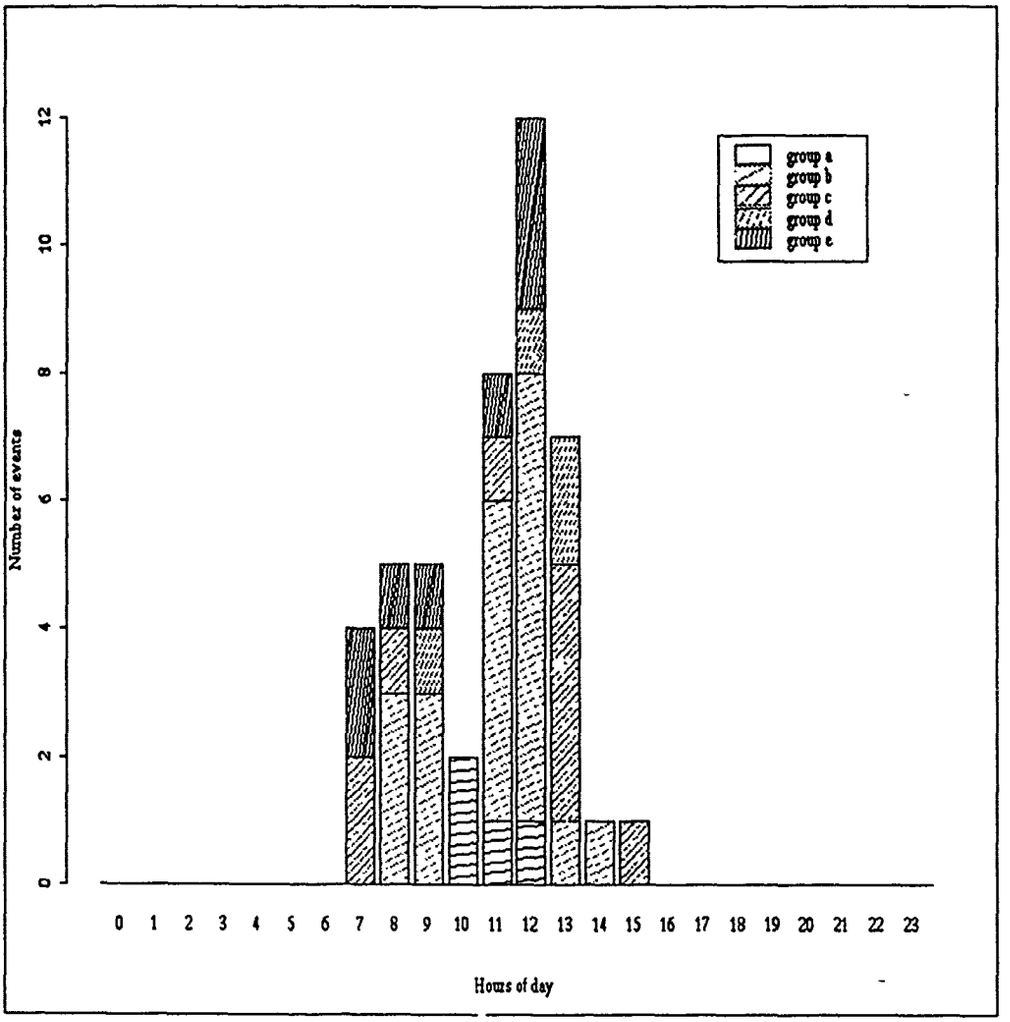

Figure 67: *Subarea IV. The origin times in this area are concentrated in the middle of the day with a lull at 10 am (Noon, local time). This is opposite to the other subareas, which show a very large number of shots between 10 am and 11 am GMT.*

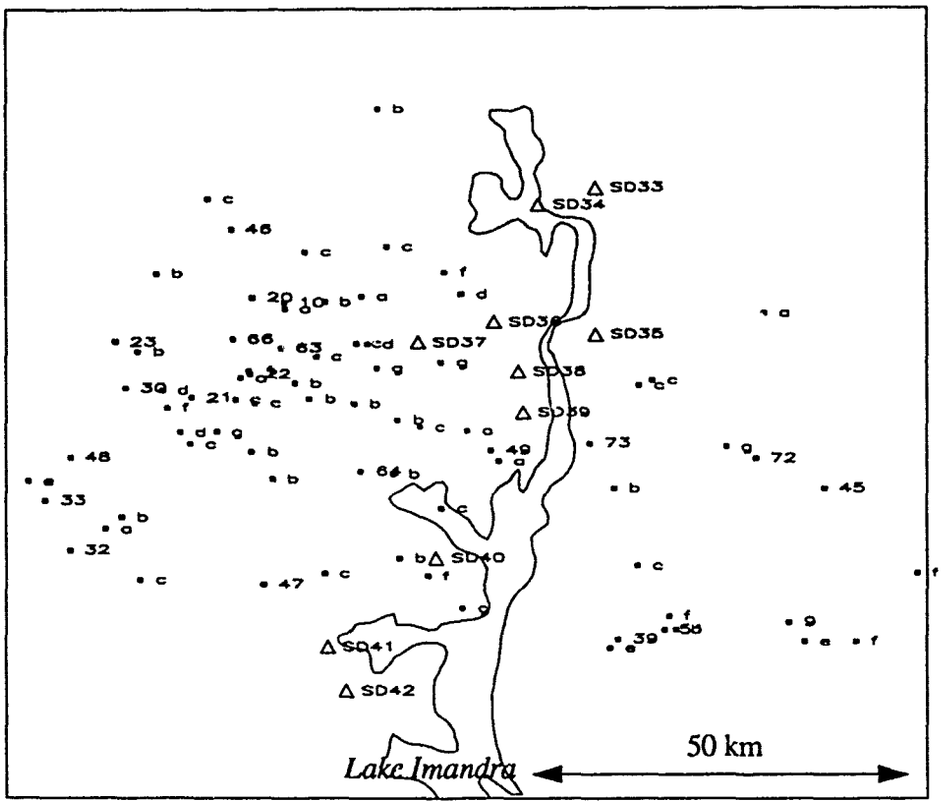

Figure 68: *Subarea V. IMS locations for 77 events (squares). Thirteen mine locations determined on SPOT photos have been reported (triangles).*

Twelve events were not classified; one had a SNR, five of them were multiple events, and the remaining six were unique but may fall in another group using Apatity events.

Figure 70 shows the distribution of the magnitudes for 237 events and Figure 71, their weekly distribution. These two histograms present the same features as the histograms plotted for subareas III and IV. That is, a majority of events have magnitudes between 1.0 and 2.5 and high level of seismic activity during the weekend, especially on Saturday. Figure 72 shows that the origin times are concentrated between 10 am and 1 pm GMT (between 12 am and 3 pm local time), and that a few events occur either very early in the

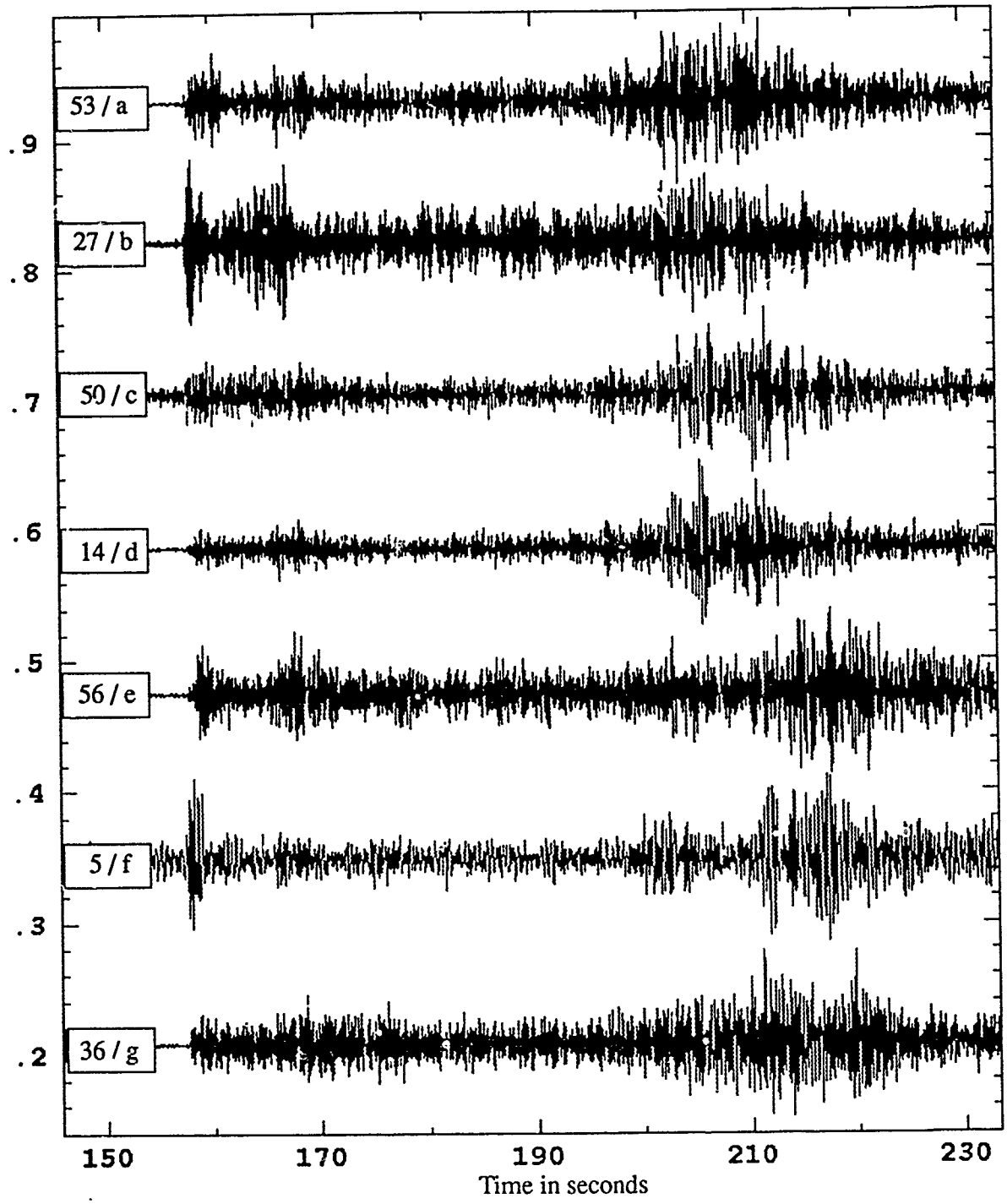

Figure 69: *Subarea V. Six events representing each of the six groups. Events can be separated into two large groups based on their Lg-P time: groups "a", "b", "c" , "d", and groups "e", "f" , "g". Events from group "f" are from the Apatity mine and match perfectly the events from group "h2" from subarea III.*

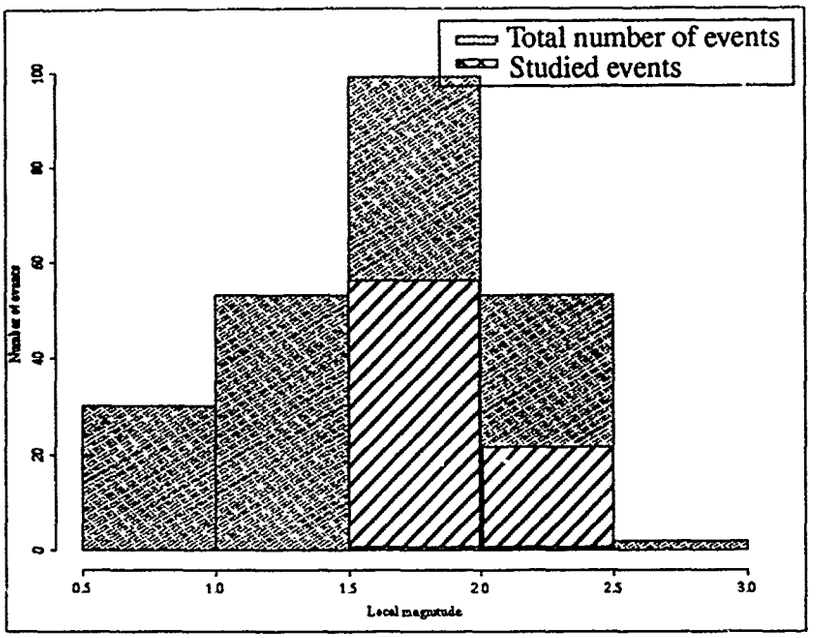

Figure 70: *Subarea V. Distribution of the magnitude for 237 events located by the IMS in this subarea. Most of the events have magnitudes between 1.0 and 2.5 and 78% have a SNR lower than 50.*

morning or very late in the evening. These late events were classified in the same group.

Subarea VI

This small part of the Kola Peninsula provided only 31 events. Three mines were located on SPOT photos in the subarea (Figure 73). Only a couple of groups could be defined with two or three events in each group. Most of the events were unique. In hindsight, the events should have been included in subarea III.

The magnitude distribution has been plotted in Figure 74 for 88 events located by the IMS in this subarea. Figure 75 shows the weekly distribution of the origin times.

Discrimination Between Earthquakes and Mine Blasts

As mentioned earlier in the introduction, the Kola Peninsula has both natural seismicity related to active faults and mining induced events. For the time interval considered in this study, 22 events were identified as having a natural origin in the Apatity bulletin. Fifteen events listed in the IMS bulletin had arrival times close enough to match with an event reported in the Apatity bulletin. Ten of them were located within the boundaries of the

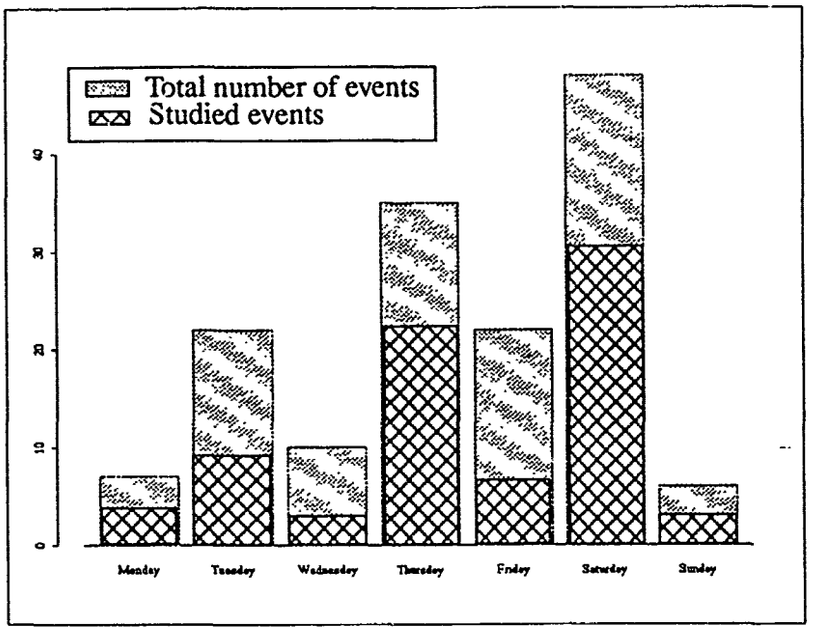

Figure 71: *Subarea V. Histogram showing the weekly distribution of the origin times. This shows that the most active day is Saturday.*

study area and were recorded at ARCESS. Waveforms for only five were useful (enough data) for the cross-correlation computation. Three events were located in subarea III, one in subarea V and one in subarea VI. Three of these events were classified into a group (indicating a mining related origin) and two were not classified. Each of the events, along with other events in their groups are plotted in Figure 76. One of these five events was associated with seven other waveforms that were nearly identical (Figure 76, left). The waveform similarities imply almost identical source parameters, so we believe that these events are either mining blasts or mining induced tremors. Two other events were associated with a group in which the similarities are not as evident (Figure 76, right upper and middle). The small number of event in these two groups prevent speculation about the origin of the events. The last two events were not associated with any group.

Summary and Conclusions

The most important feature of the Kola Peninsula is the presence of both mining activity and natural seismicity. Twenty-seven events were identified as earthquakes by the Russian scientists during 1991. Unfortunately, data were available for only a few of them. The comparison between the bulletin from Apatity seismic station, the results of cluster analysis and the visual classification illustrates the difficulties in correctly identifying the origin

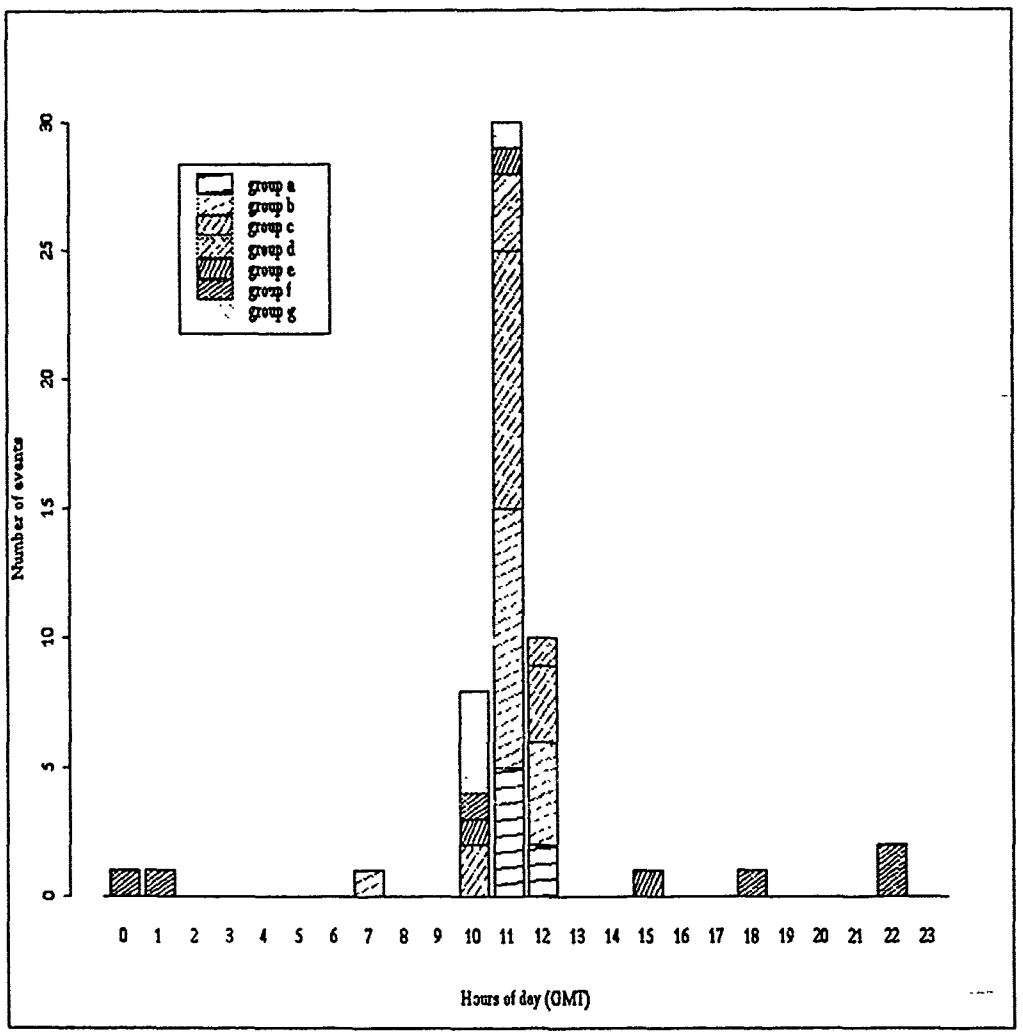

Figure 72: *Subarea V. Daily distribution of origin times. The majority of events occurred in the middle of the day. The five events that occured in the middle of the night belong to the same group.*

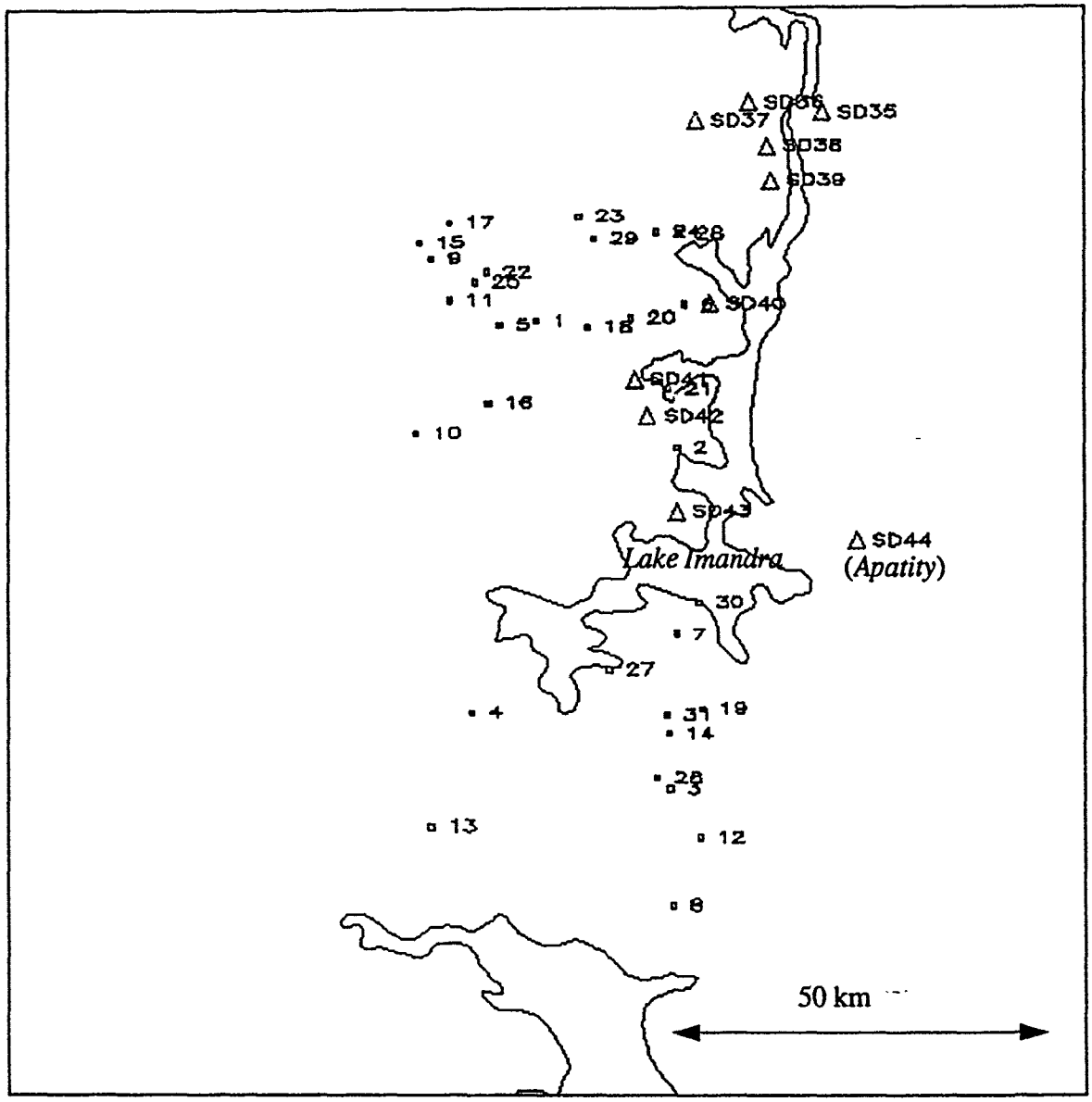

Figure 73: *Subarea VI. IMS locations for 31 events have been plotted along with the mines located in this subarea. Only four of the mines shown in the plot are within subarea VI: SD40, SD41, SD42 and SD43.*

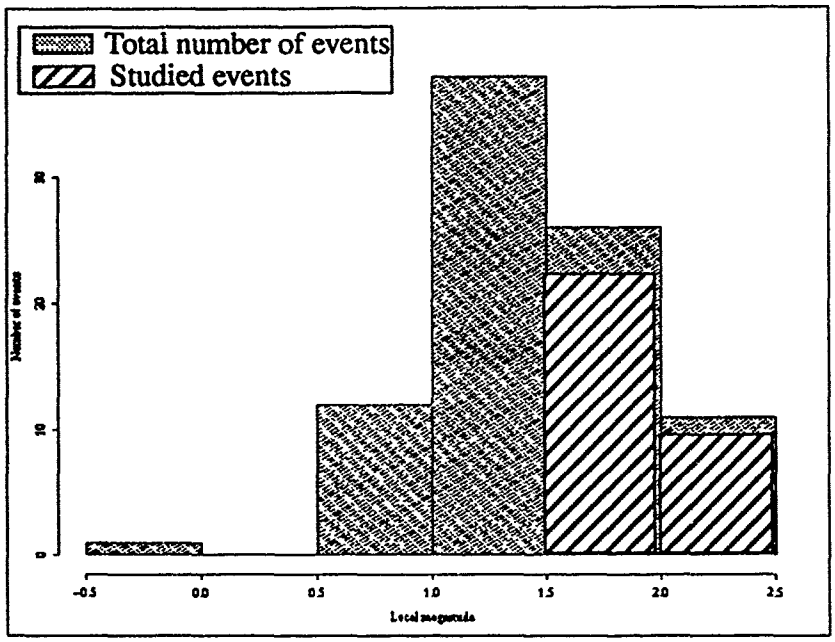

Figure 74: *Subarea VI. Distribution of the magnitude for 88 events located by the IMS in subarea VI. This histogram exhibits the same features as the histograms for subarea III and V: most of the events have a magnitude above 1.0.*

of an event. Several of the events identified as earthquakes in this bulletin may really be mining induced events (tremors).

This study shows that the computation of cross-correlation values needs to be done using customized parameters determined for each subareas. The cluster analysis provided reliable grouping of events even at the largest distances (up to 450 km), that is the groups defined on the dendrograms were in a good agreement with the analyst review of the events. Difficulties in grouping events occur for subarea III and seem to be due to the variability of the source of the events rather than to the distance from the array. Additional features of the data can corroborated the grouping such as the origin time distribution as a function of days of week and as a function of hours of day.

These weekly distributions of the origin time for the Kola Peninsula indicates that much of

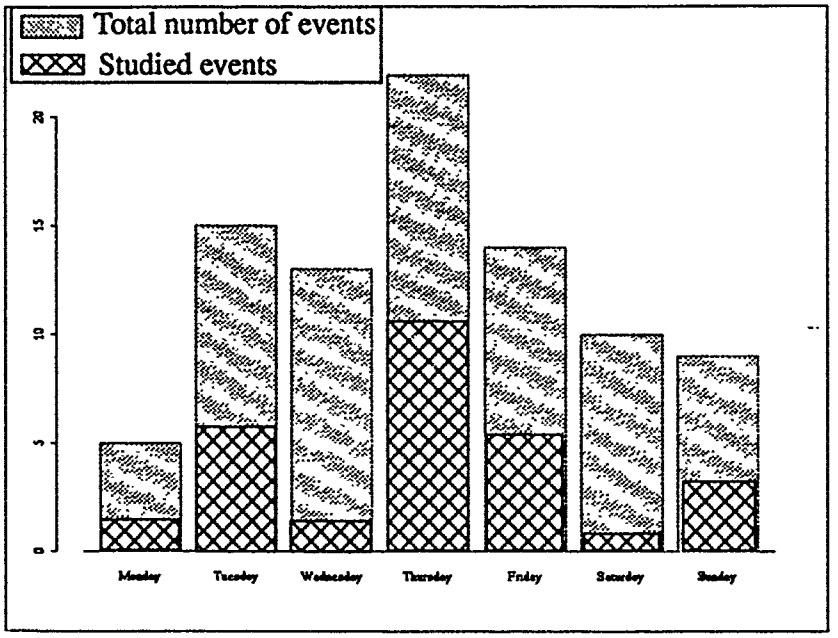

Figure 75: *Weekly distribution of the origin times. As already mentioned for subareas III, IV and V, the seismic activity is high during the weekend.*

the blasting occurs on Friday or on Saturday depending on the subarea. It is unlikely that this weekend seismic activity could be related to natural seismicity since the majority of them occur in the middle of the day.

The results show that the application of the cluster analysis can be easily extended to other areas and larger distances than what was originally done in Karelia. The method needs to be improved in cases where events from the same mine show a large variability in the signal (e.g. Apatity mine). This study of large groups of events with nearly identical waveforms, yet with locations that are widely distributed, indicates that event location could be significantly improved using automatic methods. Based on the results presented in this report, the subdivision of the Kola Peninsula into six subareas could now be revised and optimized.

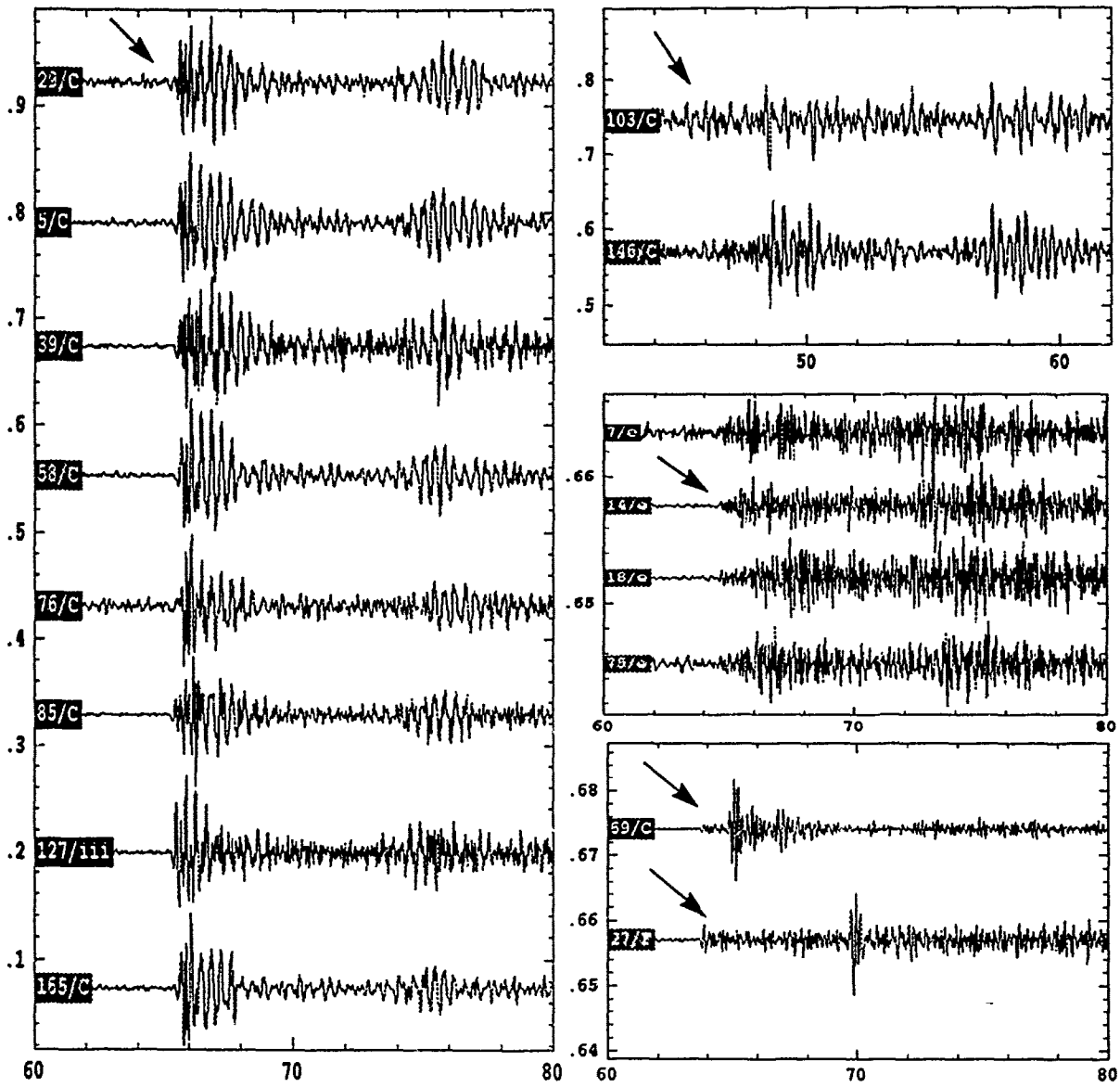

Figure 76: *The arrows show events that were identified as earthquakes in the Apatity bulletin. Upper left: Group of eight events from subarea III. Upper right: Group of two events from subarea III. Middle right: Group of four events from subarea V. Lower right: Two events from subarea III and subarea VI, respectively, that were not classified in any group.*

References

Mykkeltveit S., A. Dahle, J. Fyen, T. Kvaerna, P.W. Larsen, R. Paulsen, F. Ringdal and E.O. Kremenetskaya (1992). Norsar Scientific Report 1-91/92, Kjeller, Norway.

Rivière-Barbier F. and L. Grant (1992). Cluster Analysis of Closely Spaced Mining Blasts as a Method of Event Location. *Final Technical Report, October 1991*, PL-TR-92-2006. SAIC, Center for Seismic Studies.

Polarization Filtering of Depth Phases

Anne Suteau-Henson

Introduction

Polarization filtering has been applied to the P-wave coda of earthquakes with depth larger than 30 km to enhance the depth phases. The processing method was developed by A. Jurkevics (1986a), and is designed to enhance rectilinear signal in the direction of the initial P-wave. It was applied to 3-component recordings of events that occured during five days of reprocessed data from the GSETT-2 experiment (GSE/US/72, 1992). Compared to the vertical components, the polarization-filtered traces show enhanced signal in the time windows corresponding to the depth phases.

Method

The polarization filtering method used in this study was developed by A. Jurkevics (1986a). It is based on the calculation of the polarization ellipsoid in overlapping time windows for a set of frequency bands. For each time window and frequency band, the polarization ellipsoid is noise-corrected. Then, the signal coming within a small angle from a given direction is extracted. An aperture parameter is set specifying how much signal off the selected direction is passed. The resulting signal is multiplied by a rectilinearity factor, to a given power, so as to enhance rectilinear signal. Finally, the contributions of all time windows and frequency bands are summed.

Jurkevics (1986a) tested this method on synthetic data and showed how its performance decreases with decreasing signal-to-noise ratio (SNR). He then applied it to a short-period RSTN recording of a regional earthquake. Several bursts of rectilinear signal, both in the direction of the initial *P*-wave and with SV polarization, were observed in the *P*-wave coda of the filtered trace. A strong frequency dependence of incidence angle was also observed with higher-frequency signal emerging closer to the vertical. He also applied this technique to recordings of a suspicious event from West Kazakh at NORESS and RSTN stations (Jurkevics, 1986c). For data with sufficient SNR, polarization filtering indicated that no rectilinear energy in the *P*-wave direction could be observed in the *P*-coda beyond 10 seconds of the onset. An attempt was made to enhance depth phases in the *P*-coda of teleseismic recordings of a presumed East-Kazakh nuclear explosion at RSTN stations (Jurkevics, 1986b). Not enough time resolution, however, was achieved by this method to resolve *pP-P* time delays of less than 0.5 second, typical of scaled-depth explosions.

The Dataset

The dataset used in this study was extracted from the five days of reprocessed data for the GSETT-2 experiment (April 29 and May 30 - June 2, 1991). Which had been carefully analyst-reviewed (GSE/US/72, 1992). Events with depth > 30 km were selected, and a search for short-period waveform data from 3-component stations was performed. Finally, stations at which at least one depth phase (*pP* or *sP*) had been identified were selected. As this study required 3-component recordings, most of the usable stations were either from the US/NDC network or the IMS arrays. A total of eleven events were thus selected. The event information (from the database for the five reprocessed days of GSETT-2) is summarized in Table 11. The "orid" is the unique origin identification number, assigned to

Table 11: Event Information

Event Number	Orid	Date	Time	Lat.	Lon.	Depth (km)	m_b
1	105633	4/29/91	6:54:55	20.26S	174.38W	39	4.6
2	105697	4/29/91	15:36:29	44.46N	152.17E	41	4.2
3	105723	4/29/91	19:41:15	8.81N	126.62E	34	4.0
4	107135	5/30/91	9:06:22	23.39S	68.11W	116	5.2
5	107206	5/31/91	1:28:31	46.02N	153.13E	35	4.5
6	107264	5/31/91	17:47:3	17.57N	94.55W	139	4.0
7	109463	6/1/91	6:53:0	51.39N	173.35W	48	4.4
8	109469	6/1/91	8:56:7	54.52N	161.52W	32	5.0
9	109487	6/1/91	12:00:55	11.93N	62.67W	96	3.7
10	109555	6/2/91	16:25:27	24.82S	179.93E	495	4.4
11	109565	6/2/91	17:35:43	40.02N	143.97E	33	4.2

each event in this database. The events have m_b estimates ranging from 3.7 to 5.2. Four of the events had depths ranging from 96 to 495 km, while the remaining seven had shallower depths, between 30 and 50 km.

The locations in Table 11 compare well with the NEIS locations. For the events with depth > 50 km, the NEIS depth estimates are slightly larger (by 2-6%). Events with depth < 50

km had constrained depths in the NEIS bulletin, with three exceptions. In one case, the GSETT and NEIS depth estimates differed significantly: event 3 was assigned a depth of 74 km by NEIS and 34 km by the GSETT analyst. The GSETT depth, however, appears to be well constrained by a clear *pP* phase observed at station ARA0 (Flori Ryall, personal communication).

Depending on the event, recordings at 1-6 stations were obtained. Epicentral distances vary from 28 to 91°, except for one regional recording at 14° distance (event 6 at LTX). For each event at a given station, the theoretical azimuth and incidence angle of the initial *P*-wave were calculated based on the event and station locations and the event depth. The slowness (from Jeffreys-Bullen tables) was converted to apparent incidence angle after correction for surface reflection. The incidence angle ranges from 16 to 31° at teleseismic distances, and is 45° for the regional recording. Therefore, the polarization-filtered trace is best compared to the vertical component. Table 12 summarizes, for each event, the distance, azimuth, incidence angle, and observed depth phases at each station. The numbers in parentheses in the "*P*-Coda Phases" column give the observed time delay between the two preceding phases to the nearest second. The observed delays range from 10 to 33 seconds, except for the deepest event (10), with a *pP-P* time of 112 seconds.

Results

For the waveform data described in Table 12, two minutes of data were processed starting 30 seconds before the initial *P*-wave. A zero-phase bandpass filter of order 4 was applied with a passband adjusted to suppress low- and/or high-frequency noise. Except for particularly noisy records, the passband was set to 0.1-5 Hz. The number of time and frequency cycles was set to 4, the aperture to 20, and the rectilinearity scaling power to 1 (see Jurkevics, 1986a, for a complete description of these parameters). The direction of polarized motion was specified by the azimuth and incidence given in Table 12. Of particular interest are the data with low SNR.

Enhancement of depth phases through polarization filtering was achieved in most cases. It is particularly remarkable for events 2 and 7. Figure 77, for example, shows the three-component and the polarization-filtered traces for event 2 at ARA0. In some cases it appears that the choice of a narrower passband may improve the results by suppressing more low and/or high-frequency noise (e.g., event 1 at MAT, Figure 78). Event 4 is a large event with well enhanced depth phases at all stations (Figure 79). In particular, rectilinear signal in the *P*-wave direction can be observed at the expected time for *sP* on the polarization-filtered trace at station PFO, where this phase was not reported (Figure 80). At low

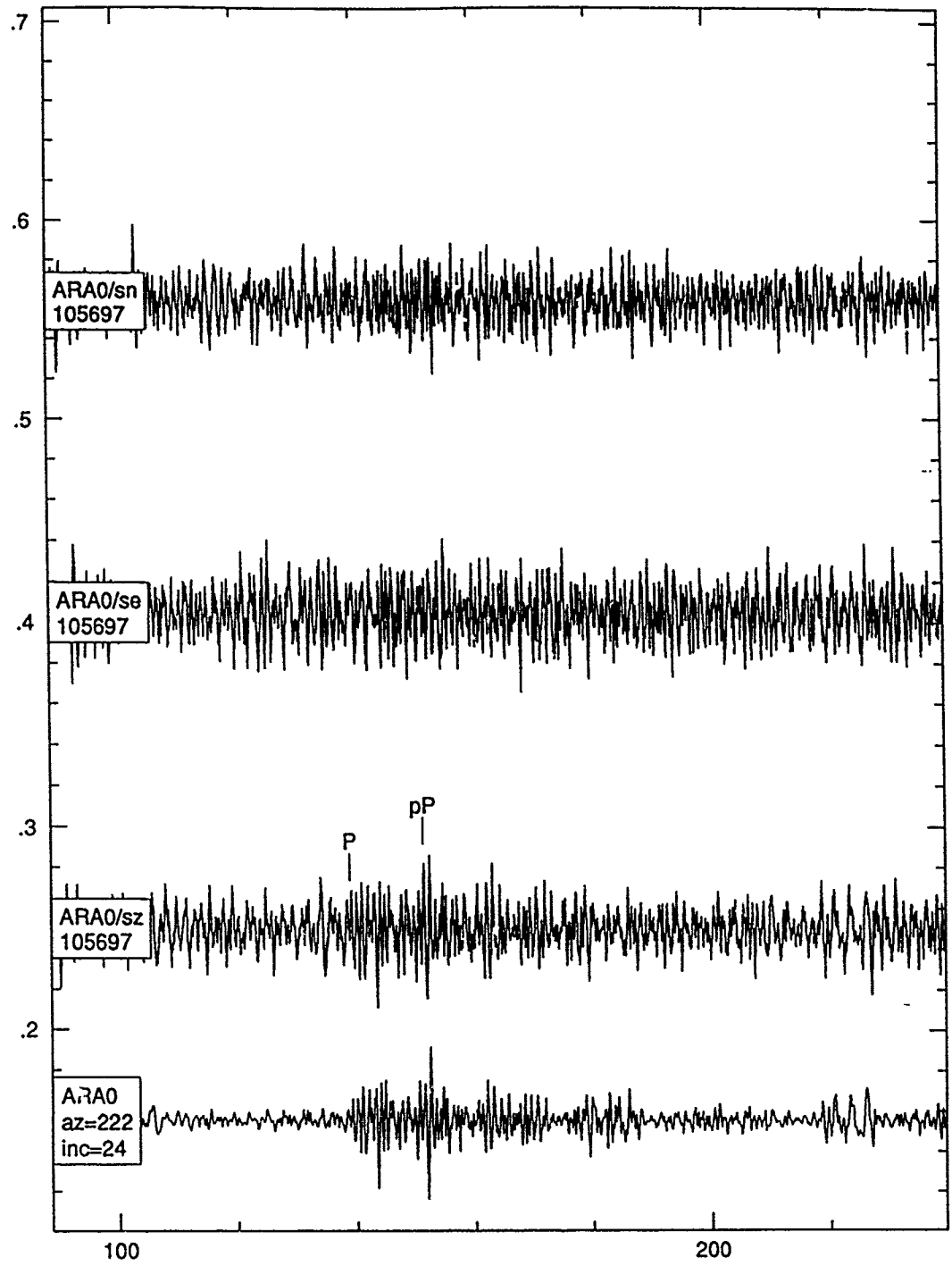

Figure 77: *Three-component and polarization-filtered traces for event 2 at ARA0. This is an example of good enhancement of the depth phases through polarization filtering.*

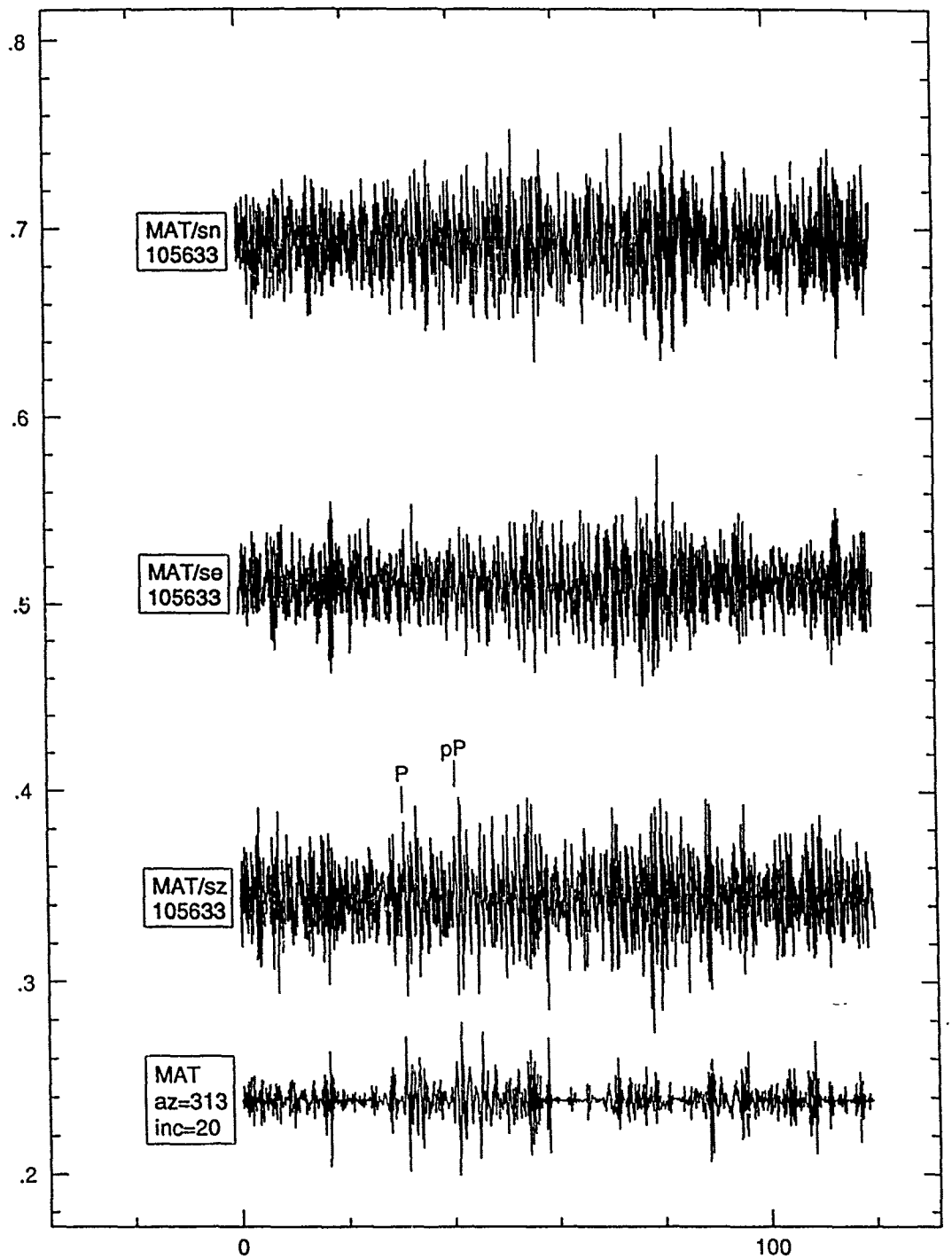

Figure 78: *Three-component and polarization-filtered traces for event 1 at MAT. In this case, a narrower bandpass filter may be necessary to improve the enhancement of depth phases.*

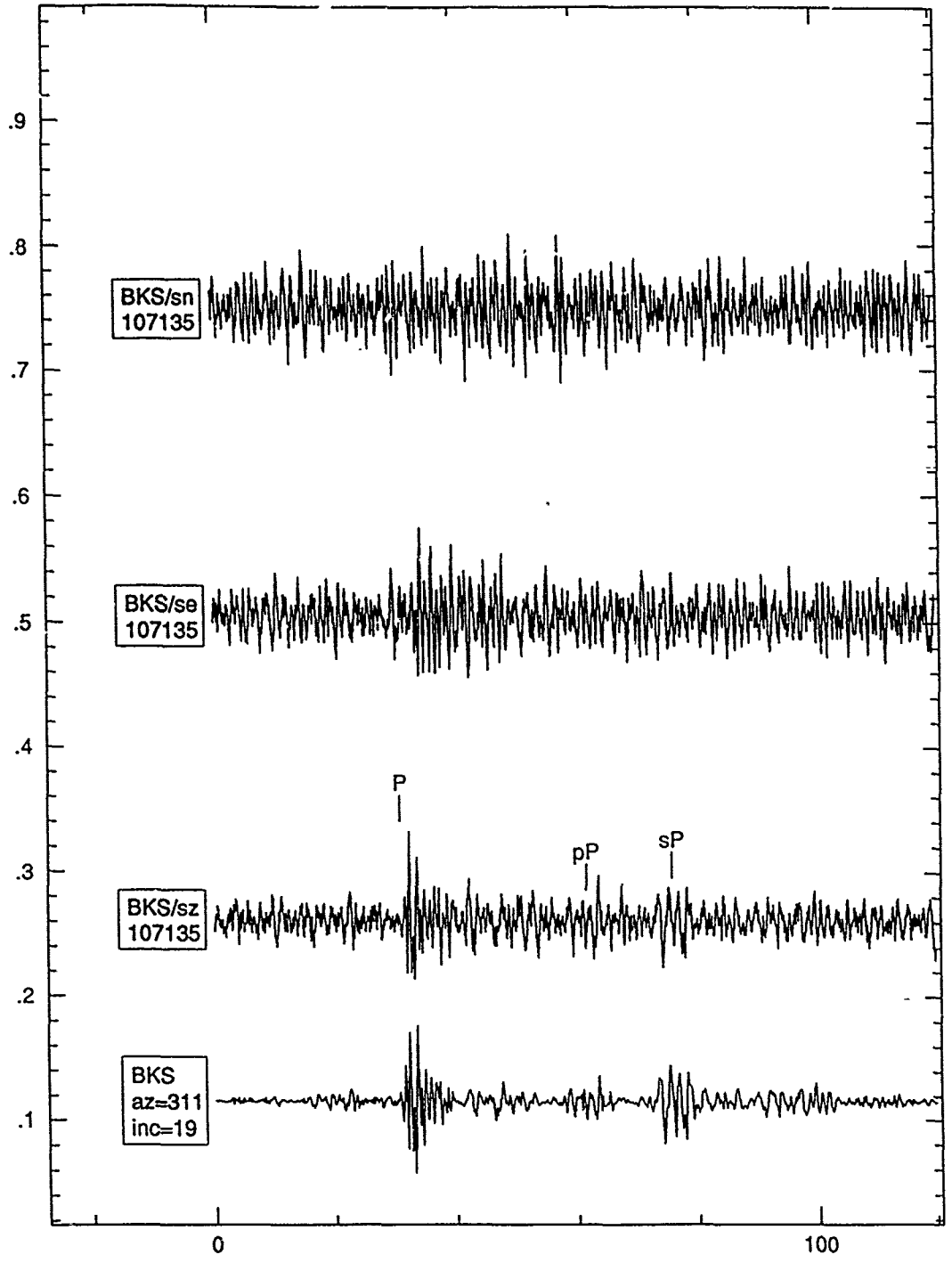

Figure 79: *Three-component and polarization-filtered traces for event 4 at BKS. The depth phases are weli enhanced by polarization filtering.*

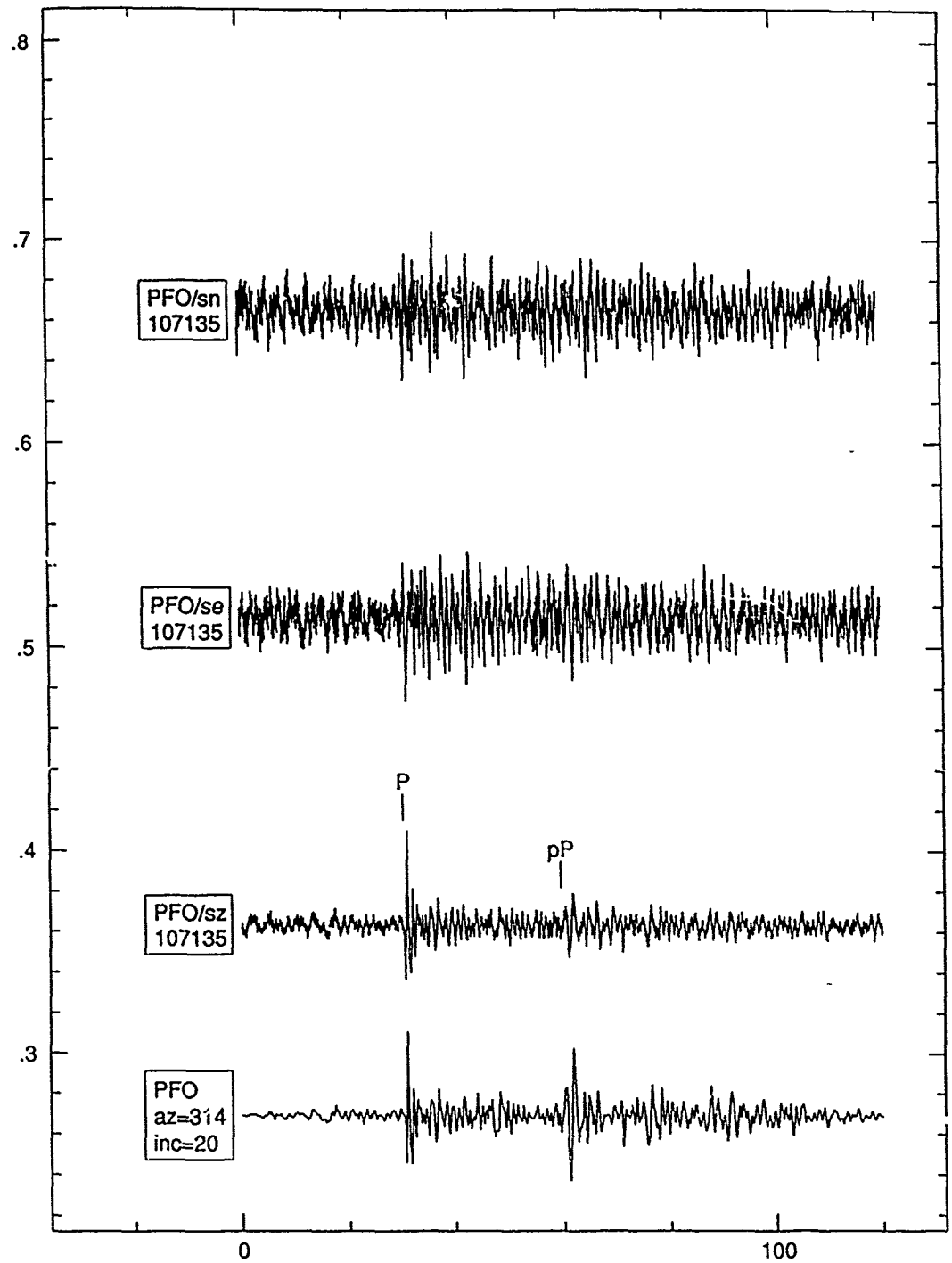

Figure 80: *Three-component and polarization-filtered traces for event 4 at PFO. Polarized signal can be seen on the filtered trace at the expected time for sP (see Fig. 79).*

Table 12: Summary of Associated Phases in *P*-Coda

Event Number	Station	Distance (°)	Azimuth (°)	Incidence (°)	*P*-Coda Phases
1	MAT	72	313	20	*P*, pP (10)
2	ARA0	60	222	24	*P*, pP (12)
2	NRA0	70	209	21	*P*, *pP* (12)
3	ARA0	86	257	17	*P*, *pP* (11)
4	BKS	79	311	19	*P*, *pP* (31), *sP* (15)
4	BLA	61	347	23	*P*, *pP* (29), *sP* (16)
4	ESLA	87	56	17	*P*, *pP* (30)
4	LTX	63	323	23	*P*, *pP* (29), *sP* (14)
4	PFO	73	314	20	*P*, *pP* (30)
4	PIN	76	321	19	*P*, *pP* (30), *sP* (14)
5	HFS	69	209	21	*P*, *pP* (11)
5	NRA0	69	208	21	*P*, *pP* (11)
5	PIN	65	130	22	*P*, *pP* (12)
6	LTX	14	323	45	*P*, *sP* (33)
6	PIN	28	328	31	*pP*, *sP* (15)
7	BLA	64	136	23	*P*, *pP* (13)
7	LTX	55	134	25	*P*, *pP* (12)
7	MAT	37	231	29	*P*, *pP* (13)
7	PFO	44	131	28	*P*, *pP* (12)
7	PIN	43	125	28	*P*, *pP* (13)
3	BLA	56	136	25	*P*, *sP* (15)
8	LTX	48	139	27	*P*, *sP* (14)
8	PFO	38	138	29	*P*, *sP* (13)
8	PIN	36	128	30	*P*, *sP* (13)
9	HFS	73	84	20	*P*, *pP* (25)

Table 12: Summary of Associated Phases in *P*-Coda

Event Number	Station	Distance (°)	Azimuth (°)	Incidence (°)	*P*-Coda Phases
9	LTX	42	286	29	*P*, *pP* (22)
10	LTX	91	62	16	*P*, *pP* (112)
11	HFS	72	218	20	*P*, *pP* (10)
11	LTX	87	135	17	*P*, *pP* (10)
11	NRA0	72	216	20	*P*, *pP* (11)

SNR, the performance decreases, and varying the processing parameters of the polarization filter may be required to improve the results (e.g., events 8 at PFO, 9, and 11). Figure 81 demonstrates this for event 8 at PFO.

Conclusions

This preliminary study of polarization filtering of depth phases for events from the five days of reprocessed GSETT-2 data shows promising results. This processing was, in general, successful in enhancing depth phases, the degree of success depending on SNR. In future work we propose to:

- Compare the results of polarization filtering with those of simple bandpass filtering to better assess the contribution of the polarization filter.
- Optimize the processing parameters at low SNR.
- Process data from the 3-component stations that did not report depth phases to evaluate the capabilities of this method for helping an analyst or automated system detect and identify them.

Acknowledgements

Carl Romney initiated this study. Flori Ryall was very helpful in the selection of the dataset. I am also grateful to Peter Davis (Teledyne Geotech) for making available most of the three-component recordings from US/NDC stations used in this study. Polarization filtering was performed with the "geotool" program, developed by Ivan Henson (Teledyne Geotech) and John Coyne (SAIC).

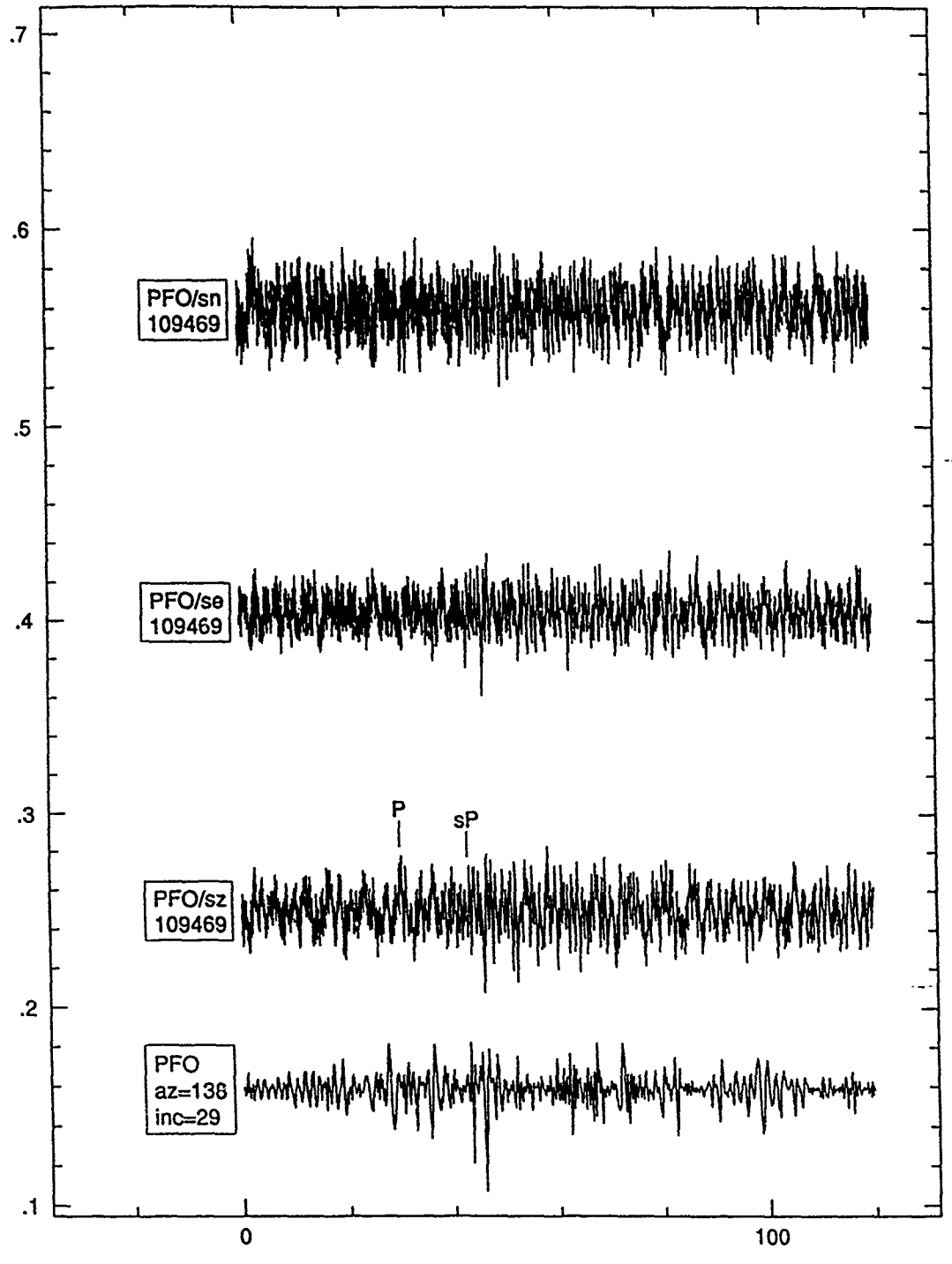

Figure 81: *Three-component and polarization-filtered traces for event 8 at PFO. This is a case of low SNR, where fine-tuning of the parameters of the polarization filter appears to be required.*

References

GSE/US/72 (1992). "Results of Washington EIDC Re-Processing of GSETT-2 Data", *United States Delegation*, March 1992, 16 pp.

Jurkevics, A. (1986a). "Polarization Processing Algorithm With Applications to RSTN Data", *Center for Seismic Studies Report C86-05*, p. 34-47.

Jurkevics, A. (1986b). "Use of Polarization Filtering to Enhance Depth Phases in P-Coda", *Center for Seismic Studies Report C86-06*, p. 2-1 - 2-9.

Jurkevics, A. (1986c). "Application of Polarization Processing to NORESS and RSTN Recordings of Two Events in West Kazakh S.S.R.", *Center for Seismic Studies Report C86-06*, p. 2-21 - 2-28.